UNIVERSITY OF TRENTO - Italy

**International PhD Program in Biomolecular Sciences**

**Department of Cellular, Computational**

**and Integrative Biology - CIBIO**

**XXXII Cycle**

# Identification of new pathways modulating *C9orf72*-derived DPRs expression


Tutor: Prof **ALESSANDRO PROVENZANI**

Department of Cellular, Computational and Integrative Biology

University of Trento

Laboratory of Genomic Screening


Ph.D. Thesis of


**NAUSICAA VALENTINA LICATA**

Department of Cellular, Computational and Integrative Biology

University of Trento

Laboratory of Genomic Screening


Academic Year 2018/2019

**Declaration of original authorship**

I Nausicaa Valentina Licata confirm that this is my own work and the use of all material from other sources has been properly and fully acknowledged.

Trento, 02/10/2020

Licata Nausicaa Valentina

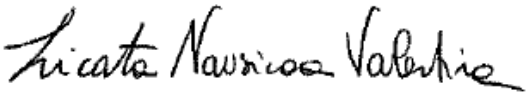

*"[…] for it is not his possession of knowledge, of irrefutable truth,*
*that makes the man of science,*
*but his persistent and recklessly critical quest for truth."*

Karl Popper, *the Logic of Scientific Discovery,* 1934

*"The point is that, whenever we propose a solution to a problem,*
*we ought to try as hard as we can to overthrow our solution,*
*rather than defend it.*
*Few of us, unfortunately, practice this precept;*
*but other people, fortunately, will supply the criticism for us*
*if we fail to supply it ourselves."*

Karl Popper, *the Logic of Scientific Discovery,* 1934

# *Abstract*

The hexanucleotide repeat expansion $GGGGCC_n$ (also known as $G4C2_n$) localizes in the first intron of the *C9ORF72* gene and is the most common genetic cause of ALS and FTD (C9ALS/FTD). The pathomechanisms proposed for C9ALS/FTD suggest that from sense $(G4C2)_n$- and anti-sense $(C4G2)_n$-containing transcripts originate two different mechanisms of toxicity: i) by the alteration of RNA processing due to binding and sequestration of RNA-binding proteins, thereby leading to impairment of RNA metabolism; and ii) by their unconventional Repeat-associated non AUG (RAN) translation into five different dipeptide-repeats (DPRs). In addition, pathological expansion of $(G4C2)_n$ reduces the *C9orf72* transcription causing loss of function of the C9ORF72 protein. The toxicity of some of these DPRs has been showed in several cell lines, in iPSC-derived neurons, in *Drosophila* and in mouse models. An impairment of the ubiquitin-proteasome system (UPS) due to aggregation of toxic proteins is largely demonstrated in neurodegenerative disorders and among the mechanisms of DPR-related toxicity. RAN translation of $(G4C2)_n$-RNAs has been recently shown to require a near-cognate start codon upstream of the repeat in frame +1 and to be triggered by stress conditions in a cap-dependent or cap-independent way. However, the mechanism regulating RAN translation is still largely unknown. Importantly, no small molecules are known to selectively modulate RAN translation, even if antisense oligonucleotides (ASOs) and small molecules binding the $r(GGGGCC)_n$ have been proposed as therapeutics for C9ALS/FTD. In addition, no effective pharmacological approach to reduce the pathological load of DPRs is currently available.

Here, I developed a high-throughput drug-screening assay to identify small molecules and relative molecular targets that can modulate the DPR level. Among the identified hits, two hits reduced DPRs expression levels triggering the protein clearance system *in vitro*. Moreover, the screening identified compounds having the same target that increased DPRs expression levels indicating the targeted pathway as a crucial modulator of the translation process of the *C9orf72* repeat-containing mRNAs. Conversely, I showed that pharmacological inhibition of the pathway reduced DPRs expression levels *in vitro*, while *in vivo* it rescued climbing ability and increased life span of *Drosophila* flies carrying G4C2X36 repeats. Moreover, genetic

ablation of the target reduced DPRs expression levels by decreasing their translation efficiency *in vitro* and rescued the pathological phenotype *in vivo*. Together, the results show the identification of new pathways as new drug targets for C9ALS/FTD.

# *Index*

***Aims of the Thesis*** ..... 1

***Introduction*** ..... 3

1. ALS and FTD: two extremes of the ALS/FTD disease spectrum ..... 4

1.1 Amyotrophic Lateral Sclerosis ..... 4

1.1.1 The genetics of ALS ..... 4

1.2 Frontotemporal Dementia ..... 6

1.2.1 The genetics of FTD ..... 6

1.3 Management of ALS and FTD ..... 6

2. The GGGGCC repeat expansion in *C9ORF72* gene ..... 8

2.1 *C9ORF72*-mediated ALS and FTD ..... 8

2.2 The *C9ORF72* gene ..... 9

2.3 Pathogenic mechanisms underlying C9ALS/FTD ..... 10

2.3.1 C9ORF72 loss of function ..... 11

2.3.2 RNA foci-mediated toxicity ..... 12

2.3.3 DPR-mediated toxicity ..... 13

2.4 C9ALS/FTD therapeutics ..... 15

3. Repeat-associated non-AUG (RAN) translation ..... 17

3.1 Canonical mechanism of translation ..... 17

3.2 RAN translation in microsatellite repeat disorders ..... 20

3.3 RAN translation of GGGGCC and CCCCGG repeat expansions ..... 21

4. Mechanisms of protein clearance ..... 24

4.1 The ubiquitin-proteasome system ..... 24

4.2 Autophagy ..... 24

5. The cAMP/PKA signalling pathway ..... 26

***Results*** ..... 29

1. Development of a HTS assay for identifying modulators of *C9ORF72*-DPRs expression 30

2. High-throughput screening compounds and confirmatory screening for identifying modulators of *C9ORF72*-DPRs expression ..... 36

3. Characterization of selected small molecules in different cell lines ..... 40

4. None of the compounds acts on inducing the autophagy system ..... 45

5. GELD and SPL enhance the activity of ubiquitin-proteasome system ..... 50

6. Insight: FSK does not block the UPS and does not interfere with CREs inside the CMV promoter-driven plasmids ..... 52

7. The PKA inhibitor H89 decreases DPRs expression ..... 54

8. The PKA inhibitor H89 does not act by modulating either the autophagy system or the UPS ..... 56

9. Genetic ablation of the PKA catalytic subunits decreases DPRs expression levels ..... 60

10. Genetic ablation of the PKA catalytic subunit β decreases DPRs expression modulating *G4C2* mRNA translation ..... 62

11. The PKA inhibition through H89 administration rescues motility defects and extends lifespan in a *Drosophila* model for C9ALS/FTD ..... 66

12. Downregulation of *Pka-C1* in C9ALS/FTD *Drosophila* improves motility defects and extends lifespan ..... 68

13. The PKA-substrate eEF2 kinase as candidate involved in modulating DPRs expression ..... 70

***Discussion*** ..... 72

***Future perspectives and ongoing works*** ..... 78

***Materials and Methods*** ..... 81

***Funding*** ..... 96

***References*** ..... 97

# *Aims of the Thesis*

My PhD project aimed at developing a high-throughput screening assay to identify and validate small molecules (hits) modulating the cytotoxic expression of *C9ORF72*-related DPRs that are produced via an AUG-independent translation.

To achieve this goal, the first arduous task was to set up an assay amenable for high-throughput screening.

The second goal related, to exploitation of the biological effect of the selected small molecules, consisted of:

i) Dissecting the molecular mechanisms underlying RAN translation by analysing the effect of the hits at different levels: transcriptional, translational and post-translational (i.e. protein clearance).

ii) Testing the protective activities of hits in C9ALS/FTD models, specifically the small molecules were tested firstly in different cell lines and in a *Drosophila* C9ALS/FTD model carrying the G4C2 repeat expansion.

# *Introduction*

# 1. ALS and FTD: two extremes of the ALS/FTD disease spectrum

## 1.1 Amyotrophic Lateral Sclerosis

Amyotrophic Lateral Sclerosis (ALS) is a neurodegenerative disease characterized by the selective death of both upper (placed in the brain) and lower (in the brainstem and spinal cord) motor neurons[1]. The progressive loss of lower motor neurons causes paralysis, impaired voluntary muscle functionality followed by atrophy and disability[1]. The survival rate for ALS patients is three to five years and often respiratory failure, resulted from pulmonary complications, represents the main cause of death[1,2]. The clinical signs seem often start at a specific body region and then disseminate elsewhere, suggesting a possible mechanism of "*prion-like propagation*"[3]. There are mainly three types of clinical onset:

1) *Limb-onset* characterized by the combination of both upper and lower motor neuron signs in the limbs. Limb-onset is the predominant type with 70% of the cases among patients[4,5].

2) *Bulbar-onset* characterized by dysarthria, dysphagia for solid or liquids and limbs symptoms, which can develop almost simultaneously with bulbar symptoms. Bulbar-onset occurs in 25% of the cases[4,5].

3) *Respiratory-onset* occurs in only 5% of the cases. Usually, it does not present limb or bulbar symptoms[5,6].

The clinical diagnosis of ALS bases on the revised El Escorial criteria[7] that includes laboratory exams as diagnostic tools to exclude differential diagnosis.

### 1.1.1 The genetics of ALS

ALS is principally classified as a sporadic disease as the majority of cases (sporadic ALS, sALS) do not apparently show a Mendelian inherited component. About 10% of ALS cases instead having a family history are grouped as familial ALS (fALS) [1,8]. All fALS cases, but also a minority of sALS case, are caused by the presence of mutations in one or more genes. The first mutations causing ALS were discovered in the *SOD1* gene in 1993[9]. After that, the discovery of mutations in the *TARDBP* gene[10] happened only in 2008. However, thanks to the arrival of the next-generation sequencing, the genetics discoveries in ALS have been took big forward steps. Among the several ALS genes known until now, *C9ORF72*, *SOD1*, *FUS* and

*TARDBP* are the most common ones[11]. Following, about thirty ALS genes are listed in **Table 1**.

| Involved in | Locus | Gene | Protein | Frequency of mutation | | Discovery |
|---|---|---|---|---|---|---|
| | | | | fALS | sALS | |
| RNA processing | q36 | *TARDBP* | TDP-43 | 5% | <1% | 2008 |
| | 16p11.2 | *FUS* | FUS | 5% | <1% | 2009 |
| | 14q11 | *ANG* | Angiogenin | <1% | <1% | 2006 |
| | 9q34.13 | *SETX* | Senataxin | NA | NA | 2002 |
| | 5q31.2 | *MATR3* | Matrin 3 | <1% | <1% | 2014 |
| | 12q24.12 | *ATXN2* | Ataxin 2 | NA | NA | 2011 |
| | 12q13.1 | *HNRNPA1* | hnRNP A1 | <1% | <1% | 2013 |
| Protein trafficking and degradation | 9p21-22 | *C9ORF72* | C9ORF72 | 25% | 10% | 2011 |
| | 2q33.1 | *ALS2* | Alsin | NA | NA | 2001 |
| | 20q13. 32 | *VAPB* | Vesicle-associated membrane protein-associated protein B/C | 0.6% | NA | 2004 |
| | 3p11.2 | *CHMP2B* | Charged multivesicular body protein 2b | <1% | NA | 2006 |
| | Xp11.23-Xp13.1 | *UBQLN2* | Ubiquilin 2 | <1% | <1% | 2011 |
| | 5q35 | *SQSTM1* | Sequestosome 1 | <1% | NA | 2011 |
| | 10p15-p14 | *OPTN* | Optineurin | 4% | <1% | 2010 |
| | 9p13.3 | *VPC* | Transitional endoplasmic reticulum ATPase | 1-2% | <1% | 2010 |
| | 12q14.1 | *TBK1* | Serine/threonine-protein kinase TBK1 | NA | NA | 2015 |
| Cytoskeletal and axonal dynamics | 2p13 | *DCTN1* | Dynactin subunit 1 | <1% | <1% | 2003 |
| | 17p13.2 | *PFN1* | Profilin-1 | <1% | <1% | 2012 |
| | 15q21.1 | *SPG11* | Spatacsin | NA | NA | 2010 |
| | 2q36.1 | *TUBA4A* | Tubulin α-4A chain | <1% | <1% | 2014 |
| | 4q33 | *NEK1* | NIMA-Related Kinase 1 | NA | NA | 2015 |
| Mitochondria | 22q11.23 | *CHCHD10* | Coiled-coil-helix-coiled-coil-helix domain-containing protein 10 | <1% | <1% | 2014 |
| Other | 21q22.11 | *SOD1* | Cu–Zn superoxide dismutase | 20% | 2% | 1993 |
| | 2q34 | *ERBB4* | Receptor tyrosine-protein kinase erbB-4 | 0.5% | NA | 2013 |

**Table 1 |** Genetics of ALS. Table adapted from [8,11,12**].**

## 1.2 Frontotemporal Dementia

Frontotemporal dementia (FTD) is the second most common form of dementia with midlife onset. FTD is characterized by progressive neurodegeneration of frontal and temporal lobes and can be divided in three subtypes based on symptoms presented: two language variants and one behavioural variant. This latter FTD subtype is often associated with motor system dysfunctions[13]. The lifespan of FTD patients goes from five to ten years after the disease onset[14].

### 1.2.1 The genetics of FTD

Several mutations have been identified in the *MAPT* and *PGRN* genes that are closely located on chromosome 17 and encode for tau and progranulin protein, respectively[15]. Moreover the abnormal repeat expansion in the *C9ORF72* gene represents the most common genetic cause of FTD (about 13% of cases)[16].

## 1.3 Management of ALS and FTD

Although enormous progress in the field of genomics are ongoing, there is no cure for ALS yet. Currently, there are two FDA-approved drugs acting on symptom management, providing modest benefits only in some patients.

- Riluzole, approved in 1995, is thought to act as inhibitor of glutamate production. In two therapeutic trials, riluzole prolonged survival by three to six months, showing a slowdown of disease progression[17,18].
- Edaravone, approved in 2017, is a free radical scavenger that is administrated in patients that receive probable or definite ALS diagnosis[19].

Moreover, antisense oligonucleotides (ASO) targeting ALS-causative genes are in diverse phases of clinical trials. Specifically, there are currently ongoing a phase III clinical trial to test ASOs targeting SOD1 in patients with familiar ALS (ClinicalTrials.gov Identifier: NCT02623699) and a phase I clinical trial of ASOs targeting the sense strand of *C9ORF72* in patients with C9ALS (ClinicalTrials.gov Identifier: NCT03626012). The main advantage in utilizing ASOs is their capability to degrade the targeted-mRNAs.

As with ALS, there are no cure for FTD yet. The only medications in use have the aim to manage the symptoms as selective serotonin reuptake inhibitor for the

behavioural FTD variant and Riluzole can be suggested as therapy in presence of motor dysfunctions[20].

# 2. **The GGGGCC repeat expansion in *C9ORF72* gene**

## 2.1 ***C9ORF72*-mediated ALS and FTD**

In the last three decades, clinical evidences on the symptomatology of ALS and FTD patients led to consider the two disorders as a continuous disease spectrum. Indeed, about 50% of ALS patients show frontal and cortical neurodegeneration and clinically behavioural symptoms, and about 20% of FTD patients with the behavioural variant show the loss of motor neurons[8]. In addition, several genes overlap with the two diseases such as *TARDBP*[10], *SQSTM1*[21], *VCP*[22], *FUS*[23], *TBK1*[24], *CHCHD10*[25], and *C9ORF72*[16].

Notably, the mutation in the *C9ORF72* gene has been significantly associated to 40% and 25% of familiar ALS and FTD cases, respectively, and to 5-15% and 6% of sporadic ALS and FTD cases, respectively[26]. Patients carrying the mutation of *C9ORF72* and showing both ALS and FTD symptomatology are referred as C9ALS/FTD patients.

Linkage analysis in several cases of ALS, FTD and ALS/FTD found that the locus on the short arm of chromosome 9 is linked to onset of disease in 2006[27,28]. Later, through studies of a risk haplotype at the 9p21 locus, a hexanucleotide repeat expansion mutation in a non-coding region of the *Chromosome 9 open reading frame 72* (*C9ORF72*) gene was independently identified in 2011 by two groups[29,30]. Between the discovery of the locus and the identification of the responsible mutation five years passed because both the intronic localization of expansion and its 100% GC content have made difficult to detect it by traditional sequencing.

Studies of genetics population on the *C9ORF72* expansion frequency suggest the idea of a common founder effect. Indeed, a high expansion frequency was found in a large Finnish population rate, but just outside from Scandinavia the expansion frequency begins to decrease[31,32]. In addition, studies on cohorts of non-European descent (limited to a small number of Asian populations), found a lower frequency of *C9ORF72* repeat expansion than that observed in European and North American cohorts[31,33,34].

The age of onset of C9ALS/FTD such as also the disease progression have a range extremely broad; it goes from 27 to 83 years of age while from 1 to 22 years for the disease duration[31,35].

In the healthy population, the repeat length is present in a range between 2 up to 25 units, while in C9ALS/FTD cases it is expanded from hundred to thousand units[29,30,36,37], even if a tract of 30 repeats has been associated with the disease[30] as well as others short expansions of 45-80 repeats[38]. Longer repeat sizes seem to correlate with an early onset of disease[38]. However, whether the increased risk and the clinical phenotype correlate with the repeat length remains uncertain yet.

The C9ALS/FTD disease is a TDP43 proteinopathy as shown by presence of SQSTM1/p62 and TDP43 positive cytoplasmic inclusions in post-mortem brain tissue of both ALS and FTD patients: specifically, they were found in motor cortex and anterior horn of the spinal cord[39]. However, in extra-motor regions, cytoplasmic and intranuclear DPRs inclusions were phospho-TDP43-negative[32,40–42]. Another characteristic of the C9ALS/FTD disease is the presence of nuclear sense and antisense RNA foci in both TDP43 and SQSTM1/p62 inclusions that cause toxicity probably through sequestration of RNA-binding proteins[43–45]

## 2.2 The *C9ORF72* gene

The *C9ORF72* gene is transcribed as three transcript variants. Transcript variants 2 and 3 encode the full-length isoform protein with 481 amino acids, while transcript variant 1 encodes an isoform of 222 amino acids[29]. The hexanucleotide repeat expansion (HRE) GGGGCC (also known as G4C2) localizes in the first intron in transcript variants 1 and 3 that corresponds to the promoter region of transcript variant 2[46,47] (**Figure 1**).

Bioinformatics analysis has suggested a number of possible functional domains for the C9ORF72 protein. In particular, secondary structure of C9ORF72 protein has high homology with the “differentially expressed in normal and neoplasia” (DENN) domain, also found in guanine exchange factors (GEF) that activate Rab GTPases[48], suggesting that C9ORF72 protein could be involved in Rab-GTPase-dependent membrane trafficking and protein degradation[49].

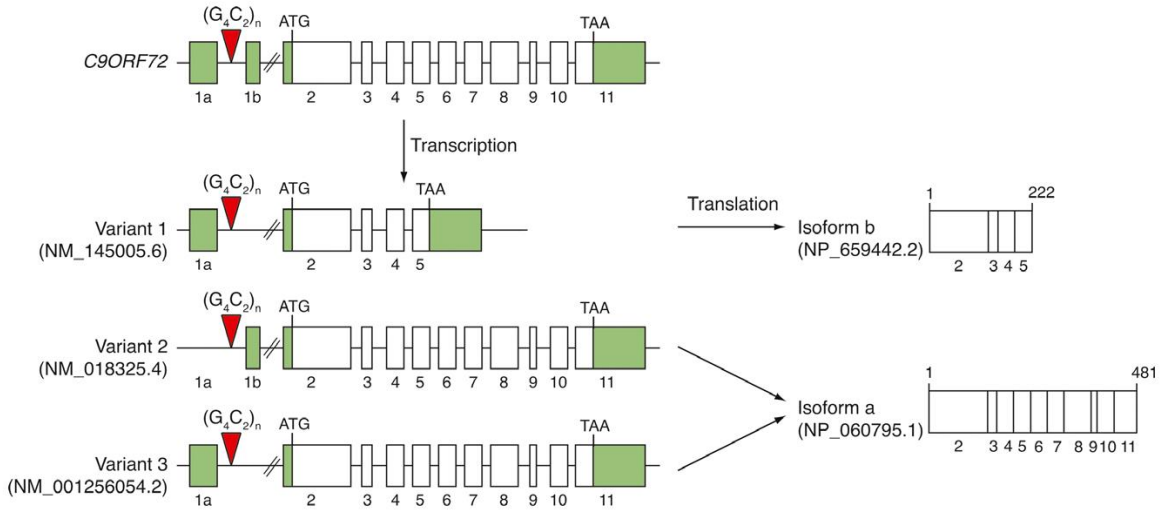


**Figure 1 | *C9ORF72* gene structure, transcription and translation**
The *C9ORF72* gene consists of 11 exons (boxes). In green are represented the non-coding exonic regions. The HRE G4C2 (red triangle) localizes in intron 1 between non coding-exons 1a and 1b. The *C9ORF72* gene is transcribed in three transcript variants. Variants 2 and 3 encode the full-length protein isoform a (481 aa), while variant 1 the short isoform b (222 aa). Figure adapted from [46].

## 2.3 Pathogenic mechanisms underlying C9ALS/FTD

Several studies demonstrated that HRE G4C2 induces neurodegeneration through three different pathogenic mechanisms (**Figure 2**) that are not mutually exclusive:

i) loss of the C9ORF72 function due to haploinsufficiency,

ii) toxic gain-of-function through formation and accumulation of HRE-containing transcripts;

iii) toxic gain-of-function due to the translation of these HRE-containing transcripts that generate dipeptide repeat proteins (DPRs).

All the three mechanisms proposed contribute to the disease to some extent and more likely at different stages of the disease, however their relative importance is still to determine and is required to develop targeted therapeutic strategies. Moreover, several other cellular processes are implicated in C9ALS/FTD and most of them have been already observed and associated to ALS and FTD (e.g glutamate excitotoxicity, impaired ubiquitin-proteasome system).

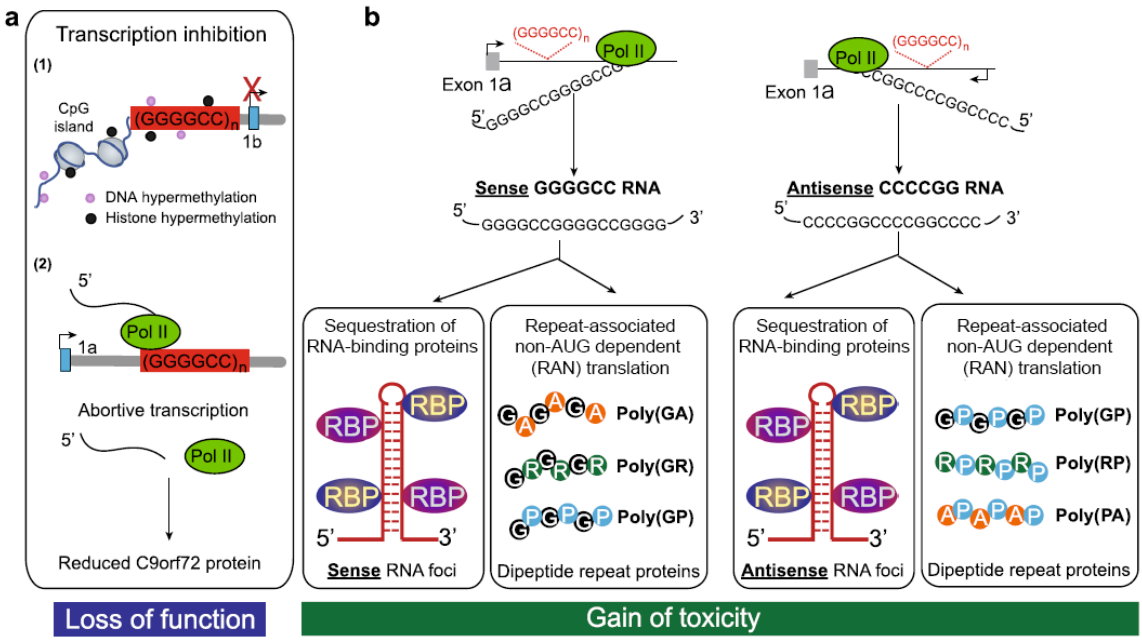


**Figure 2 |** Pathogenic mechanisms in C9ALS/FTD
(**a**) The presence of abnormal HRE sizes potentially contributes to hypermethylation of DNA and histones, and to abortive transcription thereby reducing C9ORF72 protein expression. (**b**) Bidirectional HRE-containing transcripts cause neuronal toxicity through formation of RNA foci that sequester RNA-binding proteins and through synthesis of five dipeptide repeat proteins (DPRs) by uncanonical repeat-associated non-AUG (RAN) translation. Figure adapted from [50].

### 2.3.1 C9ORF72 loss of function

Reduced expression of *C9orf72* mRNA has been reported in the presence of the abnormal HRE sizes[29,30]. A possible explanation could be that the repeat expansion induces epigenetic changes as has been described for Friedreich's ataxia and Fragile X syndrome[51,52]. Xi *et al.*[53] demonstrated that small expansions of 43-50 repeats did not reduce *C9orf72* transcription, probably because do not cause hypermethylation of a CpG island 5' placed in proximity of the HRE. Therefore, the HRE could induce DNA hypermethylation leading to decreased levels of *C9orf72* mRNAs thereby decreased levels of C9ORF72 protein[53]. Several other mechanisms have been proposed for haploinsufficiency. One is that the HRE G4C2 being GC-rich forms DNA G-quadruplex structures that could induce abortive transcription of *C9ORF72*[54] (**Figure 2a**).

*C9ORF72* knockdown and knockout mice models have been generated, but none of them reproduced the pathological features of C9ALS/FTD[44,55], suggesting that *C9ORF72* loss-of-function is not sufficient alone to induce the disease. Moreover, patients homozygous for *C9ORF72* HRE did not show more severe symptoms than patients heterozygous[56,57].

### 2.3.2 RNA foci-mediated toxicity

As previously reported, the HRE G4C2 is able to form stable G-quadruplex structures due to its abundance of GC nucleotides inducing abortive *C9orf72*-transcription but also generation of sense and antisense HRE-containing transcripts[54]. In physiological conditions, intron 1 is spliced out and degraded; however, the presence of repeat expansion might avoid this process generating different types of RNAs: spliced intron bearing the repeat, *C9orf72*-mRNA transcripts with the retained intron[58] and aborted *C9orf72*-RNA transcripts[54] (**Figure 3**).

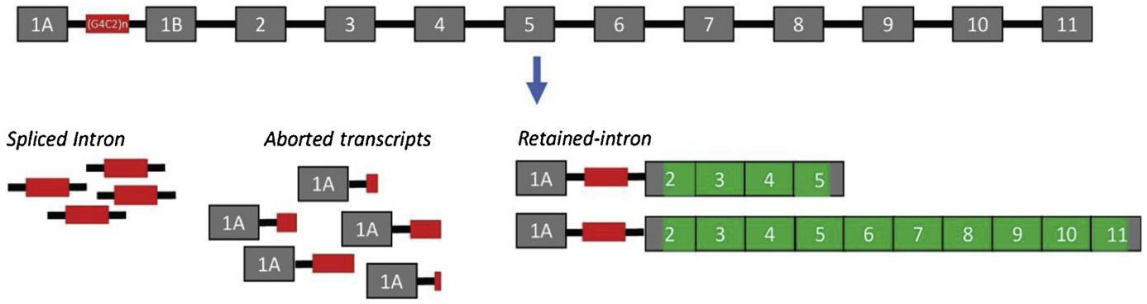


**Figure 3 |** Generation of possible different types of RNAs caused by the presence of the repeat expansion. Figure adapted from [14].

Both sense and antisense transcripts accumulate and form nuclear RNA foci in multiple neuronal cell types and in non-neuronal cells, including astrocytes and microglia[44,45]. However, non-neuronal cells show few RNA foci compare to neurons suggesting neurons are the primary sites of foci pathology[45]. Several studies reported that RNA foci induce neuronal toxicity through sequestration of several RNA-binding proteins (e.g. Nucleolin, Pur α, hnRNPs. ADARB2, SRSF1, SRSF2 and ALYREF)[54,59–63], as already observed in other non-coding repeat expansion diseases[64], disrupting several downstream molecular pathways (e.g. dysfunction in RNA processing and in granule transport, disrupted nucleocytoplasmic transport and nucleolar stress)[54,59–63] (**Figure 4**).

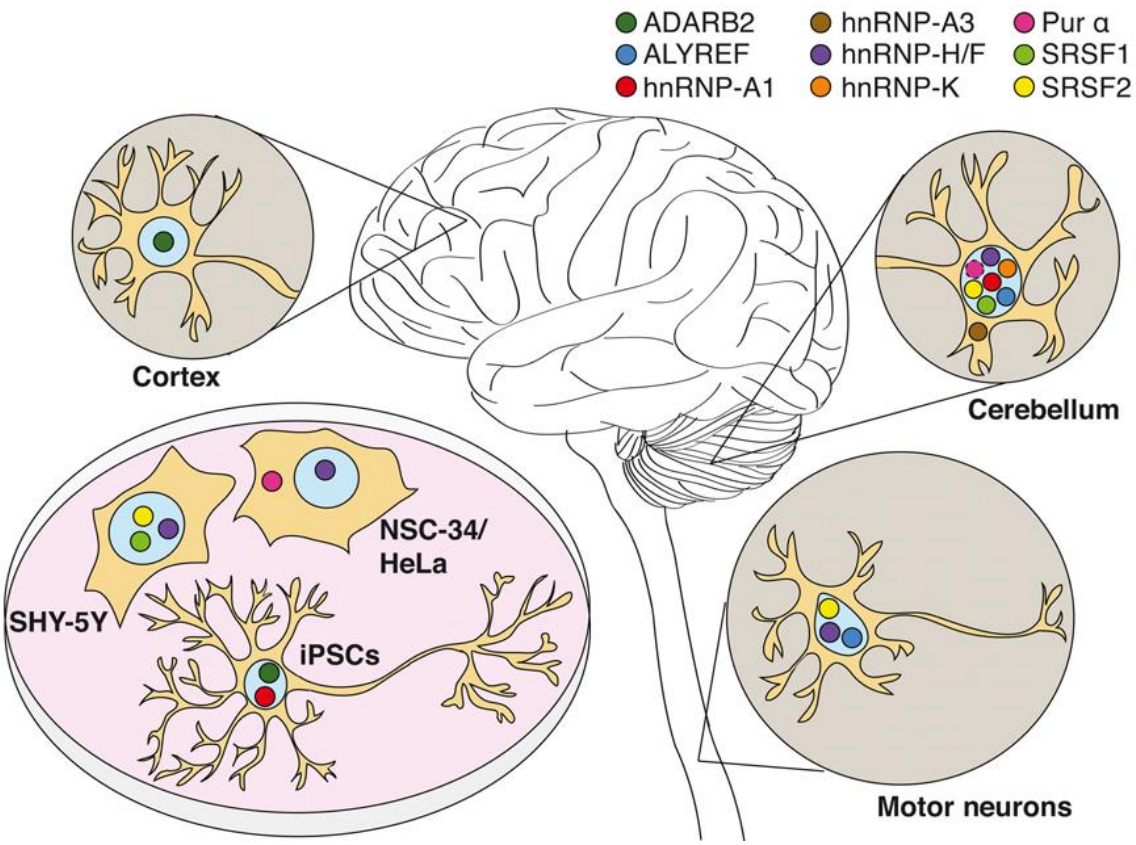


**Figure 4 |** RNA-binding proteins (RBPs) co-localizing with *C9orf72* RNA foci. RBPs are listed above and represented by a coloured point. The figure recapitulates the co-localization of RBPs with *C9orf72* RNA foci that have been seen in cells models (SHSY-5Y, NSC34, HeLa cells and iPSCs) and in patient tissues. Figure adapted from [46].

However, whether RNA foci formation is sufficient to induce neurodegeneration is still under investigation, as *Drosophila* models carrying “RNA-only” repeats (i.e. with RNA foci, but not DPRs production) did not show neurodegeneration, differently from *Drosophila* expressing both RNA foci and DPRs that showed it[65,66].

### 2.3.3 DPR-mediated toxicity

HRE-containing transcripts can also escape from the nucleus and undergo RAN translation producing up to five DPRs[54,67,68]. Poly-GA and poly-GR arise from the first and third sense strands, respectively, poly-PA and poly-PR from the first and third antisense strands, respectively, whereas poly-GP is synthesized from both second sense and antisense strands[67–71] (**Figure 5**).

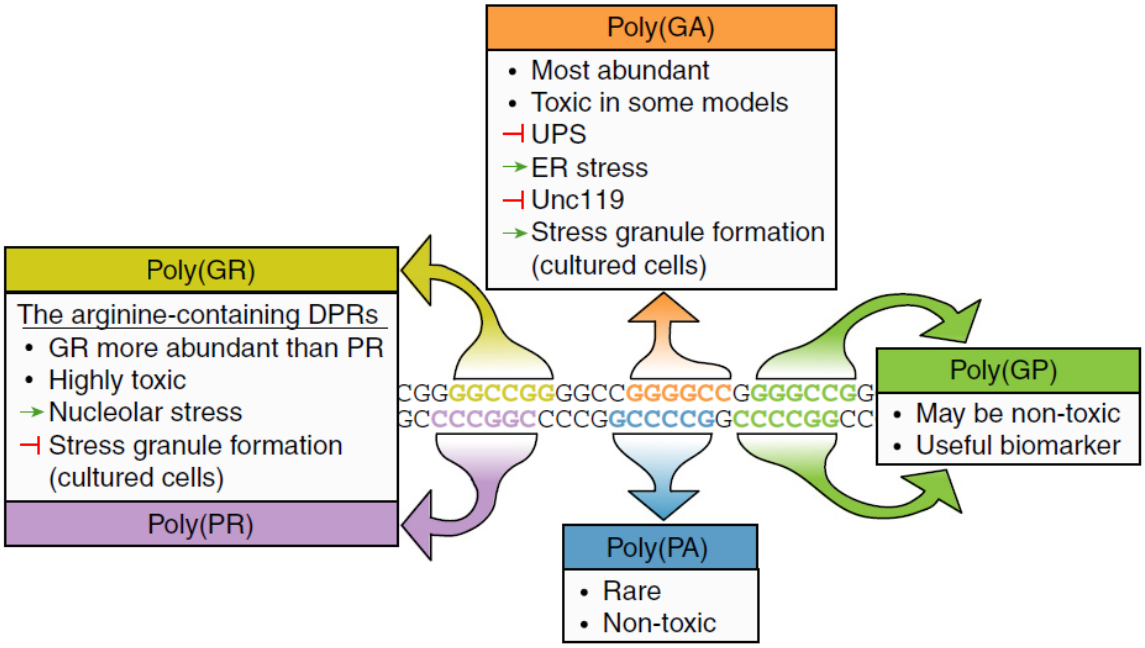


**Figure 5 |** Schematic representation of DPRs generated by RAN translation of expanded GGGGCC and CCCCGG repeats in all reading frames and their toxic effects listed in boxes. Figure adapted from [46].

All DPRs have been detected as aggregates in brain tissues of C9ALS/FTD patients [67–72]. Interestingly, soluble poly-GP can be detected in the cerebrospinal fluid of C9ALS/FTD patients[73–75], suggesting it can be used as measurable biomarker of therapeutic efficacy. Pathologically, dot-like and "star-shaped" neuronal cytoplasmic inclusions of sense and antisense DPRs are found in cerebellum, hippocampus and frontotemporal neocortex, whereas they are less frequent in the spinal cord[67–70,72]. However, the presence of DPRs in these brain regions does not correlate with neuronal loss, raising question about their pathogenicity[72]. The frequency of antisense inclusions is lower compare to the frequency of sense DPRs[76]. Moreover, DPR inclusions are found in neuronal cells types and rarely in microglia, astrocytes and oligodendrocytes, probably owing to the failure of protein quality control system, which is instead characteristic of post-mitotic cells[77]. Interestingly, several studies reported cell-to-cell transmission of DPRs suggesting that DPRs synthesis might be cell-specific and that DPRs synthesized diffuse to neighbouring cells[78,79]. Poly-GA, poly-GP and poly-GR proteins co-localizes with SQSTM1/p62-positive inclusions[68] (an autophagic marker), but only poly-GR inclusions are found co-localize with phospho-TDP43[80].

Poly-GR and poly-PR are arginine-rich DPRs and are the most toxic DPRs among all the others. Indeed, their toxicity has been demonstrated *in vitro*[81] and *in vivo*[65,82]

models inducing neurodegeneration by disrupting several downstream pathways as nucleocytoplasmic transport[82,83], RNA processing[83] and the ubiquitin proteasome system (UPS)[84]. The demethylation of arginine residues might increase protein hydrophobicity, possibly altering the aggregation properties and thus causing cytotoxicity[67]. In addition, poly-GA exerts its toxicity by inhibiting the UPS[85]. DPR-associated toxicity has been largely demonstrated also by the expression of DPRs with AUG-dependent translation and degenerate codons[84]. However, although DPR-mediated toxicity has been largely demonstrated both *in vitro* and *in vivo* models, whether the severity of disease correlates with their presence remains to determine, even if as previously said, DPRs do not localizes in brain regions with neuronal loss. An hypothesis could be that neurons expressing DPRs die and therefore at the time of autopsy they do not exist anymore[47].

## 2.4 C9ALS/FTD therapeutics

Although there is no available yet a cure for ALS or FTD, multiple therapeutic approaches for patients carrying the *C9ORF72* repeat expansion have been proposed targeting upstream or downstream the disease-signalling cascade.

a) Targeting *C9orf72* repeat expansion RNA/DNA to selectively inhibit transcription of repeat-containing RNA. This goal can be pursued by different strategies:
    - Antisense oligonucleotide. ASOs targeting the sense strand is currently in phase I clinical trial (NCT03626012)[50]. The administration of these ASOs in C9 BAC mice expressing 450 repeat expansions led to a significant decrease of both RNA foci and DPRs[86] .
    - RNA interference.
    - Small molecules as G-quadruplex or hairpin binders showed several benefits both in vitro and in vivo models decreasing foci formation thereby ablating RBPs sequestration, and DPRs accumulation[73,87–89].
    - CRISPR/Cas9 technology to genetically correct the *C9ORF72* repeat expansion[90].
b) Targeting RAN translation indirectly by using strategies mentioned above or directly for example performing an unbiased RNAi-based screen for canonical translational factors in a C9-*Drosophila* model[91,92].

c) Targeting DPRs directly by using antibodies as recently demonstrated vs poly-GA[79,85] or indirectly for example by enhancing their turnover rates through overexpression of the heat shock protein HSPB8[93]. Since soluble poly-GP can be detected in the cerebrospinal fluid of C9ALS/FTD patients[73–75], poly-GP may be used as measurable biomarker of therapeutic efficacy.

d) Targeting downstream mechanisms affected by *C9ORF72* repeat expansions, for example the nucleocytoplasmic transport (NTC) by using selective inhibitors of nuclear export (SINE). The administration of SINEs in *Drosophila* showed mitigation of NTC deficits. Currently, a SINE compound, KPT-350, has taken in clinical studies by Karyopharm Therapeutic[50]. Moreover, mitigation of NCT deficits, inhibition of stress granule assembly[94] and extension of the lifespan of TDP-43 mice[95] were obtained by reducing ataxin-2.

# 3. **Repeat-associated non-AUG (RAN) translation**

## 3.1 Canonical mechanism of translation

In eukaryotic cells, the initiation of protein synthesis is tightly regulated and consists of assembling an 80S ribosome with a capped messenger RNA (mRNA) and initiator methionyl-transfer RNA (Met-tRNAi). The translation of capped mRNAs depend on the recognition of the 5′ methyl-7-guanosine ($m^7G$) cap on mRNA by the eukaryotic initiation factor 4F (eIF4F) complex. This represents the first step of this process. The eIF4F consists of eIF4E that directly binds to $m^7G$[96], eIF4G and eIF4A. eIF4G binds to the poly-adenosine-binding protein (PABP), allowing its binding to the 3′ polyA tail on mRNAs thereby making mRNAs circularized and enhancing initiation efficiency[97]. eIF4A is an RNA helicase that, together with the accessory factors eIF4B and eIF4H, unwinds mRNA secondary structures to allow then the recruitment of 43S pre-initiation complex (43S PIC)[98]. The 43S PIC consists of 40S ribosomal subunit, eIF1, eIF1A, eIF3, eIF5, and the ternary complex, that in turn is composed of methionine-conjugated tRNA (tRNAMet) and eIF2-GTP. Once the 43S PIC is recruited, together with eIF4F complex, form the 48S pre-initiation complex that begins to scan the mRNA from the $m^7G$ cap, in 3’ direction, looking for an AUG initiation codon placed in a good Kozak context[99]. Then eIF1 dissociates from the 48S allowing the hydrolization of GTP by eIF2 with the help of eIF5. This facilitates the recruitment of eIF5B-GTP that promotes the association of the 60S subunit and displacement of most eIFs[100]. Finally, release of eIF5B-GDP and eIF1A allows the establishment of 80S ribosome that begins translation elongation[100] (**Figure 6**).

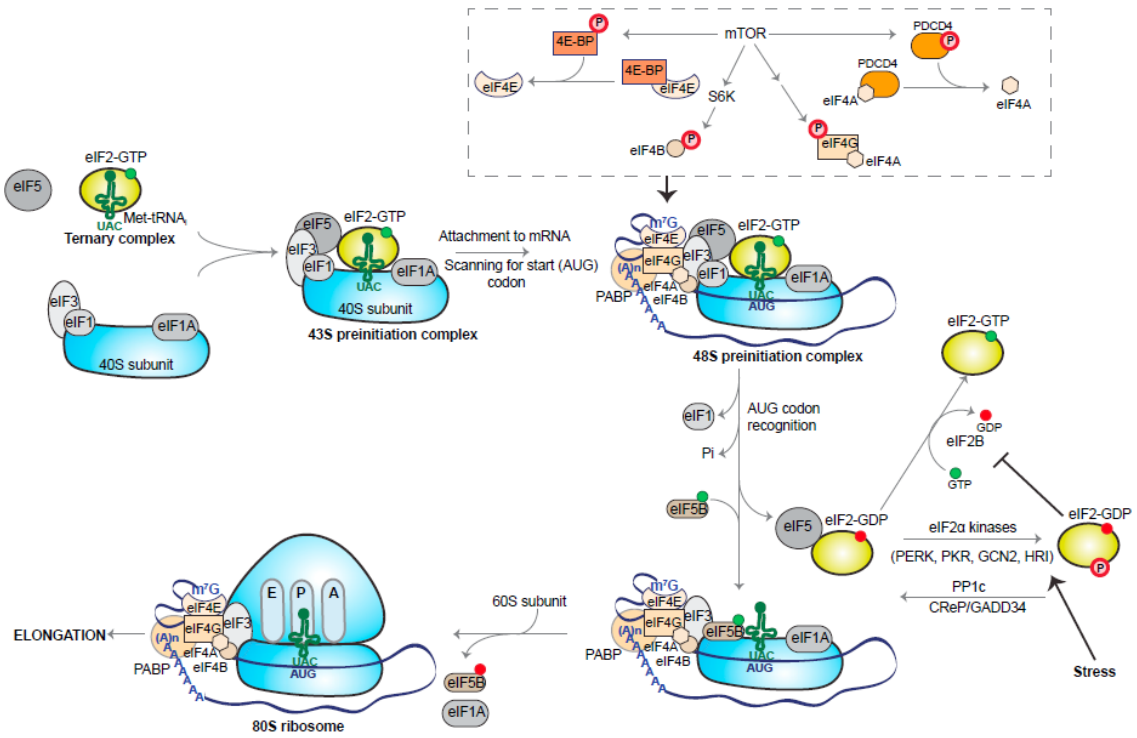


**Figure 6 |** Schematic representation of the canonical mechanism of translation initiation. Figure adapted from [101].

The elongation phase requires three eukaryotic elongation factors (eEFs). The eEF1A binds the aminoacyl tRNAs to the ribosome in a GTP-dependent way, while the eEF1B, that differs from eEF1A, being a guanine nucleotide exchange factor is required to recycle the eIF1A•GTP in the transfer of aminoacylated tRNAs to the ribosome. Once the peptide bond is formed, the eEF2 comes into play to allow in a GTP-dependent way the translocation of the ribosome from one codon to the other along mRNAs and start a new cycle of elongation[100] (**Figure 7**). The elongation phase is crucial to produce functional and correctly folded proteins and is tightly regulated. Indeed, the activity of eEF2 depend on its phosphorylation status; when the threonine 56 ($Thr^{56}$) of eEF2[102] is phosphorylated, since it is close to the site of interaction for ribosomes[103], the activity of eEF2 is inhibited slowing down the total protein synthesis rate[104].

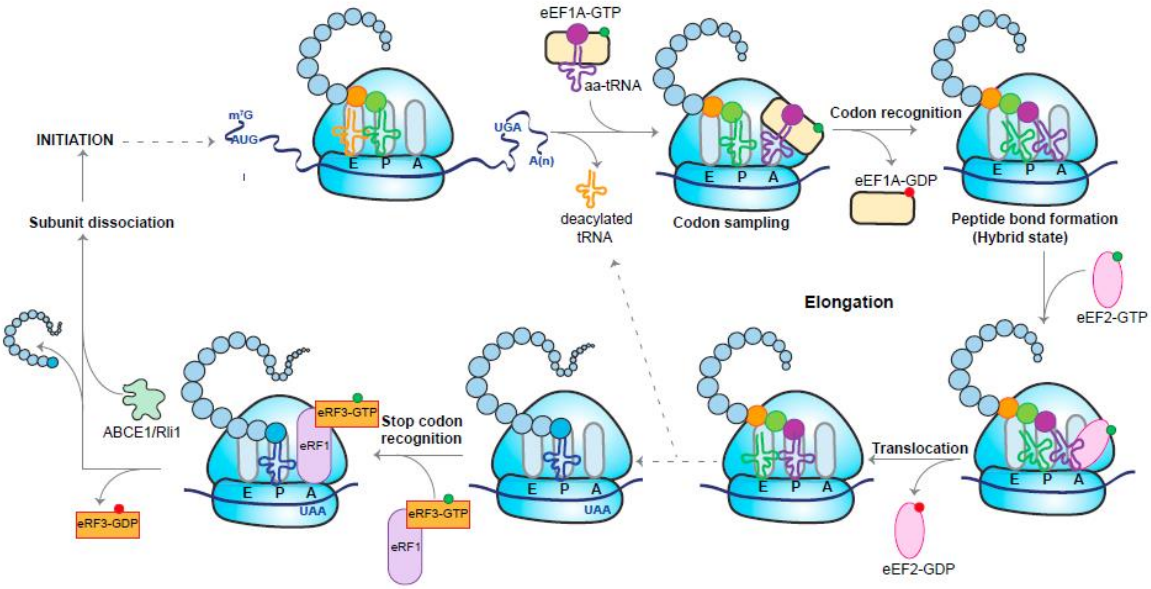


**Figure 7 |** Schematic representation of the translation elongation. Figure adapted from [101].

However, translation initiation is considered the limiting-step of protein synthesis[101]. The presence of stress cellular stimuli induces the integrated stress response (ISR) pathway that by one of the four stress-induced kinases phosphorylates the serine 51 ($Ser^{51}$) of the eIF2α[105]. Phosphorylation of $Ser^{51}$ impedes the exchange of GTP for GDP reducing the amount of ternary complex and thereby inhibiting the cap-dependent translation[101] (**Figure 6**). Moreover, under stress conditions, some mRNAs encoding proteins crucial for cell survival are translated in a cap-independent ways such as transcripts with upstream open reading frames (uORFs) (e.g. ATF4) or containing internal ribosome entry site (IRES)[101].

Indeed, some mRNAs can be translated into proteins via non-canonical forms of translation that exist in physiological and pathological conditions. RNA secondary structures, for example, play a role in regulating translation initiation. Based on their location, secondary structures upstream of an AUG start codon can inhibit initiation process, whereas when they are downstream can enhance it[106]. IRES-translation (mentioned above) is cap-independent as directly recruits 40S ribosomal subunit in the proximity of the AUG codon, bypassing the eIF4E-$m^7G$ binding[107]. Like IRES-translation, RAN translation is thought to be depend on secondary structures in the HRE.

## 3.2 RAN translation in microsatellite repeat disorders

Repeat-associated non-AUG (RAN) translation was first described in 2011 in two different diseases: spinocerebellar ataxia 8 (SCA8) and myotonic dystrophy type 1 (DM1), both caused by expansions of a trinucleotide CTG•CAG repeat[108]. This repeat localizes in the overlapping *ATXN8OS* (where OS means opposite site) and *ATXN8* genes in SCA8, whereas in MD1 it is in the 3' UTR of the *DMPK* gene. Interestingly, Zu *et al*. observed that antisense CUG expansion transcripts in both genes were translated in AUG-dependent manner producing homopolymeric (RAN) proteins[108]. Subsequently, RAN translation has been reported in other several microsatellite repeat expansion disorders associated with neurodegeneration (**Figure 8**).

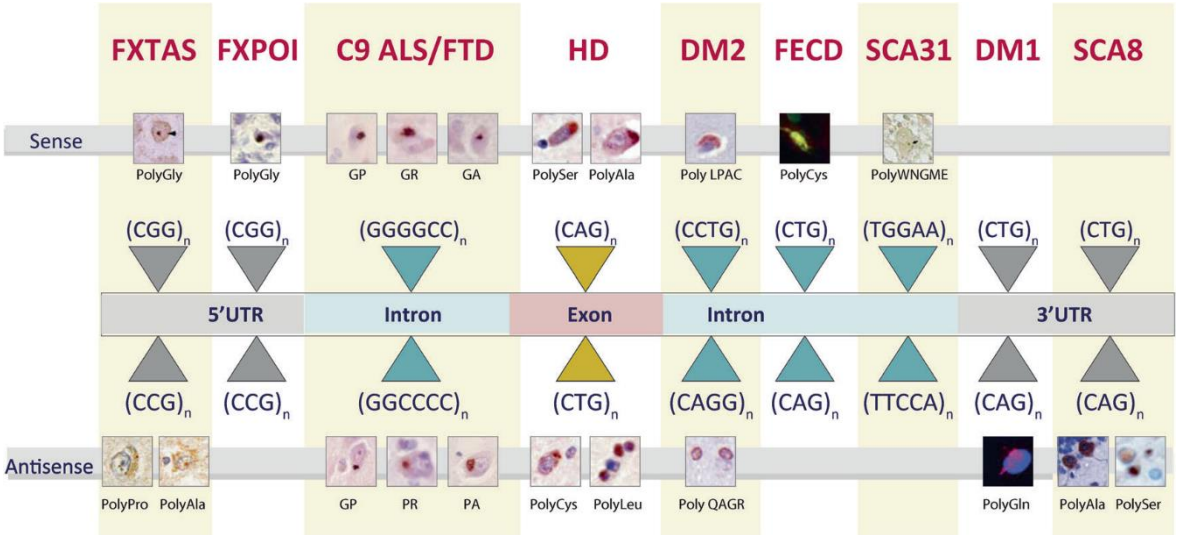


**Figure 8 |** RAN-positive diseases. Figure adapted from [109].

Although not much is known about how RAN translation occurs across the different types of repeat expansions, some common aspects have been identified. Since an AUG start codon lacks, both sense and antisense repeat-containing transcripts undergo RAN translation, resulting in the production of up to six RAN proteins as in C9ALS/FTD[42,67,68,70,72]. In the healthy population the repeat length generally does not exceed twenty repeats and becomes pathological above thirty up to thousands repeats depending on microsatellite motifs (tri-, tetra-, penta- or hexa- nucleotide). For example, 40-70 CAG repeats in a exon of *HTT* gene are required to cause HD[110], whereas hundreds to thousands of CTG[111] and GGGGCC[29,30] repeats in non-coding regions of *DMPK* and *C9ORF72* genes need to cause DM1 and C9ALS/FTD, respectively. Moreover, depending on the repeat localization inside the gene, the

repeat expansion can induce mechanisms of loss- (LOF) or gain-of-function (GOF). Indeed, the repeat expansion can localize in 5'UTR o 3'UTR regions, in an exon or in an intron[109]. Interestingly, Kearse *et al*.[112] studying RAN translation of CGG repeat in the fragile X (*FMR1*) gene demonstrated for the first time RAN translation requires a cap-dependent scanning mechanism of translation initiation.

## 3.3 RAN translation of GGGGCC and CCCCGG repeat expansions

As previously mentioned, both sense-(G4C2) and antisense-(C4G2) repeat-containing transcripts can undergo RAN translation producing five DPRs: poly-GA, poly-GP, poly-GR (from sense and antisense strands), poly-PA and poly-PR[42,67,68,70,72]. Since the discovery of RAN translation and its association with the G4C2 expansion in *C9ORF72*, there has been an intense activity to understand how this process works. Recent characteristics associated to RAN translation in *C9orf72* are set out below.

Two independently studies have been showed that RAN translation of G4C2 is cap-dependent[113,114] and requires all the components of the eIF4F complex (eIF4E[113,114], eIF4G[114] and eIF4A[113,114]). Moreover, these two studies and one more have demonstrated using different *ex vivo* models that RAN translation of G4C2 requires the presence of a near-cognate CUG start codon that is placed 24 nucleotides upstream of the repeat expansion in the first GA-reading frame[113–115]. Interestingly, this CUG codon is embedded in a perfect Kozak sequence[114]. Therefore, translation of poly-GA is thought to require the same pattern of the canonical one, while poly-GP and poly-GR could arise from the ribosome frameshift due to G-quadruplex structures[114] (**Figure 9**).

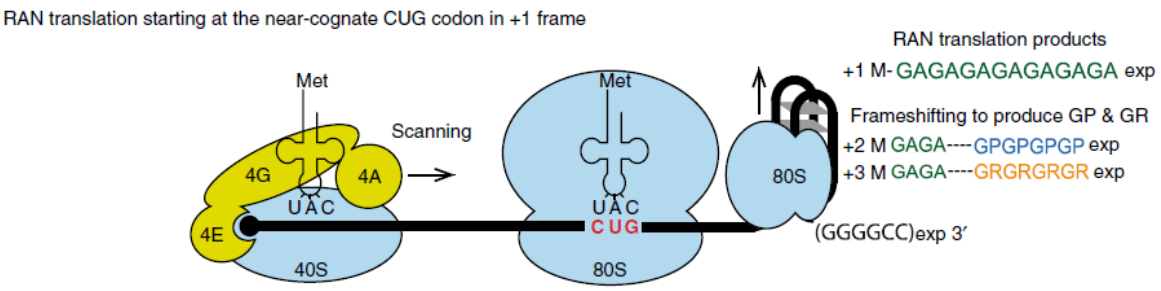


**Figure 9 |** Schematic representation illustrating how RAN translation occurs in presence of the near-cognate CUG codon in +1 frame to produce poly-GA and subsequently poly-GP (+2) and poly-GR (+3) by ribosome frameshift. Figure adapted from [114].

Noteworthy, Sonobe *et al*. demonstrated that RAN translation of poly-GA requires the non-traditional initiation factor eIF2A[115] that is required for the translation of some mRNAs during the activation of the integrated stress response (ISR) pathway. Indeed, some mRNAs such as ATF4, CHOP and BiP that are expressed under stress conditions are characterized by the presence of small upstream ORF (uORFs) in the 5' UTR region[116]. The uORF translation of these mRNAs is driven in AUG-independent way by eIF2A[116,117]. Moreover, Yamada *et al*. have recently identified another translation factor that is required by unconventional forms of translation. They identified the small ribosomal protein subunit 25 (RPS25) that as crucial factor required to an efficient RAN translation[118]. RPS25 is involved in IRES-translation of several viral[119] and cellular[120] RNAs by directly recruiting the 40S[119,120].

Although several studies have showed that RAN translation is cap-dependent, in contrast Cheng *et al*. showed that RAN translation of G4C2 is cap-independent[121]; therefore whether RAN translation is cap- dependent or independent is still under debate. It is most likely that these different results are due to the utilization of different constructs, however all these models might be right given that G4C2-containg RNAs can exist in different forms (G-quadruplex or hairpin structures)[14]. However, all these studies have shown that RAN translation can be enhanced and upregulated by eIF2α phosphorylation as a result of the activation of the integrated stress response (ISR) pathway[113–115,121,122] and other cellular stress stimuli (e.g. the increase of intracellular calcium and sodium ions)[122] (**Figure 10**). Moreover, the DPRs-mediated toxicity might in turn induce cellular stress further favouring RAN translation and thereby possibly creating a feed-forward loop[113,121].

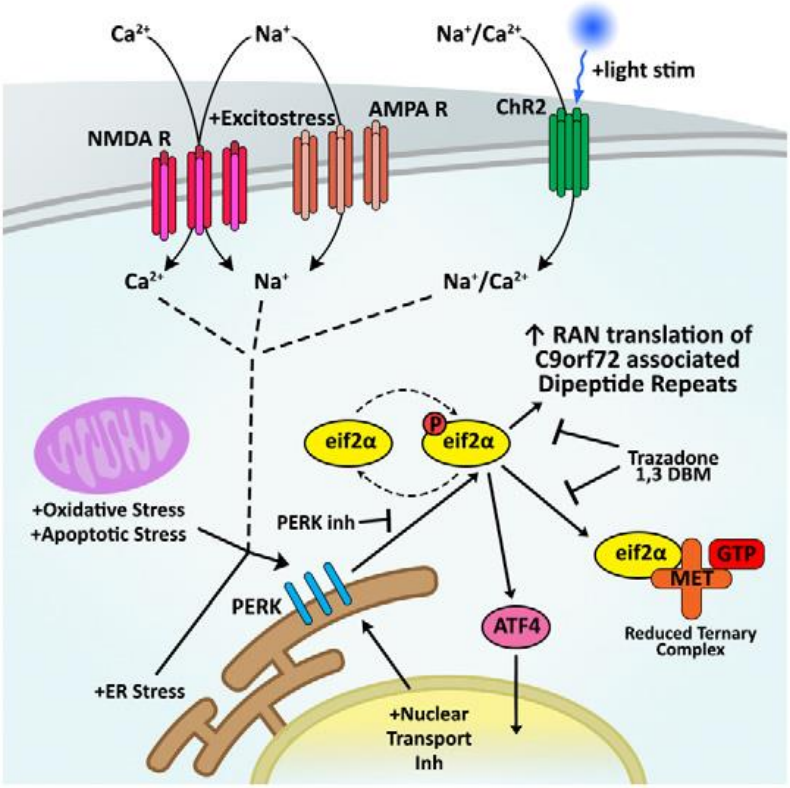


**Figure 10 |** Schematic illustration of all possible cellular stress stimuli that may contribute to induce RAN translation of G4C2 repeat expansion as a result of eIF2 α phosphorylation. Figure adapted from [122].

Noteworthy are other two studies of Goodman *et al*. in which they performed an unbiased RNAi-based screens in C9-*Drosophila* models[91,92]. In the first study, they identified the PAF1 complex as crucial modulator of G4C2-associated toxicity. PAF1 was found upregulated in C9-derived cells and in mice and flies expressing the repeat expansion[91]. In addition, they showed that downregulation of PAF1 complex led to a decrease of G4C2-associated toxicity[91]. In the second study, Goodman *et al*. used a different *Drosophila* model expressing a GFP lacking of its AUG start codon immediately downstream of G4C2x44 repeats and in frame with GR (+3)[92]. Among the translation factors screened, they further focused on eIF4B and eIF4H that are required to enhance the helicase activity of eIF4A[92,123]. Interestingly, these two accessory factors were reported to bind directly the G4C2-containg RNAs by their RNA recognition motif (RRM) domains[54,63,92,124], suggesting they are crucial for allowing the helicase activity of eIF4A on G4C2-containg RNAs[92].

Regarding the translation of the antisense G2C4 strands, it has been observed that GP and PR frames of the reverse strand contain possible AUG start codons[67].

The majority of studies, therefore, suggests that RAN translation may require some translation factors of the canonical translation[14].

# 4. **Mechanisms of protein clearance**

The main routes of protein clearance are the ubiquitin–proteasome and autophagy–lysosome systems. The ubiquitin-proteasome system (UPS) is the main route of degradation for proteins that have high turnover and for defective proteins[125], whereas autophagy of degradation for long-lived proteins, protein aggregates and damaged cellular organelles[126,127]. Dysfunction of one of these two pathways might contribute to increase the pathology of various neurodegenerative conditions[128].

## 4.1 The ubiquitin-proteasome system

The UPS is present in both nucleus and cytoplasm and plays a crucial role in protein turnover and protein quality control by degradation of nuclear and cytosolic old proteins and defective proteins[125]. The UPS is more efficient than the autophagy system; however, when the UPS is not manage to remove the abundance of defective proteins, the autophagy becomes more efficient than the UPS[128,129]. The UPS selectively degrades proteins that are ubiquitinated by post-translational modification. The ubiquitin binds to the target protein through a set of enzymatic reactions catalysed by three types of enzyme: E1 (ubiquitin-activating enzyme), E2 (ubiquitin-conjugating enzyme) and E3 (ubiquitin ligase)[128]. The ubiquitinated proteins then are recognized and degraded by the 26S proteasome[130] that consists of a catalytic core particle (20S) and of two terminal 19S regulatory particles[131,132] (**Figure 11**).

## 4.2 Autophagy

The autophagic system is the main route of degradation for long-lived proteins and of protein aggregates and damaged cellular organelles[126,127]. It is activated during nutrient starvation in order to maintain amino-acid pools[127]. The autophagy is mediated by a rearrangement of subcellular membranes that envelop cytosol or organelles and deliver them into lysosome, where the enveloped cargo is digested and recycled[133]. The autophagic process can be mainly divided into three steps: initiation, maturation, and degradation. The autophagosome formation requires the activity of several complexes mainly constituted by ATG proteins[134,135]. Among these ATG proteins, ATG8 (also known as LC3) plays a crucial role in forming autophagosome membrane. Since LC3 localizes on the surface of autophagosome

and remains bound to the membrane even after lysosome fusion, it is considered an autophagy marker indicating how many autophagosome are present[136,137] (**Figure 11**).

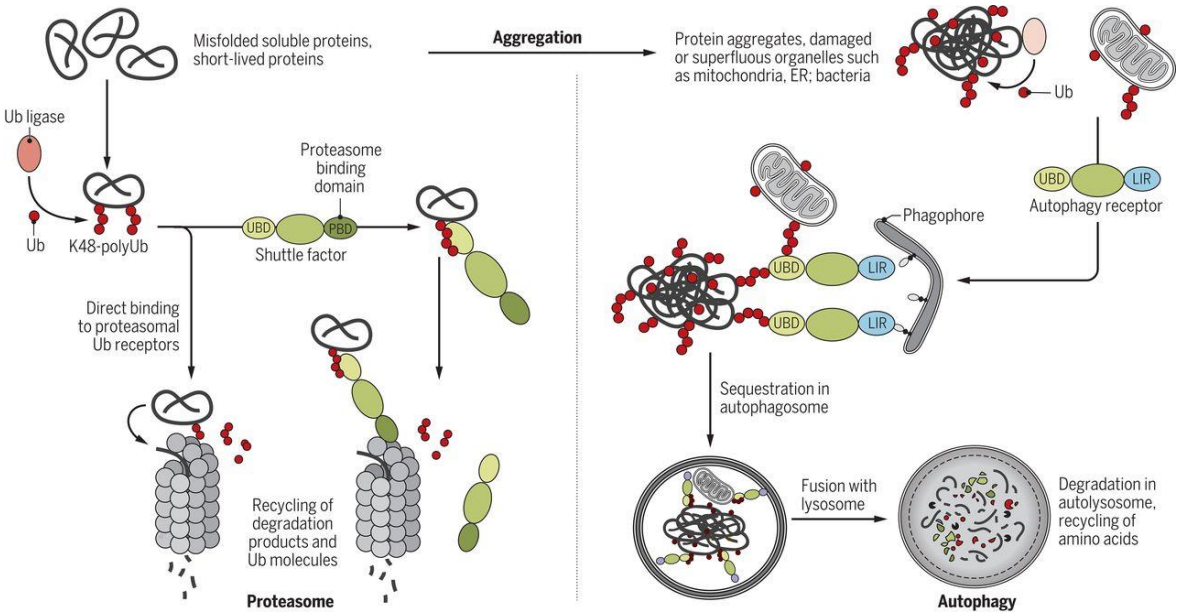


**Figure 11 |** Schematic representation of UPS and autophagy systems. Figure adapted from [138].

## 5. **The cAMP/PKA signalling pathway**

Adenosine 3'-5'-cyclic monophosphate (cAMP) is a second messenger involved in modulating several signal transduction pathways inside the cell. The enzymes adenylyl cyclase (AC) and phosphodiesterase (PDE) finely regulate the balance of intracellular cAMP level. The AC synthesizes cAMP from adenosine triphosphate (ATP). Paolo Sassone-Corsi in "The Cyclic AMP Pathway" illustrates simply and clearly how occurs the "PKA regulation"[139] (**Figure 12**). As showed in the figure "The PKA regulation"[139], the AC is activated following the activation of adenylate cyclase stimulatory G ($G_s$)-protein-coupled receptors by interaction with its α subunit, while conversely it is inhibited following the activation of adenylate cyclase inhibitory G ($G_i$)-protein-coupled receptors always by interaction with its α subunit[139]. The PDE is instead involving in degrading cAMP in adenosine monophosphate (AMP) and is regulated by different signalling pathways as for example by the calcium-signalling pathway[140,141]. The increase of intracellular cAMP level activates the protein kinase A (PKA) that in turn phosphorylates numerous substrates positively or negatively modulating their activity. PKA consists of two regulatory (R) subunits and two catalytic (C) subunits. When the cAMP level increases, two cAMP molecules bind to each R subunits allowing their dissociation and then the activation of the C subunits[142]. The C subunit activity can be inhibited by the interaction with protein kinase inhibitor (PKI) both at cytoplasmic and nuclear level[139]. Indeed, PKA can also enter into the nucleus and phosphorylates transcription factors as cAMP-response element-binding protein (CREB) allowing their interaction with transcription co-activators and then activating the transcription of genes containing cAMP-response elements (CREs)[143] (**Figure 12**).

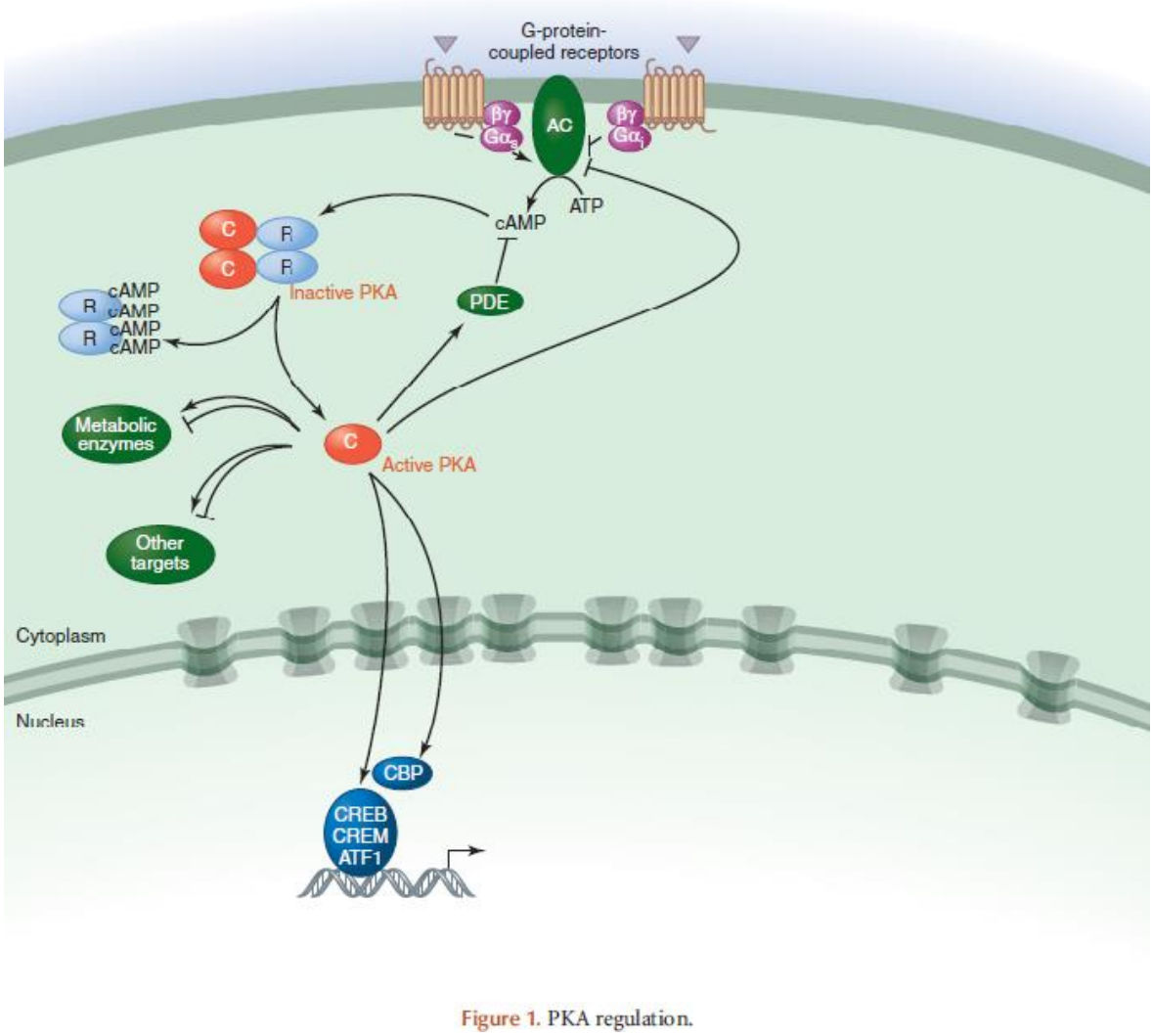


**Figure 12 |** The PKA regulation. Figure adapted from [139].

As previously said, PKA modulates several substrates that are involved in different signalling pathways as gene transcription, protein synthesis and cell growth and cell differentiation. In translation control, PKA modulates the translation elongation by phosphorylating the eEF2 kinase that is involved in regulating the eEF2 (see above). eEF2K is principally regulated by $Ca^{2+}$ and CaM (calmodulin)[144], but it can be also activated in a $Ca^{2+}$-independent way by PKA-dependent phosphorylation in serine 500 ($Ser^{500}$)[145,146] with consequence phosphorylation of eEF2[102] and then the slowdown of elongation rate.
Therefore, it is clear that a perturbation of the cAMP/PKA signalling pathway can have dangerous consequences into the cells and potentially cause various diseases[147].

Many drugs acting across the cAMP/PKA pathway have been developed. Some of them are used in research to better understand the functionality of this pathway, others are FDA-approved drugs used for the treatment of diseases. Forskolin and cholera toxin are cAMP-elevating compounds since they able to increase the intracellular level of cAMP by activating the AC[147]. The dibutyryl-cAMP is an cAMP analog that activates PKA without the activation of the AC[147]. PKA can be also activated indirectly by using PDE inhibitors that increase the level of cAMP by inhibiting its degradation to AMP[147]. Since PDEs are a superfamily consisting of 11 genes (PDE1 to PDE11)[148], several PDE inhibitors have been developed as rolipram that inhibits PDE4[149] and cilostazol that instead inhibits PDE3. Moreover, cilostazol is a FDA-approved drug used for the treatment of intermittent claudication in peripheral arterial disease[150]. Finally, H89[151,152] and KT 5720[152] inhibit PKA by competitive inhibition of the ATP site placed on the PKA-C subunit[152].

# *Results*

*Most of the results presented here are included in a manuscript submitted of which I am the first author and I personally contributed to write and prepare figures. Therefore, the discussion of results as well as the figures are the same of manuscript enriched by some further insights.*

# 1. **Development of a HTS assay for identifying modulators of *C9ORF72*-DPRs expression**

*This section presents some results, which I did not personally contributed, but they are included to allow understanding the rationale of this work.*
*I personally contributed in testing the efficiency of transfection in different cell lines and using different approach of transfection as well as in the following experiments.*

RAN translation of $(G4C2)_n$-containing RNAs is basally low if compared to the canonical translation due to the absence of an AUG start codon. Therefore, to set up an assay amenable for high-throughput screening (HTS), it had to find an appropriate construct to this purpose. Luciferase reporter was added downstream of (G4C2)x66 or x2 repeat-containing vectors (kindly provided by Dr. Leonard Petrucelli)[70] (**Figure 1a**) and their expression were tested in transiently transfected human neuroblastoma SH-SY5Y cells. However, both constructs showed a close-to-background signal that was not amenable for the HTS purpose (**Figure 1b**). Even if fluorescence is less sensitive of chemiluminescence, it gives the advantage to have pick up more parameters of analysis (i.e. cells number, number of cells transfected, and intensity of fluorescence). Therefore, two fluorescent reporter constructs were tested. The first one contains (G4C2)x58 upstream of GFP coding sequence (kindly provided by Prof Taylor)[153] (**Figure 1c**) that is in GP-reading frame. The AUG start codon between the repeat expansion and GFP was removed. The second one was generated starting from the first one cloning the AUG-RFP-STOP coding sequence upstream of the (G4C2)x58-GFP (**Figure 1c**). These plasmids were tested in transiently transfected SHSY-5Y cells. However, 24 h after transfection, any measurable level of polyGP-GFP was observed from the bicistronic vector, whereas polyGP-GFP signal from the monocistronic one was very weak (**Figure 1c**). Moreover, polyGP-GFP signal in stable SH-SY5Y cells was lost in few generations, possibly due to the toxicity of the DPR products. I also reasoned that SHSY-5Y cells may be not efficient in doing RAN translation, since RAN translation efficiently has been demonstrated to be cell type-dependent[122]. Therefore, I moved to human HEK293T cells. The initial choice to use SH-SY5Y cells was due especially to the fact that they are a human neuroblastoma cell line; however, HEK293T cells that are human embryonic kidney cell line with neuronal origin express several neuronal proteins and are easy to transfect than SH-SY5Y, then representing a good trade off. In HEK293T cells, I

observed an improvement of polyGP-GFP signal, but again not enough for HTS purpose. However, I managed to obtain a satisfactory rate of polyGP-GFP signal using a reverse transfection approach, i.e. by adding the transfection mixture into the well prior to seeding cells (**Figure 1d**). Therefore, using the reverse transfection approach, I set up the HTS assay by co-transfecting the (G4C2)x58-GFP and an AUG-RFP vector that was used as positive control for AUG-mediated translation. Cycloheximide (CHX) was used as positive control to check general translation arrest with respect to untreated cells (DMSO used as negative control). The variation in the number of GFP or RFP positive cells was used as read-out of the assay. In these conditions, the variability and the robustness of the assay were optimized to perform a HTS assuming CHX as positive control for cells expressing RFP (Z'-factor = 0.5)[154] (**Figure 1e**). I observed that CHX did not decrease the fluorescence intensity or the number of cells expressing polyGP-GFP (**Figure 1f**) as also reported by another group[155]. Kearse *et al*.[155] reported that RAN translation was not sensible to elongation inhibitors (such as CHX) more likely because the slowdown of ribosomes elongation can induce the queuing/stacking of the PICs thereby enhancing the recognition of near-cognate codons.

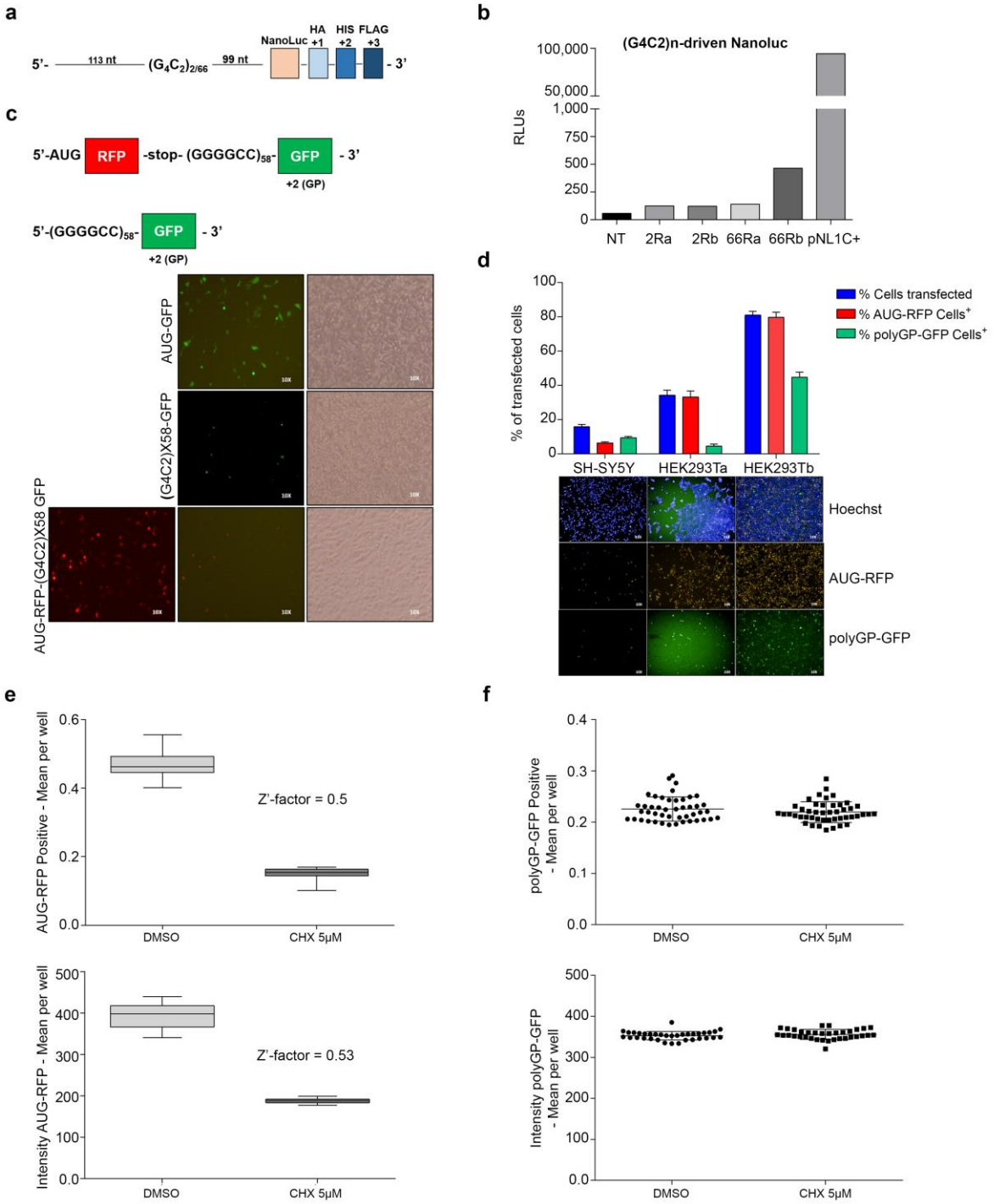
a
5'-
113 nt
$(G_4C_2)_{2/66}$
99 nt
NanoLuc
HA +1
HIS +2
FLAG +3
- 3'
b
(G4C2)n-driven Nanoluc
RLUs
100,000
50,000
1,000
750
500
250
0
NT
2Ra
2Rb
66Ra
66Rb
pNL1C+
c
5'-AUG
RFP
-stop- $(GGGGCC)_{58}$-
GFP
- 3'
+2 (GP)
5'-$(GGGGCC)_{58}$-
GFP
- 3'
+2 (GP)
AUG-GFP
(G4C2)X58-GFP
AUG-RFP-(G4C2)X58 GFP
d
% of transfected cells
% Cells transfected
% AUG-RFP Cells+
% polyGP-GFP Cells+
SH-SY5Y
HEK293Ta
HEK293Tb
Hoechst
AUG-RFP
polyGP-GFP
e
AUG-RFP Positive - Mean per well
Z'-factor = 0.5
DMSO
CHX 5μM
Intensity AUG-RFP - Mean per well
Z'-factor = 0.53
f
polyGP-GFP Positive - Mean per well
Intensity polyGP-GFP - Mean per well

**Figure 1 | Development of a HTS assay for identifying modulators of DPRs expression.**

**a** Schematic picture of the construct containing the luciferase sequence depleted for AUG and STOP codon cloned downstream of the native sequence of 99 nt. **b** Recombinant Nanoluc-containing vectors were obtained by sub-cloning the Nanoluc sequence from pNL1 plasmid into the pAG3-66R HA/His/FLAG tags-vector. Dr Vito G D'Agostino performed this experiment. **c** SH-SY5Y cells were transfected with AUG-GFP, (G4C2)x58-GFP and AUG-RFP-STOP-(G4C2)x58-GFP and images were acquired after 24 h. Dr Vito G D'Agostino performed this experiment. **d** SH-SY5Y and HEK293T cells were co-transfected with AUG-RFP and (G4C2)x58-GFP plasmids by standard or reverse transfection method. Images were acquired 24 h after using Operetta High-Content Imaging System and transfection efficiency was calculated on the ratio of cells expressing RFP/tot and cells expressing GFP/tot. **e** Distribution of cells expressing AUG-RFP (upper inset) or AUG-RFP fluorescence intensity (lower inset) in negative (DMSO) and positive (CHX) controls. Calculation of Z'-factors for the assay validation. **f** Distribution of cells expressing polyGP-GFP (upper inset) and polyGP-GFP fluorescence intensity (lower inset) in negative (DMSO) and positive (CHX) controls.
I performed experiments in (d, e and f).

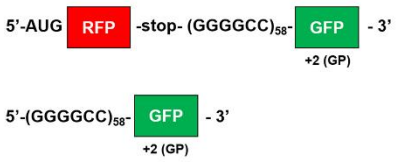


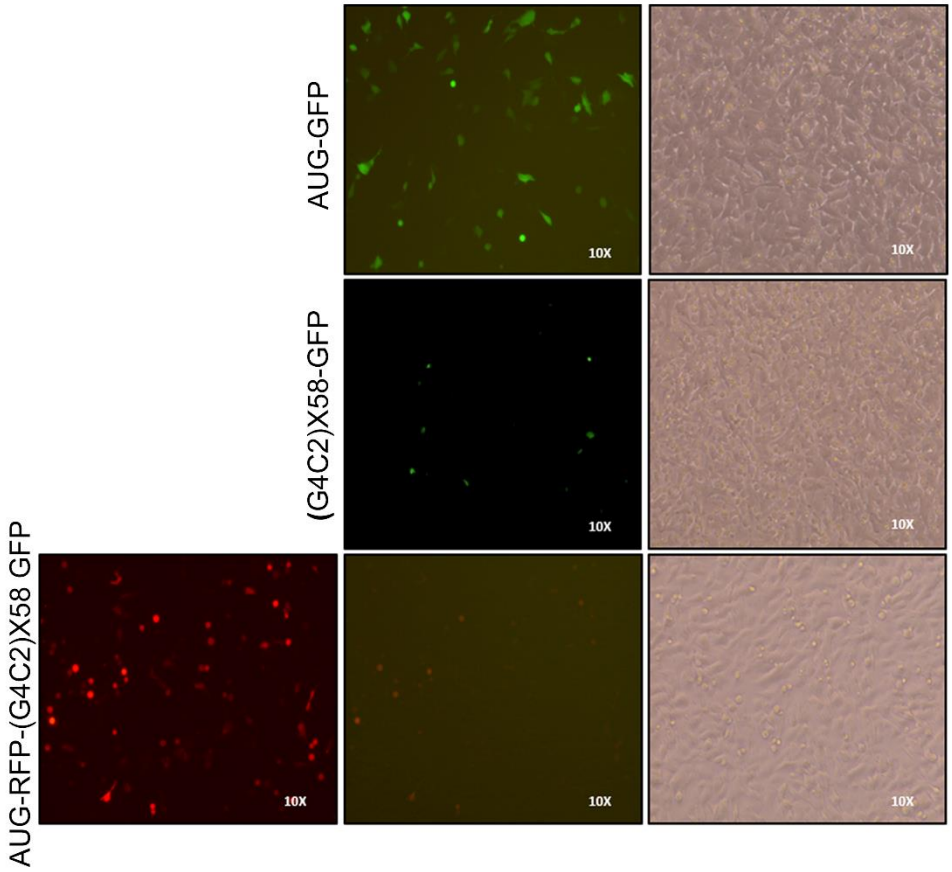


**Magnification of microscopy images in Figure 1c**

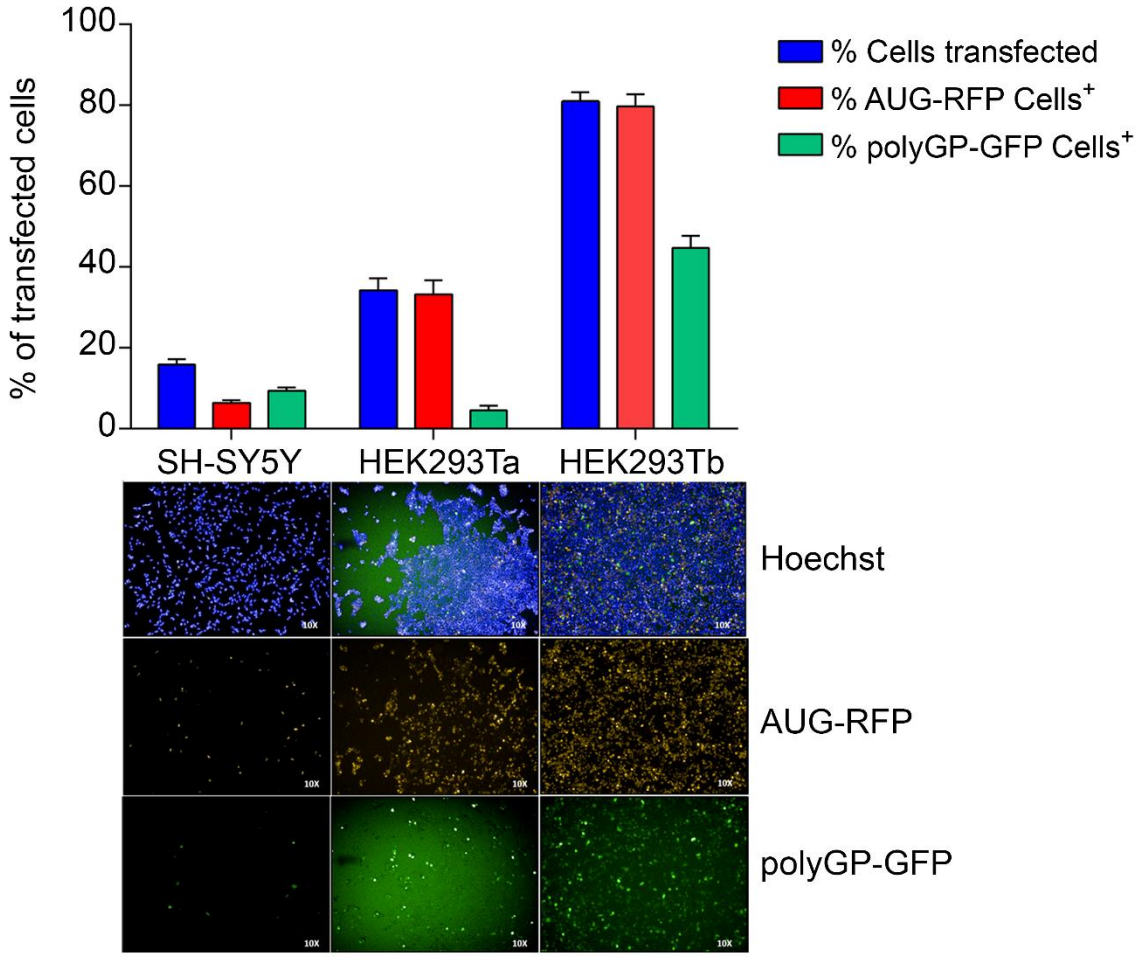


**Magnification of microscopy images in Figure 1d**

## 2. **High-throughput screening compounds and confirmatory screening for identifying modulators of *C9ORF72*-DPRs expression**

*I personally contributed in performing all the experiments. The HTS and confirmatory screening were performed with the support of the "HTS & Validation Core Facility".*

I performed the HTS assay by co-transfecting the (G4C2)x58-GFP and an AUG-RFP vectors (**Figure 2a**). I screened about 2,500 compounds with biological activity from different chemical libraries (see Material and Methods). Treatments were started 3 h after plasmids co-transfection, and GFP and RFP reporter signals were measured 36 h later. Plotting the Z-score of the number of cells expressing CAP-products (RFP, Y axis) *vs* the Z-score of the number of cells expressing DPR-products (polyGP-GFP, X axis), I obtained a graphical representation of the simultaneous effect of the small molecules either on the accumulation of canonical translation-dependent or on RAN translation-dependent products (**Figure 2b**). Effective small molecules were basically divided into four categories: positive CAP and RAN products modulators (C-I), negative DPR products modulators and positive CAP products modulators (C-II), negative CAP and DPR products modulators (C-III), positive DPR products modulators and negative CAP products modulators (C-IV) (**Figure 2b**). The majority of tested compounds did not modify the expression level of the two fluorescent reporters, indirectly proving the quality of assay. I gated effective molecules by excluding the central cloud of non-effective compounds, using an arbitrary threshold of cells expressing polyGP-GFP ±1.5 and ±1 for AUG-derived positive cells. The highly toxic compounds were excluded using the threshold Z-score nuclei ≤-2, indicating that the number of surviving cells accounted for less than 50%.

A confirmatory screening was performed as above, but further increasing the number of replicates from one to four. As expected, only few compounds were able to reduce significantly RAN products, while many showed an opposite effect (**Figure 2c**). This comes as no surprise, because the majority of the RAN-increasing compounds were blockers of the degradative pathways (e.g. Thapsigargin, Tunicamycin or MG132). I selected five hit compounds according to their ability of specifically decrease/increase the number of cells expressing polyGP-GFP and/or the fluorescence intensity of GFP (**Table 1**). These five compounds were: Spironolactone (SPL), an aldosterone antagonist; Geldanamycin (GELD), an inhibitor of Heat Shock Protein 90 (HSP90); Forskolin (FSK), a cAMP-elevating compound which acts as a direct stimulator of the Adenylyl Cyclase (AC) enzyme, and I also

included two phytochemicals, Erysolin (ERY) and Helenin (HLN), with undefined mechanism of action.

Interestingly, FSK, by activating AC and enhancing intracellular cAMP levels, triggers a multitude of PKA-dependent and/or –independent pathways resulting in pleiotropic effects into the cells. These events include the activation of many intracellular signalling cascades and of the cAMP Response Elements Binding (CREB) family of transcription factors that, upon phosphorylation, regulates the expression level of genes containing CREs in their promoters [156–158].

I then performed dose-response experiments by treating cells with two concentration ranges of the selected compounds (**Figures 2d** and **2e**), checking their toxicity and the effects on DPRS expression. All the compounds confirmed their activity to modulate the number of polyGP-GFP positive cells, although to various extent. The most potent one was FSK that selectively increased polyGP-GFP positive cells compared to AUG-RFP positive cells. HLN decreased both products, while ERY, GELD and SPL decreased more efficiently the polyGP-GFP products than the AUG-RFP. All these compounds were moderately toxic at concentrations higher than 40 μM, being HLN the most toxic one. Therefore, I excluded HLN due to its toxicity and prosecuted with SPL, GELD, ERY and FSK to gain information about their molecular mechanism of action.

Collectively, the screening identified modulators of polyGP-GFP expression level. However, the phenotypic approach used for HTS did not give me information about the mechanism of action of these compounds in modulating the polyGP-GFP expression level. Therefore, I subsequently investigated the mechanism of action of each compound.

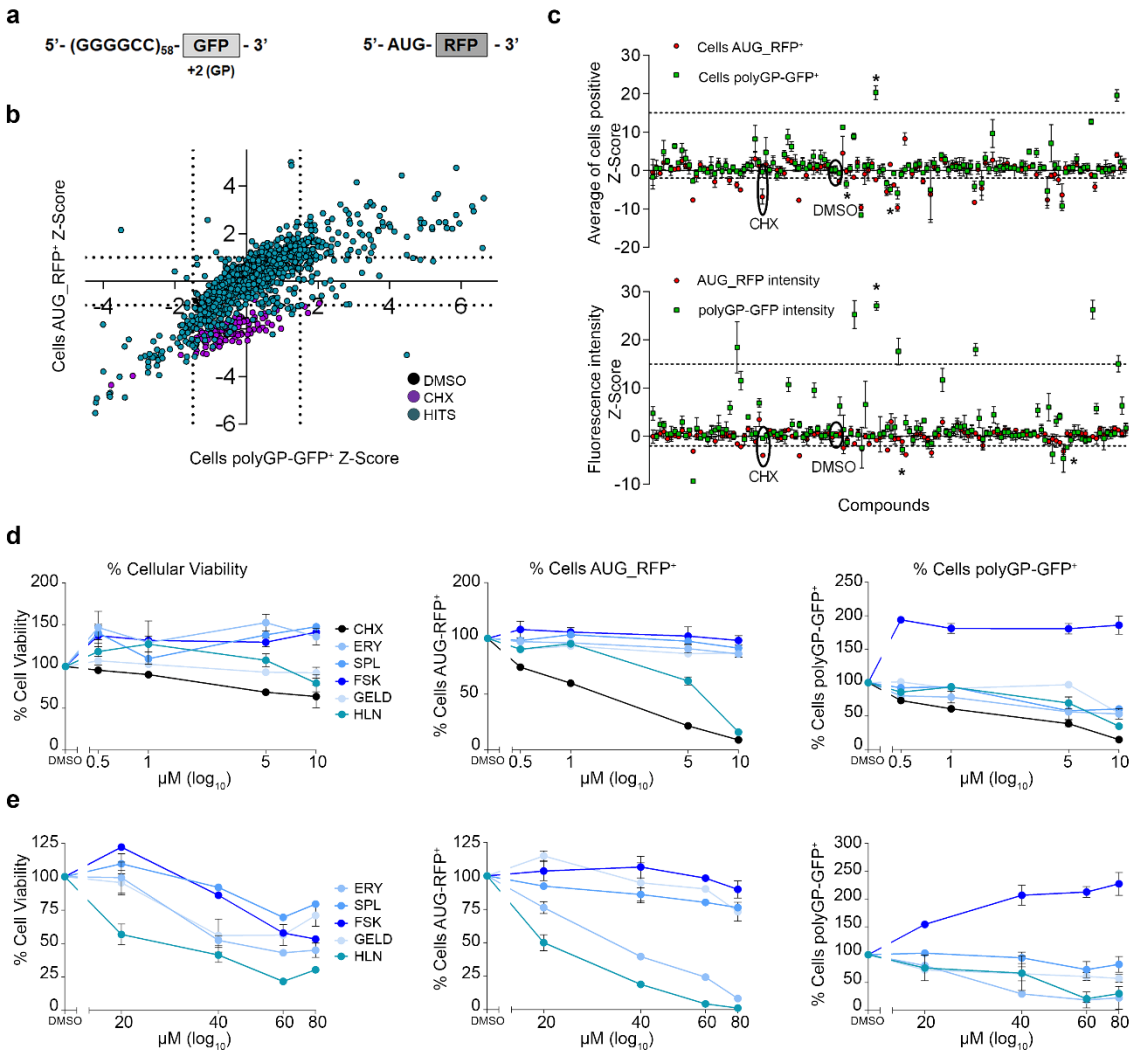


**Figure 2 | High-throughput screening compounds and confirmatory screening for identifying modulators of *C9ORF72*-DPRs expression.**

**a** Schematic representation of the constructs utilized for the screening. The first construct contains 58 $G_4C_2$ repeats upstream of the GFP, whose AUG was deleted. GFP sequence is in the +2 frame (polyGP-GFP). The second construct contains RFP, whose translation is under the AUG start codon. **b** Primary screening. Scatter plot shows distribution of 2,500 compounds. Y axis represents cells expressing AUG-RFP, while X axis the ones expressing polyGP-GFP. DMSO (black dots) and CHX 5 μM (purple dots) were used as negative and positive control, respectively. After the addition of transfection mix, HEK293T cells were seeded and incubated at 37°C for 3 h to allow their adhesion to the bottom of the well. Cells then were treated with drugs (5 μM). Images and data acquisition were collected after 36 h of treatment. Grid lines represent the threshold set up around DMSO to select effective compounds for the counter-screening and eliminate the ones without any effect. I performed HTS with the support of the HTS & Validation Core Facility (Dr Valentina Adami and Dr Micheal Pancher). **c** Confirmatory screening. Schematic distributions of cells expressing polyGP-GFP and AUG-RFP (upper inset) and the fluorescence intensity of polyGP-GFP and AUG-RFP relative to each compound (lower inset). (*) represent small molecules selected. I performed confirmatory screening with the support of the HTS & Validation Core Facility (Dr Valentina Adami and Dr Micheal Pancher). **d** and **e** Dose-response analysis of selected compounds: ERY, SPL, GELD, FSK and HLN. Cells were co-transfected with AUG-RFP and polyGP-GFP plasmids and treated with two concentration ranges 0.5, 1, 5 and 10 μM (d) and 20, 40 and 60 μM (e) for 24 h. Data are mean ± SEM from three biological replicates.

**Table 1 | List and Z-score values of hits selected by confirmatory screening**

| Hit | Cells polyGP-GFP$^{+}$ | Cells AUG-RFP$^{+}$ | polyGP-GFP Fluorescence | AUG-RFP Fluorescence | Cell Viability |
|---|---|---|---|---|---|
| **Erysolin** | -3.5 | -0.2 | -1.34 | -0.7 | -1.1 |
| **Forskolin** | 20.3 | -2.4 | 27 | -0.8 | 0.05 |
| **Geldanamycin** | -5 | 1.6 | 0.002 | 3 | -2.6 |
| **Helenin** | -1.05 | -0.7 | -2.8 | -1.1 | -1.3 |
| **Spironolactone** | -0.5 | 0.7 | -2.3 | 0.6 | -0.9 |

# 3. **Characterization of selected small molecules in different cell lines**

*This section presents some results, which I did not personally contributed. Specifically, I was not involved in all the experiments conducted in NSC34 and in SHSY-5Y cells that were performed by my collaborators from the University of Milano.*

Firstly, I investigated whether the four selected DPR modulators (**Figure 3a**) affected general transcription and translation. To this purpose, I used the incorporation of the modified nucleoside 5-ethynyl uridine (EU) to evaluate general RNA transcription and of the O-propargyl-puromycin (OPP) to evaluate *de-novo* protein synthesis. GELD marginally induced general transcription (**Figure 3b**), but none of the compounds had an effect on translation (**Figure 3c**).

The molecular mechanism of RAN translation initiation is still matter of debate and a near-cognate CUG start codon within the first intron has been suggested to play a key the role in *C9ORF72* gene RAN translation[114]. The CUG codon embedded in a perfect Kozak sequence is placed 24 nucleotides upstream of the repeat expansion in the GA-reading frame[113–115].

Therefore, to evaluate whether the effect of these compounds was CUG independent, I used the construct containing 66 G4C2 repeats and including 113 nt of 5′, with then the near-cognate CUG start codon, and 99 nt of 3′ flanking sequence[70,114]. Moreover, this construct offers the possibility to detect all the three sense-reading frames that are tagged each one with a specific tag. However, the FLAG-tagged GR-reading frame was not visible probably due to low RAN translation efficiency at the third sense-reading frame.

Immunoblot analysis in HEK293T cells showed that GELD and SPL reduced, while FSK increased the accumulation of poly-GA (HA-tagged) also in the presence of the upstream CUG codon (**Figures 3d** and **3e**). As previously said, RAN translation efficiency is cell type-dependent, therefore basal expression of DPR products can be higher in some cell lines than in others[122]. Since HEK293T has high basal expression of DPRs production, in collaboration with the laboratory of Prof Poletti (University of Milano), compounds were also tested in immortalized mouse motor neuronal cell line, NSC34. Using NSC34 cells, the efficacy of compounds was tested by checking the poly-GP expression via both immunoblot analysis and filter retardation assay (FRA). FRA is a technique that allows quantifying the PBS-insoluble species by the proteins or protein aggregates retention on acetate cellulose membrane with pore size of 0.22 µm by vacuum application. GELD and SPL significantly reduced both the soluble levels and the PBS-insoluble species of poly-GP in NSC34 cells

and FSK significantly increased the soluble levels and the PBS-insoluble species of poly-GP (**Figures 3f**, **3g** and **3h**). In contrast, ERY did not show any effect in modulating both total soluble and PBS insoluble species of poly-GP (**Figures 3f**, **3g** and **3h**).

I then assessed whether the modulation of DPRs expression was dependent on different amount of *G4C2* mRNA. To this purpose, RT-qPCR data were normalized for transfected plasmid (Ct of ampicillin) using the following formula:

$2^{-\Delta\Delta Ct}$, where $\Delta\Delta Ct$ is $(Ct_{G4C2}/Ct_{Amp}) - Ct_{GAPDH}$

The modulation of DPR expression was not dependent on different amount of *G4C2* mRNA and did not show significant differences due to the various treatments (**Figures 3i** and **3j**).

Once excluded the involvement of compounds in modulating the transcription of G4C2, among the possible post-transcriptional/post-translational mechanisms underlying modulatory effect of the selected small molecules, I started investigating their activity on DPRs clearance.

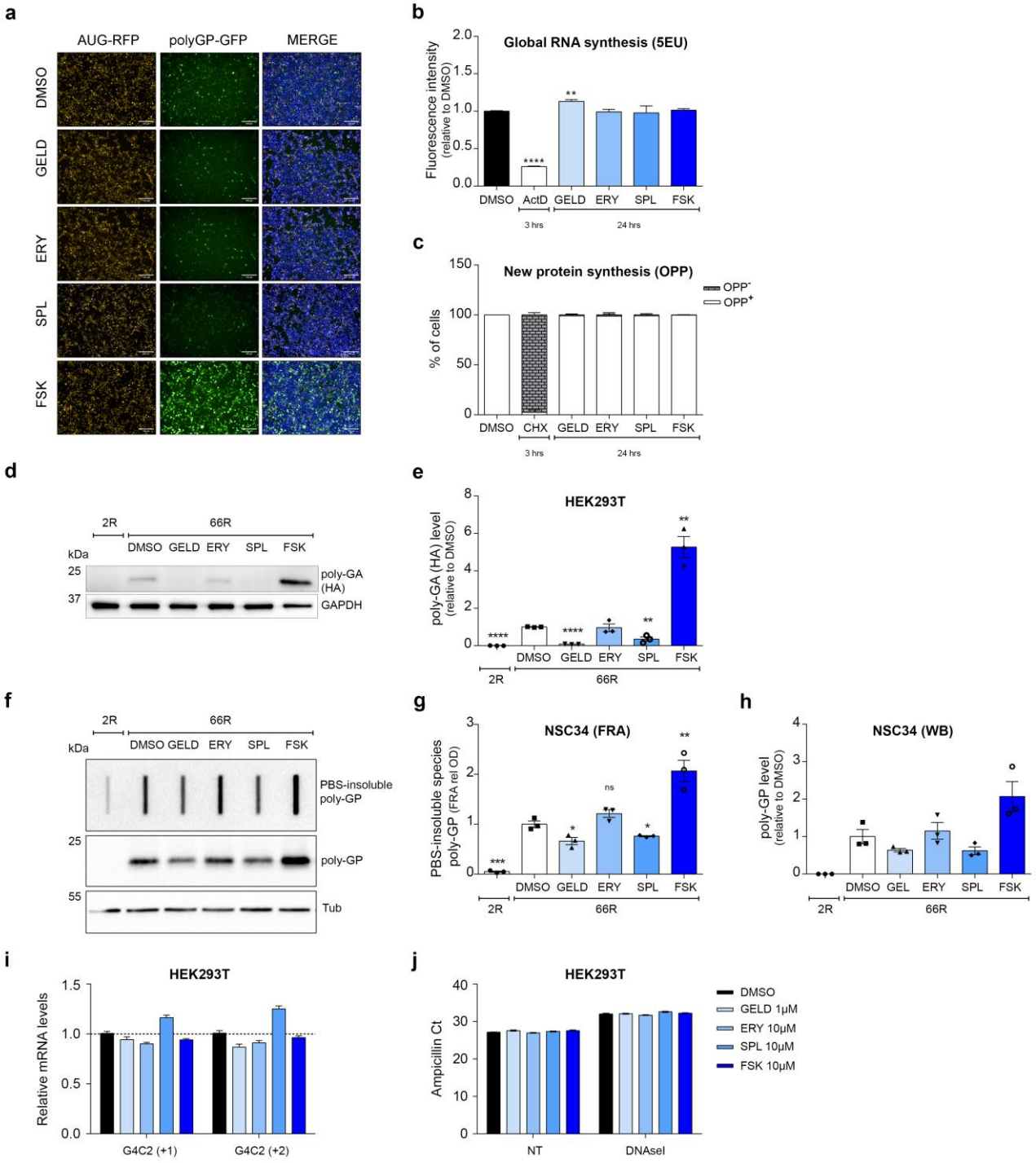
a
AUG-RFP
polyGP-GFP
MERGE
DMSO
GELD
ERY
SPL
FSK
b
Global RNA synthesis (5EU)
Fluorescence intensity (relative to DMSO)
DMSO ActD GELD ERY SPL FSK
3 hrs
24 hrs
c
New protein synthesis (OPP)
% of cells
OPP-
OPP+
DMSO CHX GELD ERY SPL FSK
3 hrs
24 hrs
d
2R
66R
kDa
DMSO GELD ERY SPL FSK
25
poly-GA (HA)
37
GAPDH
e
HEK293T
poly-GA (HA) level (relative to DMSO)
DMSO GELD ERY SPL FSK
2R
66R
f
2R
66R
kDa
DMSO GELD ERY SPL FSK
PBS-insoluble poly-GP
25
poly-GP
55
Tub
g
NSC34 (FRA)
PBS-insoluble species poly-GP (FRA rel OD)
ns
DMSO GELD ERY SPL FSK
2R
66R
h
NSC34 (WB)
poly-GP level (relative to DMSO)
DMSO GEL ERY SPL FSK
2R
66R
i
HEK293T
Relative mRNA levels
G4C2 (+1)
G4C2 (+2)
j
HEK293T
Ampicillin Ct
DMSO
GELD 1μM
ERY 10μM
SPL 10μM
FSK 10μM
NT
DNAseI

**Figure 3 | Effects of hits in different cell lines.**

**a** Images of the HTS representing the effect of the selected small molecules. Scale bar,100 µm**. b** HEK293T cells were treated for 24 h, then general RNA synthesis was monitored using the Click-it chemistry by the incorporation of the nucleoside analogue 5-ethynyl uridine (EU). Actinomycin D 5 µM was used as positive control to block RNA synthesis. Two-tailed, unpaired t-test; ****P*<0.001, ***P* 0.0047). **c** Global protein synthesis was monitored as above by the incorporation of the O-propargyl-puromycin (OPP). CHX 350 µM for 3 h was used as positive control to check general translation arrest. **d** Lysates from HEK293T cells, transfected with 2R or 66R and treated with selected compounds for 24 h, immunoblotted using antibodies for poly-GA expression (HA tagged). **e** Quantification of **d** from three biological replicates. Data are mean ± SEM. Two-tailed, unpaired t-test; *****P*<0.0001, ****P*<0.001, ***P* 0.0052 for SPL *versus* DMSO, ***P* 0.0016 for FSK *versus* DMSO). **f** Lysates from NSC34 cells, transfected with 2R or 66R and treated with selected compounds for 24 h, immunoblotted for insoluble (upper inset) and total soluble (lower inset) poly-GP expression. These experiments were performed by Dr Riccardo Cristofani from the laboratory headed by Prof Angelo Poletti (University of Milano) **g** Quantification of insoluble poly-GP in **f** from three biological replicates. Data are mean ± SEM. Two-tailed, unpaired t-test; ****P*<0.001, ***P* 0.0087,**P* 0.0256 for GELD *versus* DMSO, **P* 0.0229 for SPL *versus* DMSO. **h** Quantification of total soluble poly-GP in **f** from three biological replicates. Data are mean ± SEM. No significant results using two-tailed, unpaired t-test. 1-way ANOVA followed by Uncorrected Fisher's LSD, *P*** 0.0034 for FSK *versus* DMSO. **i** Relative expression level of *G4C2 (+1)* and *(+2)* mRNAs in HEK293T cells treated for 24 h. Data are mean ± SEM from three biological replicates. **j** Cycle threshold (Ct) values of Ampicillin antibiotic-resistance gene of 66R plasmid in samples treated ± with DNaseI. Ct values of Ampicillin were used to check and normalize differences in transfection efficiency for each condition. Data are mean ± SEM from three biological replicates.
I performed experiments in (a, b, c, d, e, i and j): Dr Riccardo Cristofani from the laboratory headed by Prof Angelo Poletti (University of Milano) performed experiments in (f, g and h).

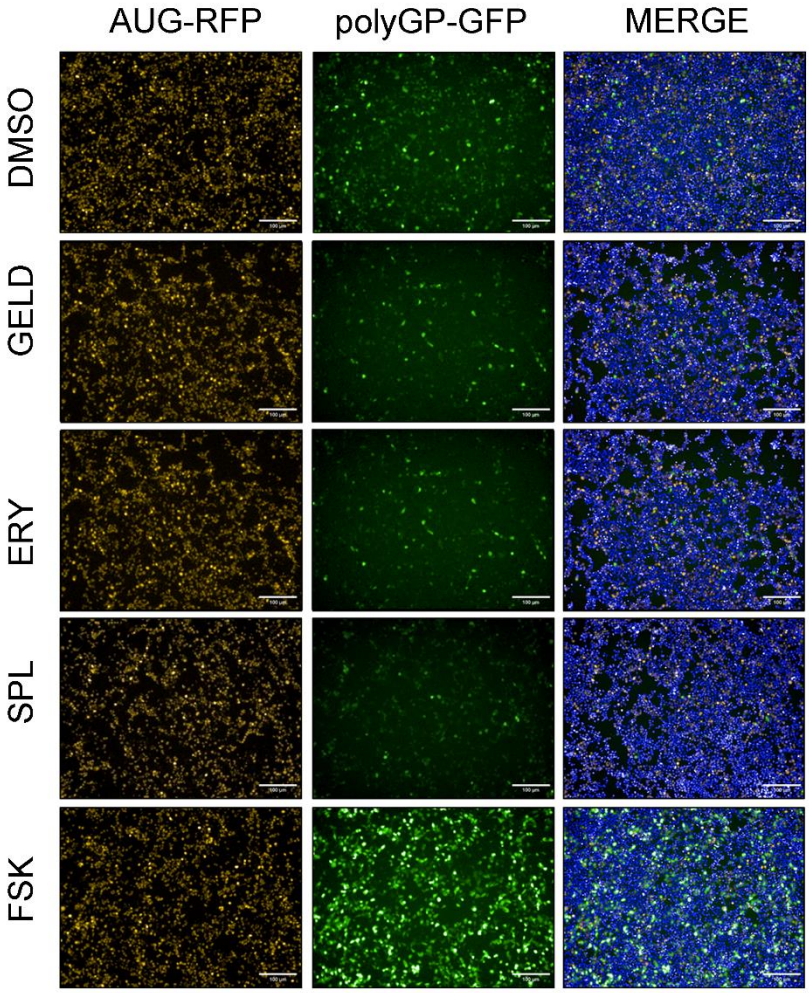


**Magnification of microscopy images in Figure 3a.**

## 4. None of the compounds acts on inducing the autophagy system

*This section presents experiments all performed by my collaborators from the University of Milano, but they are included to allow understanding the rationale of this work and are included in the manuscript.*

With the collaboration of the University of Milano, I then evaluated whether these small molecules could modulate DPR level by enhancing their clearance through autophagy and/or ubiquitin proteasome system (UPS). DPRs mainly rely upon autophagy for their degradation, while, in basal condition, only poly-GP is degraded by the UPS[84,93,159]. However, dysfunctions in protein quality control machinery have been largely demonstrated in ALS, C9ALS/FTD as well as in other neurodegenerative disorders[84,160–162]. Therefore, the expression level of autophagy markers (p62/SQSTM1, LC3, HSPB8, BAG3) was evaluated using as positive control the natural compound trehalose that promotes autophagy via the activation of TFEB[163]. None of the compounds induced neither the protein expression (**Figures 4a** and **4b**) nor the transcripts level of autophagy markers in NSC34 (**Figure 4c**) or in SH-SY5Y (**Figure 4d**) cells. Immunofluorescence analysis also showed that p62/SQSTM1 and LC3 intracellular distribution were not modified by the treatment with the various compounds in NSC34 cells (**Figures 4e** and **4f**). These data ruled out a role of autophagy in the mechanism of action of the hits.

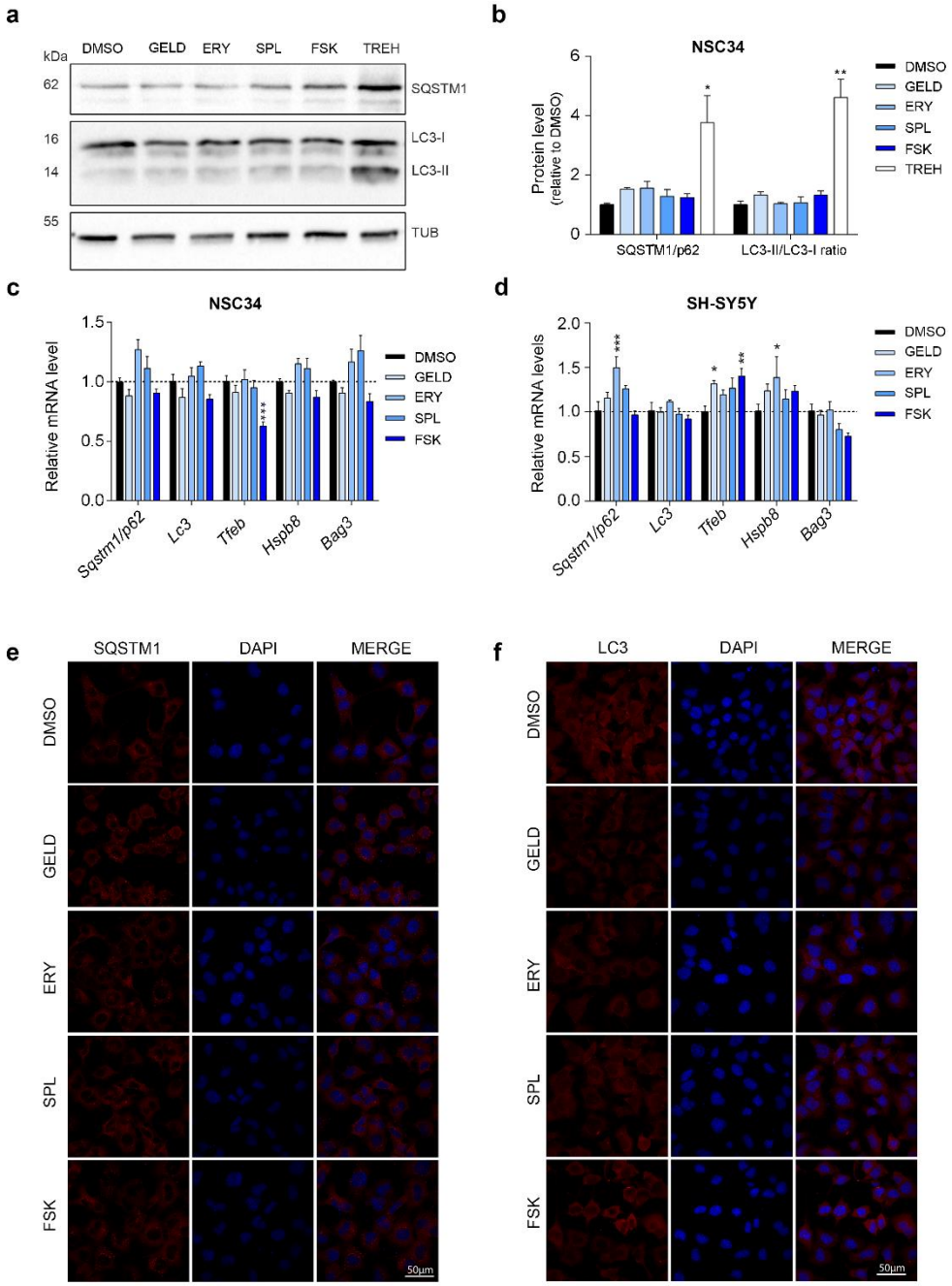
a
kDa
DMSO
GELD
ERY
SPL
FSK
TREH
62
SQSTM1
16
LC3-I
14
LC3-II
55
TUB
b
NSC34
Protein level
(relative to DMSO)
SQSTM1/p62
LC3-II/LC3-I ratio
DMSO
GELD
ERY
SPL
FSK
TREH
c
NSC34
Relative mRNA level
Sqstm1/p62
Lc3
Tfeb
Hspb8
Bag3
d
SH-SY5Y
Relative mRNA levels
e
SQSTM1
DAPI
MERGE
f
LC3
50µm

**Figure 4 | None of the compounds acts on inducing the autophagy system.**

**a** Lysates from NSC34 cells treated for 24 h and immunoblotted for SQSTM1/p62 and LC3 expression. **b** Quantification of (a) from three biological replicates. Data are mean ± SEM. Two-tailed, unpaired t-test, ***P* 0.0047, **P* 0.0393. **c** Relative expression level of *Sqstm1/p62*, *Lc3*, *Tfeb*, *Hspb8* and *Bag3* mRNAs in NSC34 cells treated for 24 h. Data are mean ± SEM from three biological replicates. 2-way ANOVA followed by Dunnett's multiple comparisons test, **P*>0.05. **d** Relative expression level of *Sqstm1/p62*, *Lc3*, *Tfeb*, *Hspb8* and *Bag3* mRNAs in SH-SY5Y cells treated for 24 h. Data are mean ± SEM from three biological replicates. 2-way ANOVA followed by Dunnett's multiple comparisons test, *Sqstm1/p62* ***P* 0.0006; *Tfeb* **P* 0.0442 DMSO *versus* GELD, ***P* 0.006 DMSO *versus* FSK; *Hspb8* ***P* 0.0098 DMSO *versus* ERY. **e** and **f** Immunufluorescence analysis of NSC34 cells treated with DMSO or compounds for 24 h. In (e) SQSTM1 (red). Nuclei were stained with DAPI (blue). Scale bars 50 µm.

All the experients were perfomed by Dr Riccardo Cristofani from the laboratory headed by Prof Angelo Poletti (University of Milano).

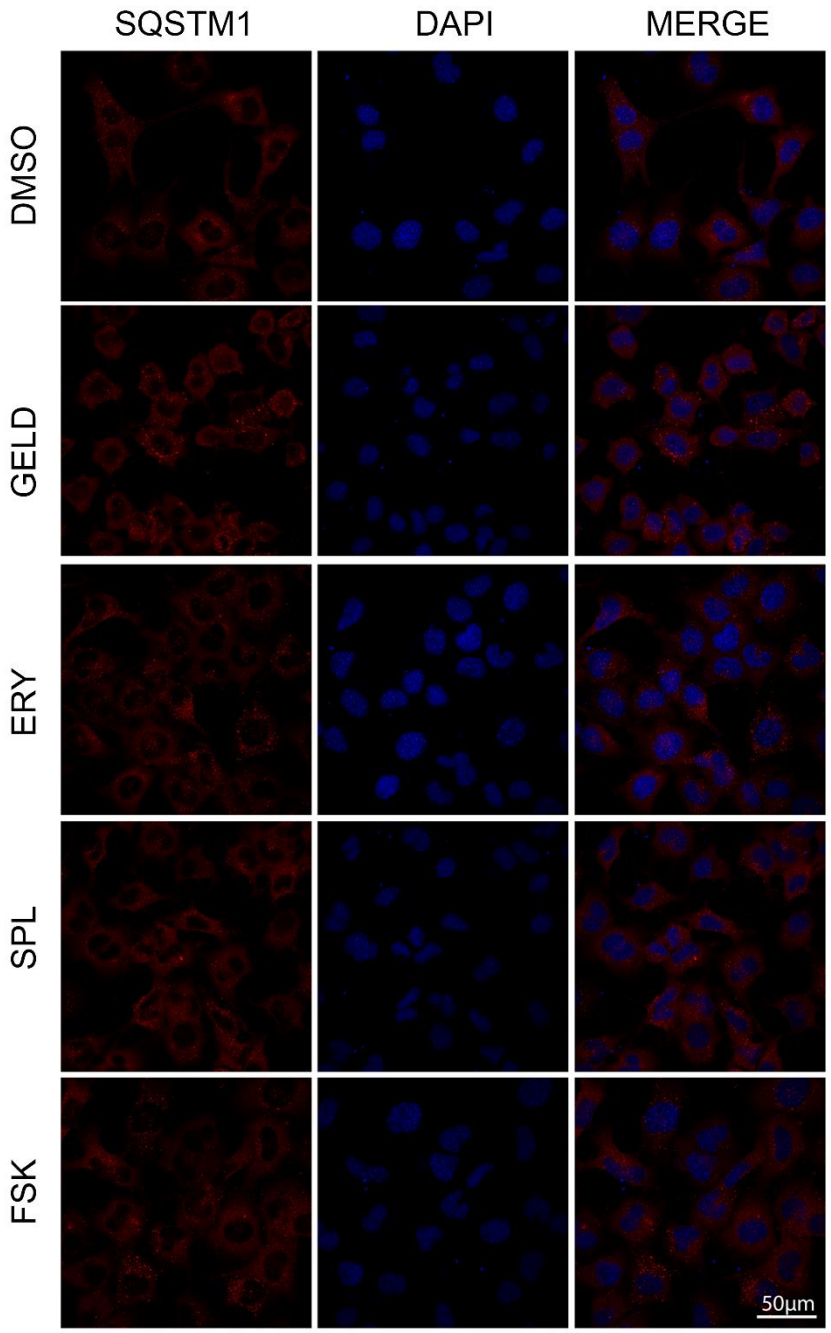


**Magnification of microscopy images in Figure 4e.**

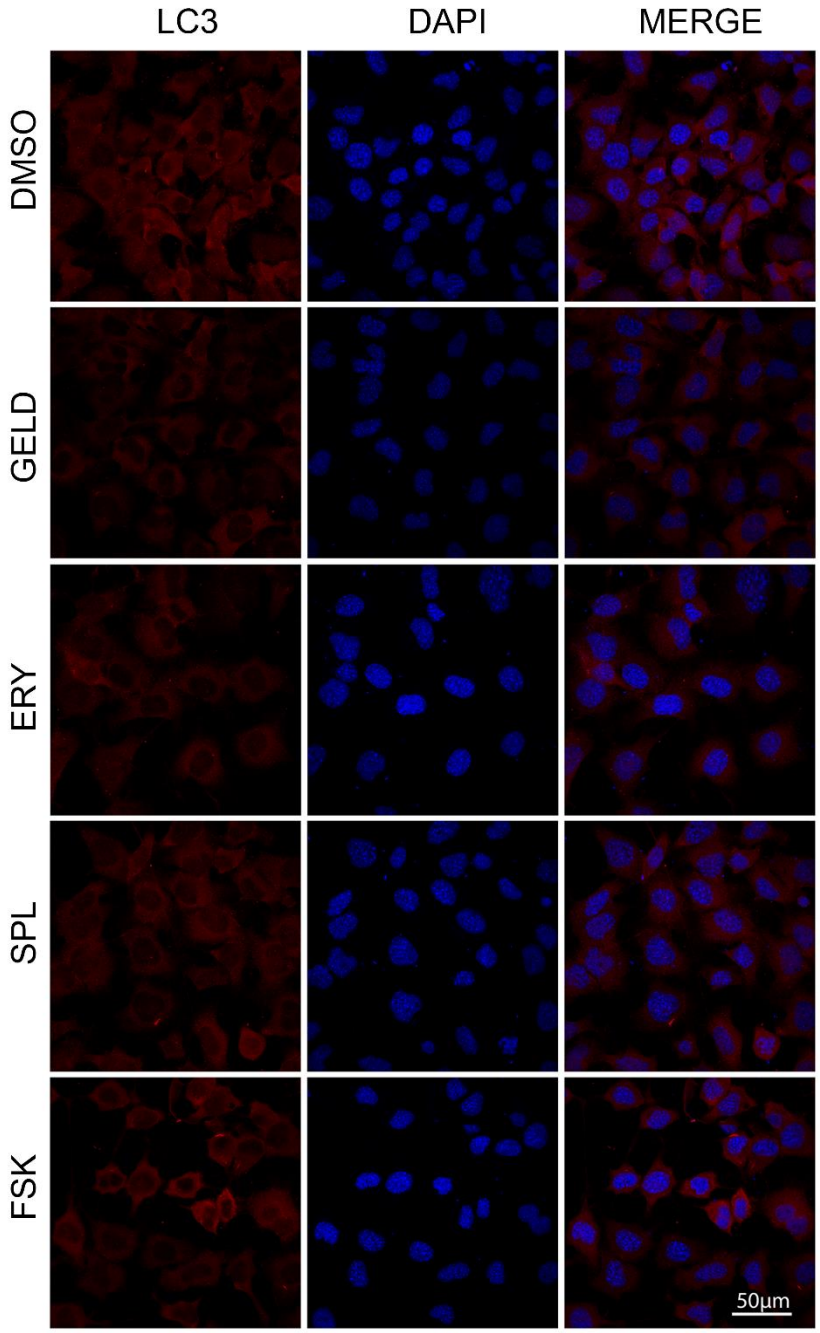


**Magnification of microscopy images in Figure 4f.**

# 5. **GELD and SPL enhance the activity of ubiquitin-proteasome system**

*This section presents experiments all performed by my collaborators from the University of Milano, but they are included to allow understanding the rationale of this work as well as are included in the manuscript.*

Since none of the compounds activated the autophagy pathway, the involvement of ubiquitin-proteasome system was assessed. Firstly, the activity of proteasome was tested by transfecting cells with a GFP construct tagged with a short degron (CL1) (GFPu) (**Figure 5a**) that directs the reporter protein to the proteasome for its degradation[159,164]; thus, the UPS impairment correlates with GFPu accumulation. GELD and SPL increased the functionality of the UPS to degrade the reporter GFPu, while ERY did not, and FSK led to a marked GFPu accumulation into both NSC34 (**Figure 5b**) and SH-SY5Y (**Figure 5c**) cells. Collectively, these data suggest that GELD and SPL enhance the function of the UPS pathway, without interfering with the autophagy machinery. However, these results do not show whether the decreased level of DPRs observed with GELD and SPL is due to the degradation by UPS. Therefore, to answer to this question, cells were co-treated with the proteasome inhibitor MG132. In particular, in this experiment cells were transfected using a new construct expressing poly-GP. Specifically, in this construct the expression of poly-GP is AUG-dependent, therefore G4C2 repeats are replaced with degenerate codons [84,93,159]. The co-treatment GELD and MG132 showed an increase of the total soluble and PBS-insoluble species of poly-GP (**Figure 5d** and **5e**) then confirming that the reduction of DPRs by GELD is, most likely elicited by enhancing the activity of the UPS. Moreover, as the translation of poly-GP is AUG-dependent and arise from degenerate codons, these results further confirm that the effect of GELD is not RAN-dependent.

Surprisingly, the co-treatment SPL and MG132 did not show any increase of AUG-polyGP total or PBS-insoluble (**Figure 5d** and **5e**), suggesting that SPL acted on DPRs expression level through different ways. Anyway, SPL alone reduced the level of AUG-polyGP (**Figure 5d** and **5e**), suggesting that as GELD, the effect of SPL might be RAN-independent. However, I cannot exclude further mechanisms of action of SPL, at present.

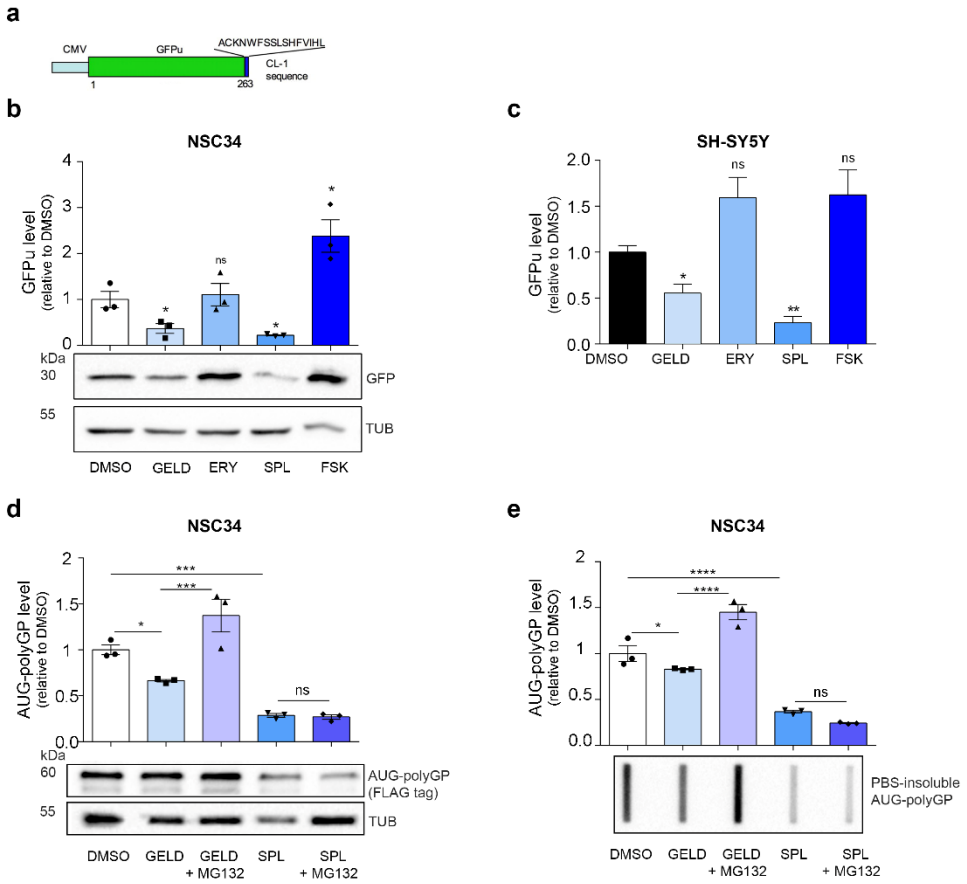


**Figure 5 | Geldanamycin and Spironolactone enhance the activity of the UPS.**

**a** Schematic representation of GFPu construct tagged with a CL-1 degron sequence specific for ubiquitination and degradation by the proteasome. Picture adapted from [165]. **b** Lysates from NSC34 cells transfected with a proteasome activity reporter (GFPu), treated for 24 h and immunoblotted for GFP expression. Quantification from three biological replicates. Data are mean ± SEM. Two-tailed, unpaired t-test, *$P$ 0.0398 GELD *versus* DMSO, *$P$ 0.0124 SPL *versus* DMSO, *$P$ 0.0253 FSK *versus* DMSO. **c** SH-SY5Y cells were transfected for 48 h with a proteasome activity reporter (GFPu), treated for 24 h and immunoblotted for GFP expression. Quantification from three biological replicates. Data are mean ± SEM. Two-tailed, unpaired t-test, *$P$ 0.0202 GELD *versus* DMSO, **$P$ 0.0015 SPL *versus* DMSO. **d** NSC34 cells were transfected for 48 h with FLAG-AUG-polyGP$_{(100)}$ reporter, treated for 24 h with DMSO, GELD and SPL ± 10 µM MG132 (16 h) and immunoblotted for polyGP expression using an antibody anti FLAG. Quantification from three biological replicates. Data are mean ± SEM. 1-way ANOVA, multiple comparisons uncorrected Fisher's LSD, *$P$ 0.0186 DMSO *versus* GELD, ***$P$ 0.0001 GELD *versus* GELD + MG132, ***$P$ 0.0001 DMSO *versus* SPL, ns SPL *versus* SPL + MG132. **e** NSC34 cells were transfected for 48 h with FLAG-AUG-polyGP$_{(100)}$ reporter, treated for 24 h with DMSO, GELD and SPL ± 10 µM MG132 (16 h) and immunoblotted for PBS- insoluble polyGP expression using an antibody anti FLAG. Quantification from three biological replicates. Data are mean ± SEM. 1-way ANOVA, multiple comparisons uncorrected Fisher's LSD, *$P$ 0.0495 DMSO *versus* GELD, ****$P$ < 0.0001 GELD *versus* GELD + MG132, ****$P$ < 0.0001 DMSO *versus* SPL, ns SPL *versus* SPL + MG132.
(ns = non-significant).
All the experients were perfomed by Dr Riccardo Cristofani from the laboratory headed by Prof Angelo Poletti (University of Milano).

## 6. **Insight: FSK does not block the UPS and does not interfere with CREs inside the CMV promoter-driven plasmids**

*My collaborators from the University of Milano mainly contributed in producing a large part of these results. I personally contributed in designing the experiments.*

The initial result obtained by FSK showed GFPu accumulation suggesting a block in the UPS. However, I found in literature several studies demonstrating that cAMP-signalling pathway positively regulates the UPS[166,167]. Therefore, I tried to better elucidate why the experiments showed a GFPu accumulation by FSK. The CHX chase experiment showed that the GFPu accumulation by FSK was not due to a block in the UPS since the degradation kinetic was identical between FSK and control condition (**Figures 6a** and **6b**). Moreover, there was no an increase of *GFPu* mRNA (**Figure 6c**).

FSK indirectly activates PKA and since among its substrates, there are also the transcription factor CREBs, and since the cytomegalovirus (CMV) promoter contains cAMP-response elements (CREs), I decided to investigate the effect of FSK more deeply. Therefore, I assessed whether FSK at the concentration used in my experiments interfered with the CREs contained in the CMV promoter. To this purpose, the expression of two β-galactosidases under two different promoters, CMV or SV40 was checked and a plasmid-independent effect on the expression of ectopic β-galactosidase under the control of different promoters was observed (**Figure 6d**), excluding then that FSK interfered with CREs present in the CMV promoter. Moreover, I checked the transcript level of one of the endogenous CREs-genes, *NR4A2*, and I found that FSK affected the expression level of *Nr4a2* that underwent a strong 3.5 fold increase (**Figure 6e**). Therefore, the results suggest that FSK, at the condition used in this work, is able to induce the transcription of endogenous but not that of ectopic genes containing CREs.

Since FSK did not have an effect on inhibiting the UPS and, given the known molecular target of FSK, I decided to further investigate on the mechanism of action elicited by this molecule.

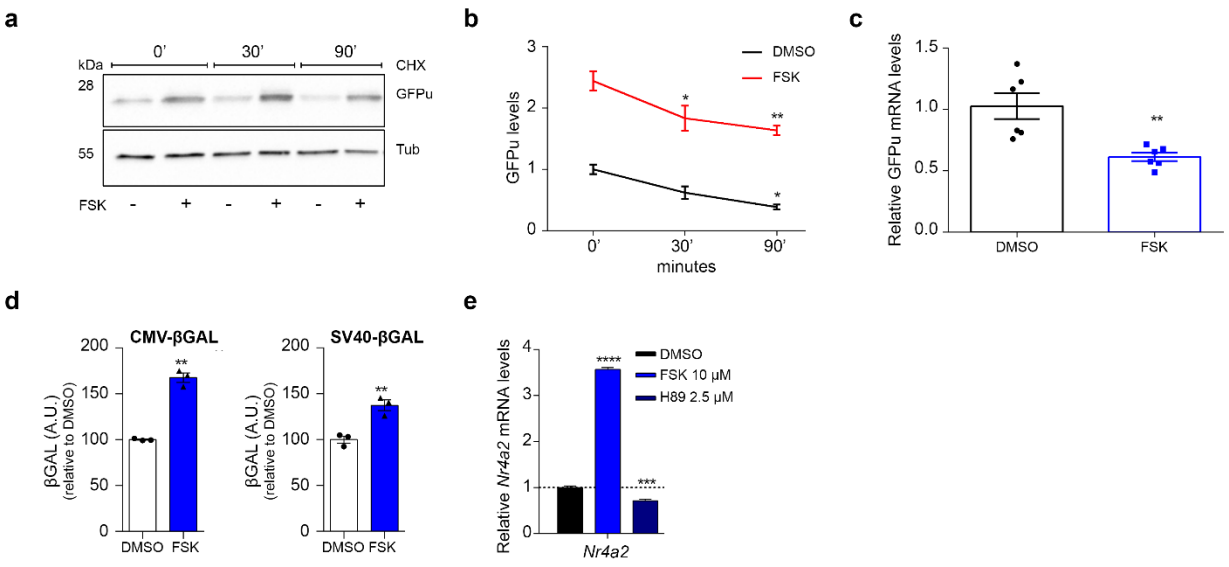


**Figure 6 | FSK does not interfere with CREs inside the CMV promoter-driven plasmids**

**a** Lysates from NSC34 cells transfected for 48 h with a proteasome activity reporter (GFPu), treated for 0', 60' and 90' with CHX 250μM or negative control (DMSO) and immunoblotted for GFP expression. **b** Quantification of **a** from three biological replicates. Degradation rate of GFPu is the same in the two conditions. Data are mean ± SEM. 2-way ANOVA followed by Dunnett's comparisons test, **P* 0.0335 DMSO 0' *versus* DMSO 30', **P* 0.0347 FSK 0' *versus* FSK 30', ***P* 0.0088 FSK 0' *versus* FSK 90'. **c** Relative expression level of *GFPu* mRNAs in HEK293T cells treated with DMSO or FSK for 24 h. Data are mean ± SEM from two biological replicates. Two-tailed, unpaired t-test, ***P* 0.004. **d** NSC34 cells were transfected with CMV- (left) or SV40- (right) β-galactosidase plasmids and treated with DMSO or FSK for 24 h. Quantification from three biological replicates. Data are mean ± SEM. Two-tailed, unpaired t-test, ****P* 0.0002 CMV-βgal FSK *versus* CMV-βgal DMSO, ***P* 0.0061 SV40-βgal FSK *versus* SV40-βgal DMSO. **e** Relative expression level of *Nr4a2* mRNAs, endogenous gene with CRE elements in their promoter, in HEK293T cells treated for 24 h. Data are mean ± SEM from three biological replicates. 2-way ANOVA followed by Dunnett's multiple comparisons test, *FosB* ****P* 0.001 DMSO *versus* FSK, ***P* 0.0012 DMSO *versus* H89; *NR4A2* *****P* < 0.0001 DMSO *versus* FSK, ****P* 0.0002 DMSO *versus* H89.

Experiments (a, b, and d) were performed by Dr Riccardo Cristofani from the lab headed by Prof Angelo Poletti (University of Milano). Experiment in (c and e) were performed by me.

# 7. **The PKA inhibitor H89 decreases DPRs expression**

*This section presents some results, which I did not personally contributed. Specifically, I was not involved in experiments conducted in NSC34 cells that were performed by collaborators from the University of Milano.*

FSK is a derivative of the geranylgeranyl pyrophosphate (GGPP), characterized by the insertion of an heterocyclic ring of tetrahydropyran-derivated[168], and differs from the analogous geranylgeranyl acetone (GGA), which is a potent inducer of HSP70, HSPB8 and HSPB1[169,170] (thus a modulator of the protein quality control system and autophagy). As an internal additional validation of the screening results, I observed that other compounds increasing cAMP (e.i. Dibutyryl cAMP·Na, Desacetylcolforsin, Colforsin and Cilostazol) were able to increase the amount of DPRs within HEK293T cells (**Figure 7a**).

To prove the importance of the AC/PKA pathway in increasing RAN product, I re-tested Cilostazol (CLZ), a phosphodiesterase III (PDE III) inhibitor that increases cAMP level by reducing its degradation, and tested the PKA inhibitor, H89 (**Figure 7b**). In HEK293T cells, CLZ showed an effect similar to FSK, while H89 reduced poly-GA (**Figures 7c** and **7d**). As suggested by the co-administration of FSK and H89, the increase of RAN products due to the cAMP stimulation was blocked by H89. This result suggests the importance of PKA, more than of cAMP, in determining the accumulation of DPRs. The same results were obtained in NSC34 cells, in which poly-GP expression and PBS insoluble fractions were decreased following H89 treatment, and the increase due to FSK was dampened by H89 (**Figures 7e**, **7f** and **7g**).

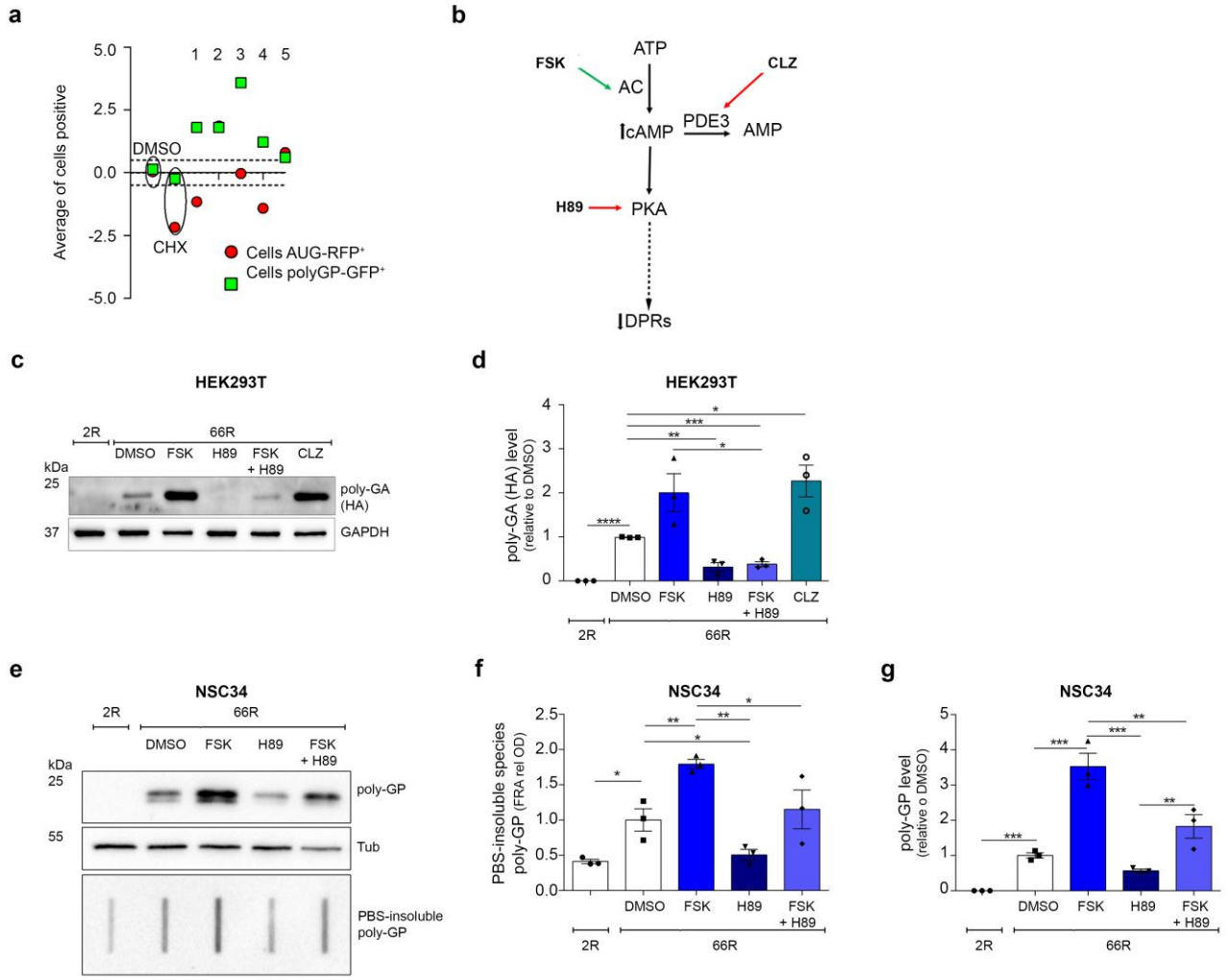


**Figure 7 | PKA inhibition decreases DPRs expression levels.**

**a** Distribution of fluorescence intensity of polyGP-GFP and AUG-RFP relative to cAMP-elevating compounds into primary screening. Legend: 1 FSK, 2 dibutyryl cAMP-Na, 3 desacetyl colforsin, 4 colforsin, 5 cilostazol. **b** Schematic representation showing where the compounds act along the AC/PKA signalling pathway. **c** Lysates from HEK293T cells, transfected with 2R or 66R and treated with selected compounds for 24 h, immunoblotted using antibody for poly-GA expression (HA–tagged). **d** Quantification of (b) from three biological replicates. Data are mean ± SEM. Two-tailed, unpaired t-test, ****$P$<0.0001, **$P$<0.0027 H89 *versus* DMSO, ***$P$ 0.0004 FSK + H89 *versus* DMSO, *$P$ 0.0234 CLZ *versus* DMSO, *$P$<0.0209 FSK + H89 *versus* FSK. **e** Lysates from NSC34 cells, transfected with 2R or 66R and treated with selected compounds for 24 h, immunoblotted for insoluble (above) and total soluble (below) poly-GP expression. **f** insoluble poly-GP in (d) from three biological replicates. Data are mean ± SEM. 1-way ANOVA followed by uncorrected Fisher's LSD, *$P$ 0.0196 2R *versus* 66R DMSO, **$P$<0.0039 FSK *versus* DMSO, *$P$<0.0418 H89 *versus* DMSO, **$P$ 0.0017 H89 *versus* FSK, *$P$ 0.0364 FSK + H89 *versus* FSK. **g** Quantification of total soluble poly-GP in (d) from three biological replicates. Data are mean ± SEM. 1-way ANOVA followed by uncorrected Fisher's LSD, ****$P$<0.0001 2R *versus* 66R DMSO, ***$P$ 0.0001 FSK *versus* DMSO, ****$P$<0.0001 H89 *versus* FSK, **$P$ 0.0015 FSK + H89 *versus* FSK, **$P$ 0.0082 H89 *versus* FSK +H89.

Dr Riccardo Cristofani from the lab headed by Prof Angelo Poletti (University of Milano) performed experiments in (e, f and g). I performed all the other experiments in (a, c and d).

## 8. The PKA inhibitor H89 does not act by modulating either the autophagy system or the UPS

*My collaborators from the University of Milano mainly contributed in producing a large part of these results.*

As previously done, I also checked the *G4C2* mRNA level under H89 treatment and observed that H89 slightly reduced the mRNA expression level of RAN transcripts (**Figures 8a** and **8b**). I then assessed whether H89 modulated the two main degradative pathways. H89 did not induce an autophagic response, as it did not modulate SQSTM1/p62 or LC3 levels in both NSC34 (**Figures 8c**, **8d**, **8e**, **8f** and **8g**) and SH-SY5Y cells (**Fig.8h**). Moreover, H89 did not induce the degradation of the GFPu reporter containing the CL1 degron, supporting that FSK and H89 may exert their effect via a mechanism, which does not involve protein degradation by the UPS (**Figures 8i** and **8j**). As further controls, it remains to perform experiments with the co-treatment of H89 +/- MG132 in the presence of DPRs (using both RAN and AUG-polyGP plasmids). The utilization of both types of plasmids will also allow confirming whether the effect of H89 is RAN-dependent or independent.

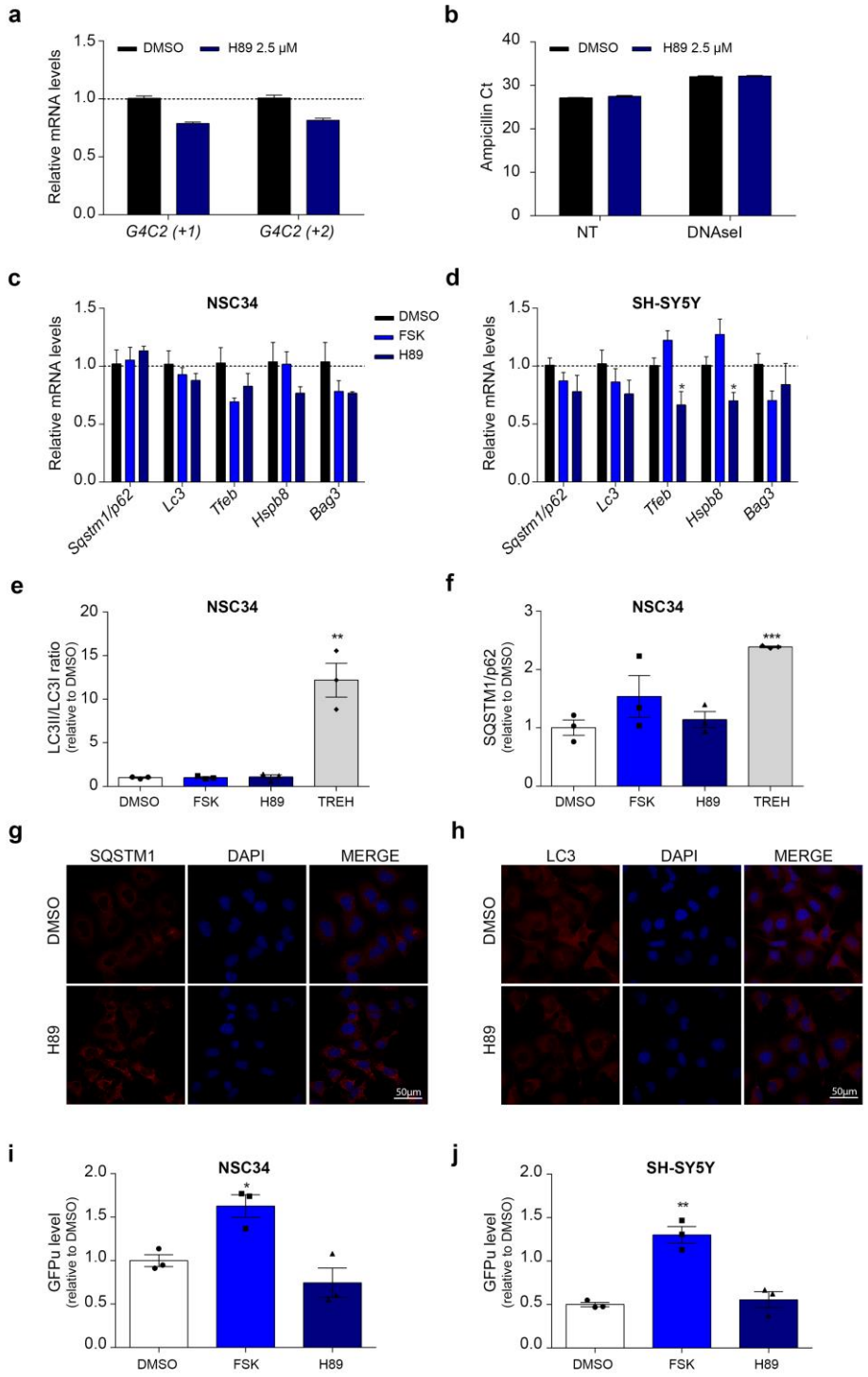
a
DMSO
H89 2.5 μM
Relative mRNA levels
G4C2 (+1)
G4C2 (+2)
b
DMSO
H89 2.5 μM
Ampicillin Ct
NT
DNAseI
c
NSC34
DMSO
FSK
H89
Relative mRNA levels
Sqstm1/p62
Lc3
Tfeb
Hspb8
Bag3
d
SH-SY5Y
Relative mRNA levels
Sqstm1/p62
Lc3
Tfeb
Hspb8
Bag3
e
NSC34
LC3II/LC3I ratio
(relative to DMSO)
DMSO
FSK
H89
TREH
f
NSC34
SQSTM1/p62
(relative to DMSO)
DMSO
FSK
H89
TREH
g
SQSTM1
DAPI
MERGE
DMSO
H89
50μm
h
LC3
DAPI
MERGE
DMSO
H89
50μm
i
NSC34
GFPu level
(relative to DMSO)
DMSO
FSK
H89
j
SH-SY5Y
GFPu level
(relative to DMSO)
DMSO
FSK
H89

**Figure 8 | The PKA inhibitor does not act by modulating either the autophagy system or the UPS**

**a** Relative expression level of *G4C2 (+1)* and (+2) mRNAs in HEK293T cells treated for 24 h. Data are mean ± SEM from three biological replicates. **b** Cycle threshold (Ct) values of Ampicillin antibiotic-resistance gene of 66R plasmid in samples treated ± with DNaseI. Ct values of Ampicillin were used to check and normalize differences in transfection efficiency for each condition. Data are mean ± SEM from three biological replicates. **c** Relative expression level of *Sqstm1/p62*, *Lc3*, *Tfeb*, *Hspb8* and *Bag3* mRNAs in NSC34 cells treated for 24 h. Data are mean ± SEM from three biological replicates. **d** Relative expression level of *Sqstm1/p62*, *Lc3*, *Tfeb*, *Hspb8* and *Bag3* mRNAs in SH-SY5Y cells treated for 24 h. Data are mean ± SEM from three biological replicates. 2-way ANOVA followed by Dunnett's multiple comparisons test, *Tfeb* **P* 0.0183 DMSO *versus* H89; *Hspb8* **P* 0.0397 DMSO *versus* H89. **e** and **f** NSC34 cells treated for 24 h and immunoblotted for LC3 (e) and SQSTM1/p62 (f) expression. Quantification from three biological replicates. Data are mean ± SEM. Two-tailed, unpaired t-test, LC3II/LC3I ratio ***P* 0.0045; SQSTM1/p62 ****P* 0.0005. **g** and **h** Immunofluorescence analysis of NSC34 cells treated with DMSO or H89 for 24 h. In (g) LC3 (red) and in (h) SQSTM1 (red). Nuclei were stained with DAPI (blue). Scale bars 50 µm. **i** NSC34 cells were transfected for 48 h with a proteasome activity reporter (GFPu), treated for 24 h and immunoblotted for GFP expression. Quantification from three biological replicates. Data are mean ± SEM. Two-tailed, unpaired t-test, **P* 0.0132. **j** SH-SY5Y cells were transfected for 48 h with a proteasome activity reporter (GFPu), treated for 24 h and immunoblotted for GFP expression. Quantification from three biological replicates. Data are mean ± SEM. Two-tailed, unpaired t-test, ***P* 0.0013. All the experiments (with the exception of ones in a and b) were performed by Dr Riccardo Cristofani from the lab of Prof Angelo Poletti (University of Milano). Experiments in (a and b) were performed by me.

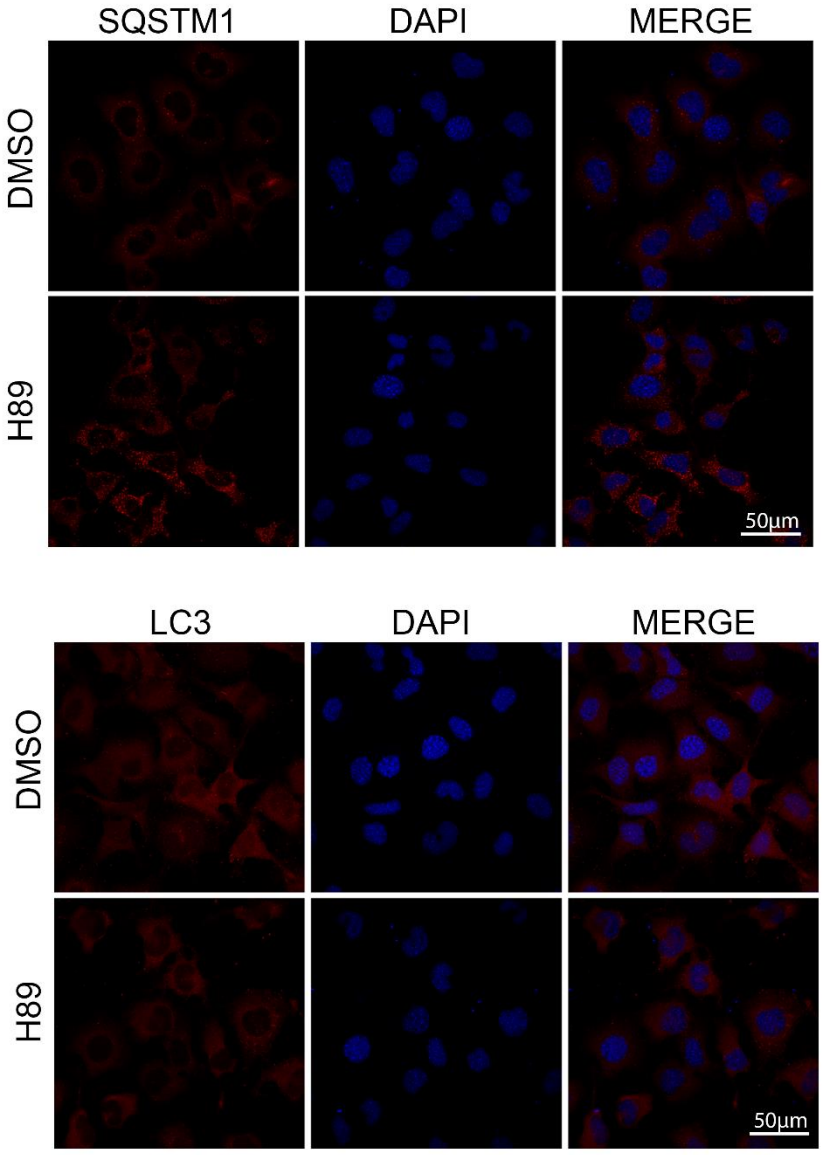


**Magnification of microscopy images in Figures 8g (SQSTM1) and 8h (LC3).**

# 9. **Genetic ablation of the PKA catalytic subunits decreases DPRs expression levels**

*I performed all the experiments described in here.*

Then I kept focused on examining whether PKA was necessary in modulating the DPRs expression level. Although H89 is defined as a specific PKA inhibitor, when used at concentration ≥ 10 μM, it loses specificity showing some PKA-independent activities and making uncertain the interpretation of the cellular effects[151,152,171,172]. Indeed, H89 reduces the phosphorylation of PKA substrates in a dose dependent manner (**Figure 9a**), and it loses its PKA-specificity at high doses, also becoming toxic (IC50 20 μM on HEK293T cells) (**Figure 9b**). Therefore, to assess whether PKA played a role in modulating the expression of DPRs, PKA expression was silenced. In humans, *PRKACA* and *PRKACB* are two genes encoding for the PKA catalytic subunits α (Cα) and β (Cβ), respectively. Using RNA interference, I genetically ablated the expression of the Cα or the Cβ subunits. A marked reduction of Cα expression (42%) slightly decreased the level of poly-GA (26.4%) (**Figures 9c**, **9d** and **9e**). In contrast, the low reduction of Cβ expression (23%) significantly reduced the level of poly-GA (37.4%) (**Figures 9f**, **9g** and **9h**). Interestingly, checking their relative mRNA levels, I observed a marked reduction of *Prkaca* mRNA upon *PRKACB* silencing (**Figure 9i**), but I did not observe the contrary under silencing of *PRKACA* gene (**Figure 9j**), suggesting a stronger inhibition of PKA activity during *PRKACB* silencing. Next, I checked whether the total expression level of *G4C2* transcripts was changed during the silencing of *PRKACA* and *PRKACB* genes. In both conditions, the level of *G4C2* transcripts was not changed (**Figure 9k**).

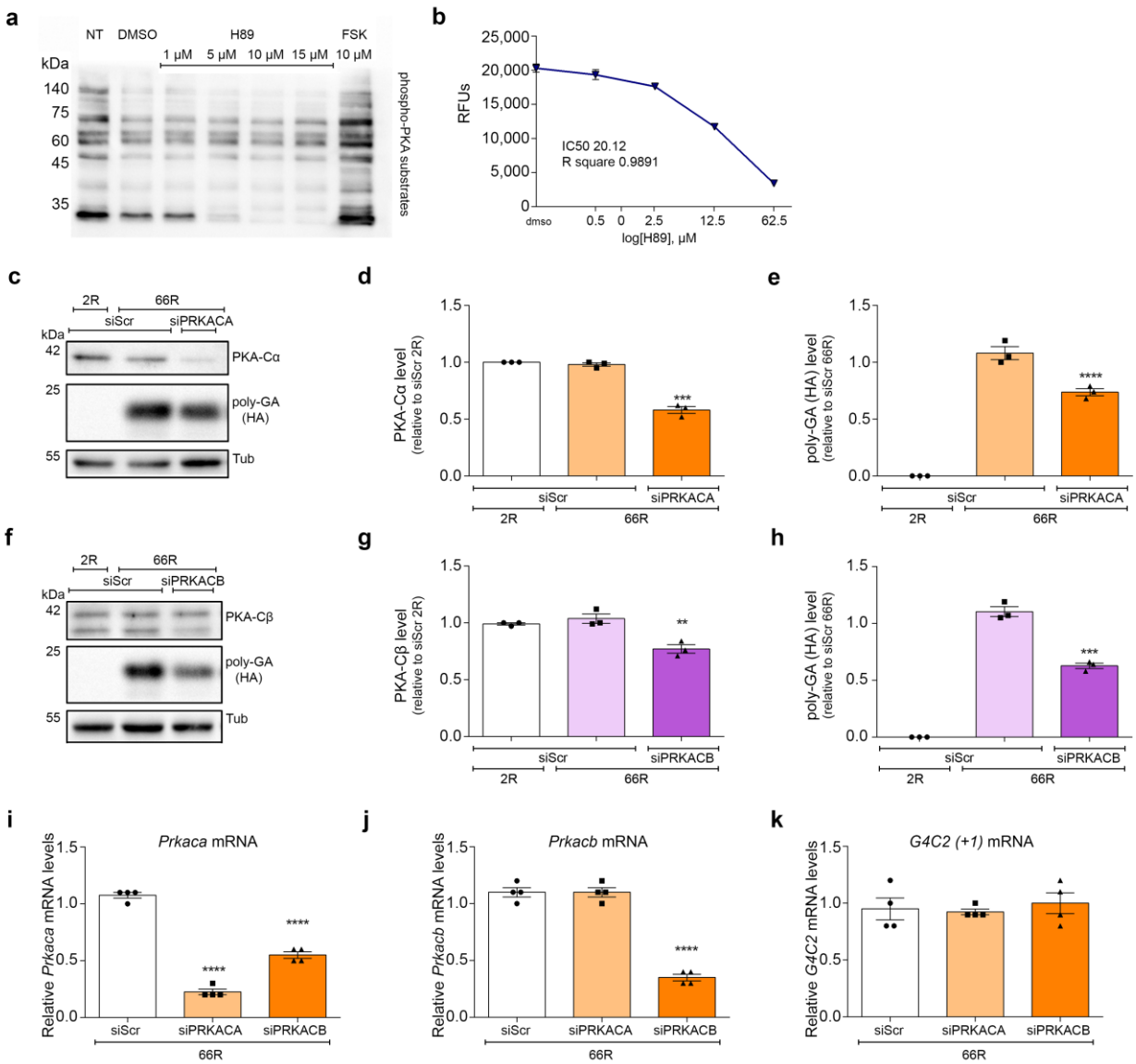


**Figure 9 | Genetic ablation of the PKA catalytic subunits decreases DPRs expression levels**

**a** Lysates from HEK293T cells treated for 24 h with DMSO, FSK or different concentration of H89 and immunoblotted for phospho-PKA substrates. **b** HEK293T cells were treated with different concentration of H89 for 24 h. Viability was measured by OZ-Blue assay. Data are mean ± SEM from three biological replicates. **c** Lysates from HEK293T cells, transfected with RNAi scramble or RNAi PRKACA (72 h) and with 2R or 66R (24 h), immunoblotted using antibodies for poly-GA (HA tagged) and PRKACB expression. **d** Quantification of PRKACA expression in (c) from three biological replicates. Data are mean ± SEM. Two-tailed, unpaired t-test, ***$P$ 0.0002 siPRKACA 66R *versus* siScr 66R. **e** Quantification of poly-GA expression in (c) from three biological replicates. Data are mean ± SEM. Two-tailed, unpaired t-test, ****$P$<0.0001 siPRKACA 66R *versus* siScr 66R. **f** Lysates from HEK293T cells, transfected with RNAi scramble or RNAi PRKACB (72 h) and with 2R or 66R (24 h), immunoblotted using antibodies for poly-GA (HA tagged) and PRKACB expression. **g** Quantification of PRKACB expression in (f) from three biological replicates. Data are mean ± SEM. Two-tailed, unpaired t-test, **$P$ 0.0091 siPRKACB 66R *versus* siScr 66R. **h** Quantification of poly-GA expression in (f) from three biological replicates. Data are mean ± SEM. Two-tailed, unpaired t-test, ****$P$ 0.0007 siPRKACB 66R *versus* siScr 66R. **i**, **j** and **k** HEK293T cells were silenced for 72 h with siScr, siPRKACA and siPRKACB and transfected for 24 h with 66R. Data are mean ± SEM from three biological replicates. Two-tailed, unpaired t-test, ****$P$ < 0.0001. **i** Relative expression level of *Prkaca* mRNA. **j** Relative expression level of *Prkacb* mRNA. **k** Relative expression level of *G4C2* (+1) mRNA. I perfomed all the experiments.

# 10. Genetic ablation of the PKA catalytic subunit β decreases DPRs expression modulating *G4C2* mRNA translation

*I performed all the experiments described in here. The polysomal profiling was conducted in collaboration with IBF-CNR (Trento).*

Therefore, I reasoned whether PKA could act at the translational level and I checked the polysomal loading of *G4C2* RNA under either silencing of *PRKACA* or *PRKACB*. Surprisingly, I found that ablation of *PRKACA* slightly shifted *G4C2* RNA from heavy to light polysomes (**Figure 10a**, upper inset), compared to the control condition, while the silencing of *PRKACB* strongly repressed the translation of *G4C2* transcript (**Figure 10b**, upper inset). In addition, the silencing of *PRKACB* marginally changed the polysomal loading of *Gapdh* mRNA (**Figure 10b**, lower inset), whereas the silencing of *PRKACA* showed a non-significant change of polysomal loading on *Gapdh* mRNA (**Figure 10b**, lower inset). Finally, I did not observe any significant change in *de-novo* protein synthesis under the silencing of *PRKACA* and *PRKACB* (**Figures 10c**, **10d**, **10e** and **10f**) supporting that effects on polysomal loading of *G4C2* transcripts under silencing of *PRKACA* and *PRKACB* might be linked to a specific molecular mechanism and not to a general modification of the translational process. Collectively, these data demonstrate that PKA, and more specifically the PKA-Cβ subunit, effectively plays a role in modulating DPRs level, without affecting the degradation of DPRs, but by affecting the translatability of the aberrantly expanded *G4C2* mRNA sequence.

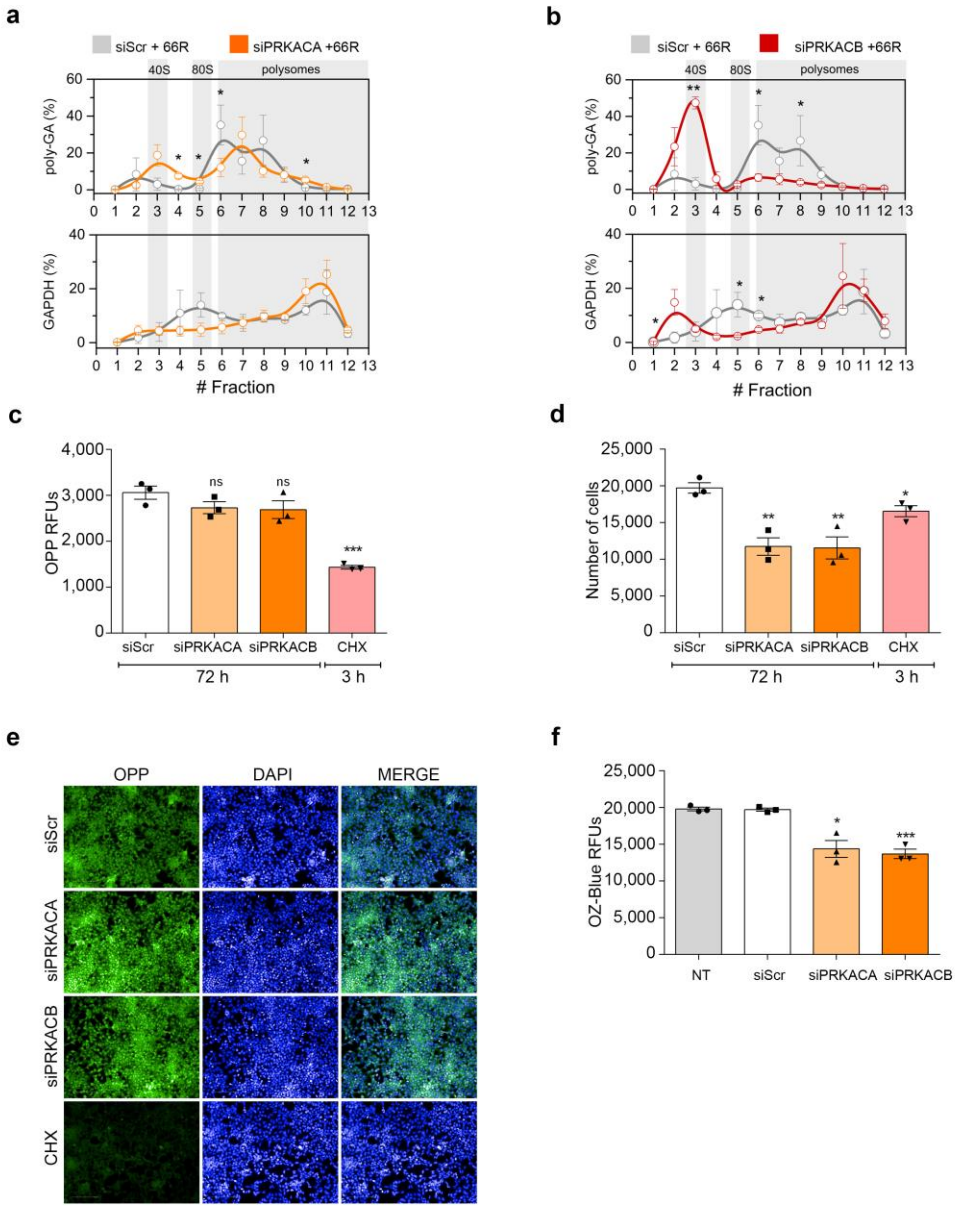
a
siScr + 66R
siPRKACA +66R
40S
80S
polysomes
poly-GA (%)
GAPDH (%)
# Fraction
b
siScr + 66R
siPRKACB +66R
40S
80S
polysomes
poly-GA (%)
GAPDH (%)
# Fraction
c
OPP RFUs
ns
ns
***
siScr
siPRKACA
siPRKACB
CHX
72 h
3 h
d
Number of cells
**
**
*
siScr
siPRKACA
siPRKACB
CHX
72 h
3 h
e
OPP
DAPI
MERGE
siScr
siPRKACA
siPRKACB
CHX
f
OZ-Blue RFUs
*
***
NT
siScr
siPRKACA
siPRKACB

**Figure 10 | RNA interference *versus* PKA catalytic subunit β reduces DPRs expression levels by repressing G4C2 translation.**
**a** Co-sedimentation profile of poly-GA (upper panel) and GADPH (lower panel) mRNAs along the sucrose gradient fractions of polysomal profiles from control (grey lines) and PRKACA-depleted (orange lines) cells. Data are mean ± SEM from three independent biological replicates. t-test, one-tailed, *$P < 0.05$; **$P < 0.01$.**b** Co-sedimentation profile of poly-GA (upper panel) and GADPH (lower panel) mRNAs along the sucrose fractions of polysomal profiling from control (grey lines) and PRKACB-depleted (red lines) cells. Data are mean ± SEM from three independent biological replicates. t-test, one-tailed, *$P < 0.05$; **$P < 0.01$. The polysomal profiling was conducted in collaboration with IBF-CNR (Trento). **c** and **d** HEK293T cells were silenced for 72 h with siScr, siPRKACA and siPRKACB, and then global protein synthesis was monitored by the incorporation of the OPP. CHX 350 µM for 3 h was used as positive control to check general translation arrest. Data are mean ± SEM from three biological replicates. **c** Relative fluorescence intensity of OPP incorporated. Two-tailed, unpaired t-test, ***$P$ 0.0004. **d** Cell viability measured by the number of nuclei selected into the fields analysed for OPP(18 per well in 96-well plate). Two-tailed, unpaired t-test, **$P$ 0.0045 siPRKACA *versus* siScr, **$P$ 0.008 siPRKACB *versus* siScr, *$P$ 0.0382 CHX *versus* siScr. **e** Immunofluorescence images from OPP assay. Scale bars, 100 µm. **f** HEK293T cells were silenced for 72 h with siScr, siPRKACA and siPRKACB. Cell viability was measured by OZ-Blue assay. Data are mean ± SEM from three biological replicates. Two-tailed, unpaired t-test, *$P$ 0.0105 siPRKACA *versus* siScr, ***$P$ 0.0009 siPRKACB *versus* siScr. I performed all the experiments described in here.

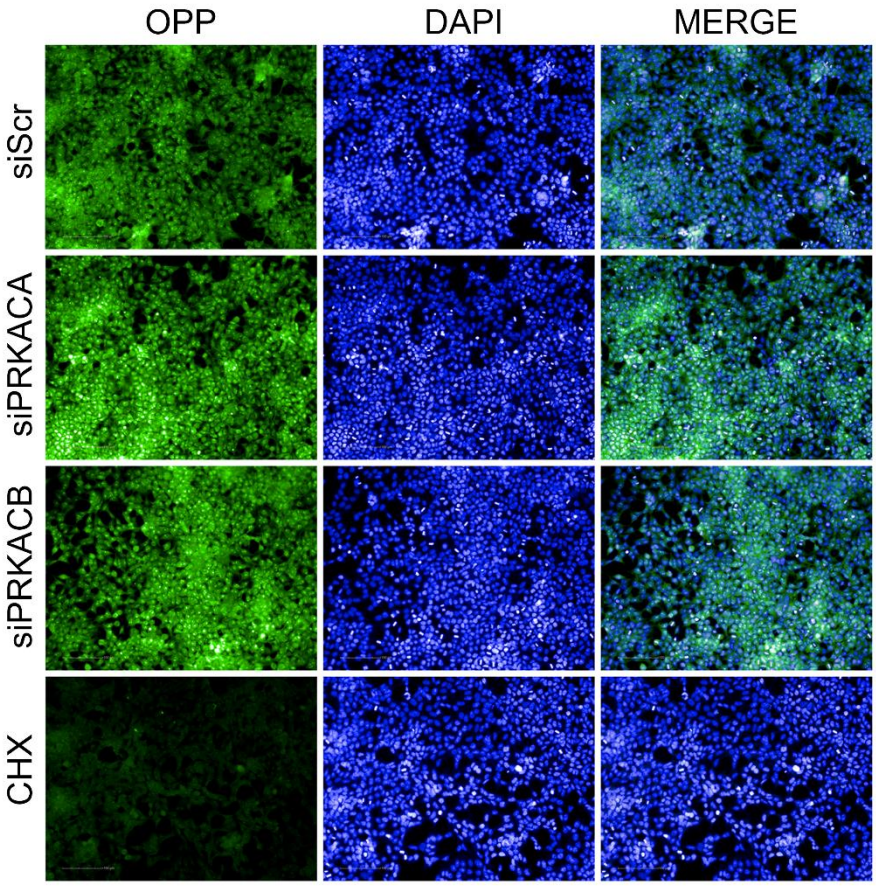


**Magnification of microscopy images in Figure 10e.**

# 11. The PKA inhibition through H89 administration rescues motility defects and extends lifespan in a *Drosophila* model for C9ALS/FTD

*The results presented in this section were obtained by experiments performed with the collaboration of Prof Paola Bellosta that has great expertise in manipulating Drosophila.*

I wondered whether the PKA inhibitor H89 could be effective in *in vivo* models. To date, many animal models have been used to study the G4C2 repeat RNA and DPR protein toxicity: yeast, *C. elengans*, *Drosophila*, mouse and zebrafish. Each animal model has its advantages and disadvantages. For example, mouse *C9orf72* is homologous to human *C9ORF72*, but it lacks the G4C2 repeats, therefore mouse can represent a useful model to study the C9ORF72 loss of function (several knockout mice models have been generated) [44,55], while to study the RNA and DPRs gain-of-function, one has to ectopically express the repeats. Instead, in *Drosophila* there is not the human *C9ORF72* homolog, however, ectopically expression of the G4C2 repeats well reproduces the pathogenic phenotype in *Drosophila* more than in mice models[173]. Moreover, *Drosophila* offers other advantages; is an expensive animal model with rapid generation time (10 days) and is highly valuable to test drugs and therapeutic compounds[174].

Therefore, to assess the effect of PKA inhibition *in vivo* I used, with the collaboration of Prof Paola Bellosta, a *Drosophila* model for C9ALS/FTD to test the efficacy of H89 by evaluating their ability to climb up. The C9ALS/FTD *Drosophila* model used expresses a sequence of 36 G4C2 repeats of the *C9ORF72* gene in neurons by using the *elav-Gal4* driver[65]. These transgenic flies show a reduction in lifespan[65] and a progressive loss of motility (**Figures 11a** and **11c**). Therefore, *Elav-C9orf72-G4C2* adults were treated daily from 1 day after eclosion (DAE) with 10 µM H89 and their ability to climb was tested every two days[175]. H89 significantly improved the motility of the flies carrying the repeats starting from the 3 DAE, while did not show any significant effect in *wild type elav-w$^{1118}$* flies (**Figures 11a** and **11c**). *Elav-C9orf2-G4C2* female flies showed a significant improvement in their climbing activity with a 50% of success that increased in the presence of H89 from 7 to 10 days DAE, while in *elav-/w1118* control females the treatment with H89 did not show any significant effect (**Figure 11a**). In males the ability of H89 to ameliorate the motility of *elav-C9orf72-G4C2* animals was also significant, but with a less extend (*$p$<0.05) than in females (***$p$<0.001) flies (**Figure 11c**). Moreover, H89 increased the viability in both female and male *elav-C9orf72-G4C2* flies compared to the mutants treated with negative control (**Figures 11b** and **11d**), suggesting a beneficial effect also on animal survival.

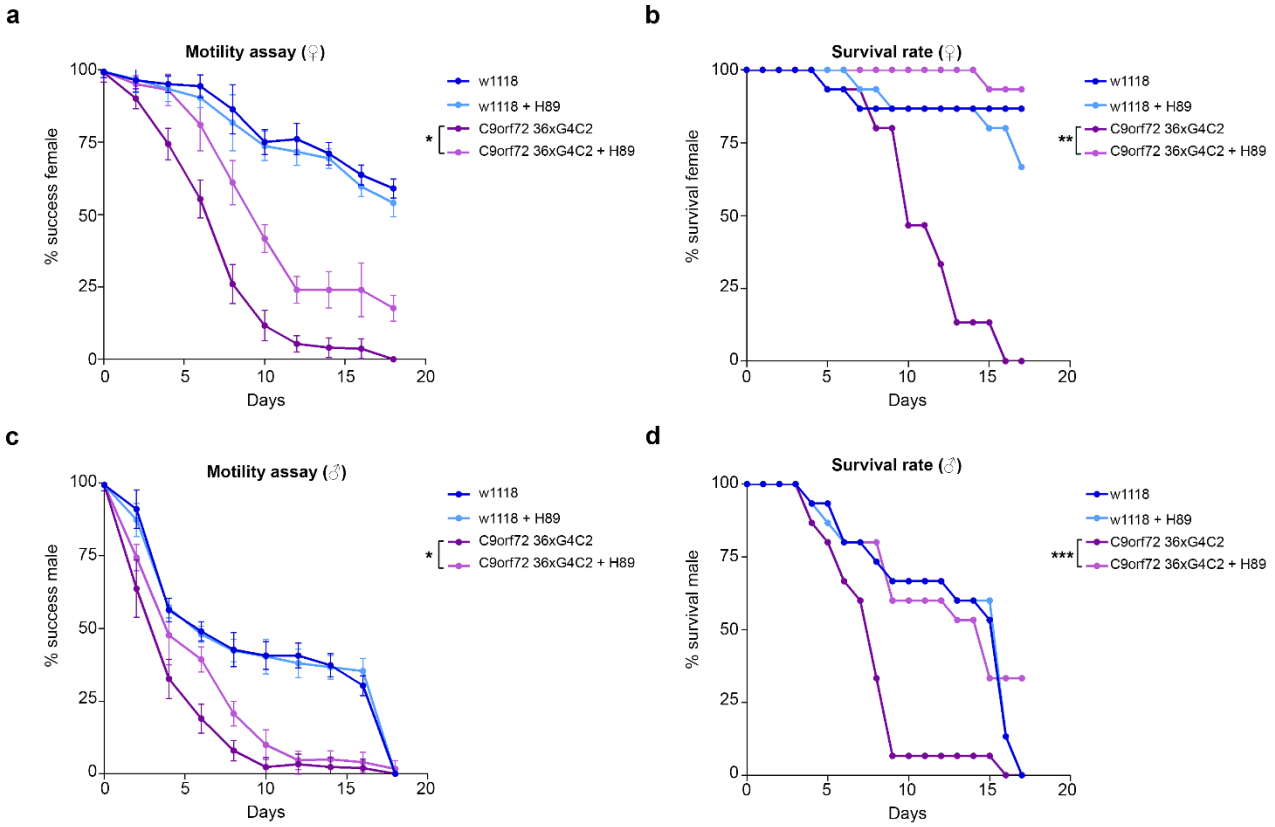


**Figure 11 | PKA inhibition through H89 administration improves motility defects and extends lifespan in a *Drosophila C9orf72* model.**

**a** Graph showing the climbing ability of female flies (♀) carrying the indicated transgenes in neurons using the *elav-gal4* promoter upon treatment with H89 10 µM diluted with 0.1 % of DMSO and 5% sucrose. Data are mean ± SD. 1-way ANOVA followed by Dunnet's multiple comparisons, ****P* 0.0007 C9ORF72 36xG4C2 *versus* C9ORF72 36xG4C2 + H89. **b** Survival curves of female flies (♀) reported in (a). Data are mean. 1-way ANOVA followed by Dunnet's multiple comparisons, ***P* 0.0018 C9ORF72 36xG4C2 *versus* C9ORF72 36xG4C2 + H89. **c** Graph showing the climbing ability of male flies (♂) carrying the indicated transgenes in neurons using the *elav-gal4* promoter upon treatment with H89 10 µM diluted with 0.1 % of DMSO and 5% sucrose. Genotypes as in (a). Data are mean ± SD. 1-way ANOVA followed by Dunnet's multiple comparisons, **P* 0.0215 C9ORF72 36xG4C2 *versus* C9ORF72 36xG4C2 + H89. **d** Survival curves of male flies (♂) reported in (c). Data are mean. 1-way ANOVA followed by Dunnet's multiple comparisons, ****P* 0.0001 C9ORF72 36xG4C2 *versus* C9ORF72 36xG4C2 + H89.
Experiments performed by Prof Paola Bellosta (University of Trento).

# 12. Downregulation of *Pka-C1* in C9ALS/FTD *Drosophila* improves motility defects and extends lifespan

*The results presented in this section were obtained by experiments performed with the collaboration of Prof Paola Bellosta that has great expertise in manipulating Drosophila. I did RNA extraction from larvae and RT-qPCR to check the transcript level of the PKA-C1.*

To further prove the PKA relevance in mediating the expansion toxicity, I decided to test the ability to climb up of C9ALS/FTD *Drosophila* in which PKA was downregulated. *Drosophila* encodes three catalytic subunits of PKA, *Pka-C1*, *Pka-C2* and *Pka-C3*, but only the functions of *Pka-C1* have been studied. Interestingly, *Pka-C1* is homologous to the human *PRKACB.* The downregulation of *Pka-C1* was obtained using a RNA interference (RNAi) construct (*UAS-RNAi* line) (**Figure 12a**). The data clearly demonstrated that the downregulation of *Pka-C1* significantly ameliorated both motility defects (**Figures 12b** and **12d**) and lethality (**Figures 12c** and **12e**) in both adult female and male flies expressing *C9orf72*-G4C2, strongly indicating the relevance of PKA in mediating the toxicity of the *C9orf72*-G4C2 expansion.

Finally, whether the improvement in motility observed in C9 flies under the treatment with H89 and in presence of *Pka-C1* downregulation is due to a decrease of poly-GP level remains to be assessed

I attempted to detect poly-GP protein via immunoblot analysis, but I did not obtained the expected results, at the present. Indeed, I did not see the band at the expected height (that is at about 15 kDa). I used different protocols to isolate the head of flies, different protocols of protein extraction and different conditions of transfer systems. I also used the protocol published in Mizielinska *et al*[65]. I also checked the poly-GP protein expression using flies at different ages. I think then the problem most likely is the antibody I used.

Among all five DPRs, poly-GR expression in the *Drosophila* eye shows a strong degenerative phenotype and it has been used for RNAi-screening to identify translational factors involved in RAN translation[92]. Therefore, another idea could be to verify whether H89 and *Pka-C1* downregulation mitigate the GR-mediated toxicity. To pursue this aim, I would use the same model already utilized by Goodman *et al*[92]. Indeed their C9 *Drosophila* model also express GFP in GR-frame, allowing detecting the DPR by immunoblot analysis. Moreover, flies expressing poly-GR from a non-*G4C2* transcript[92] are also commercially available and they could be used to show if H89 and *Pka-C1* downregulation act downstream of toxic GR-production (RAN-independent effect).

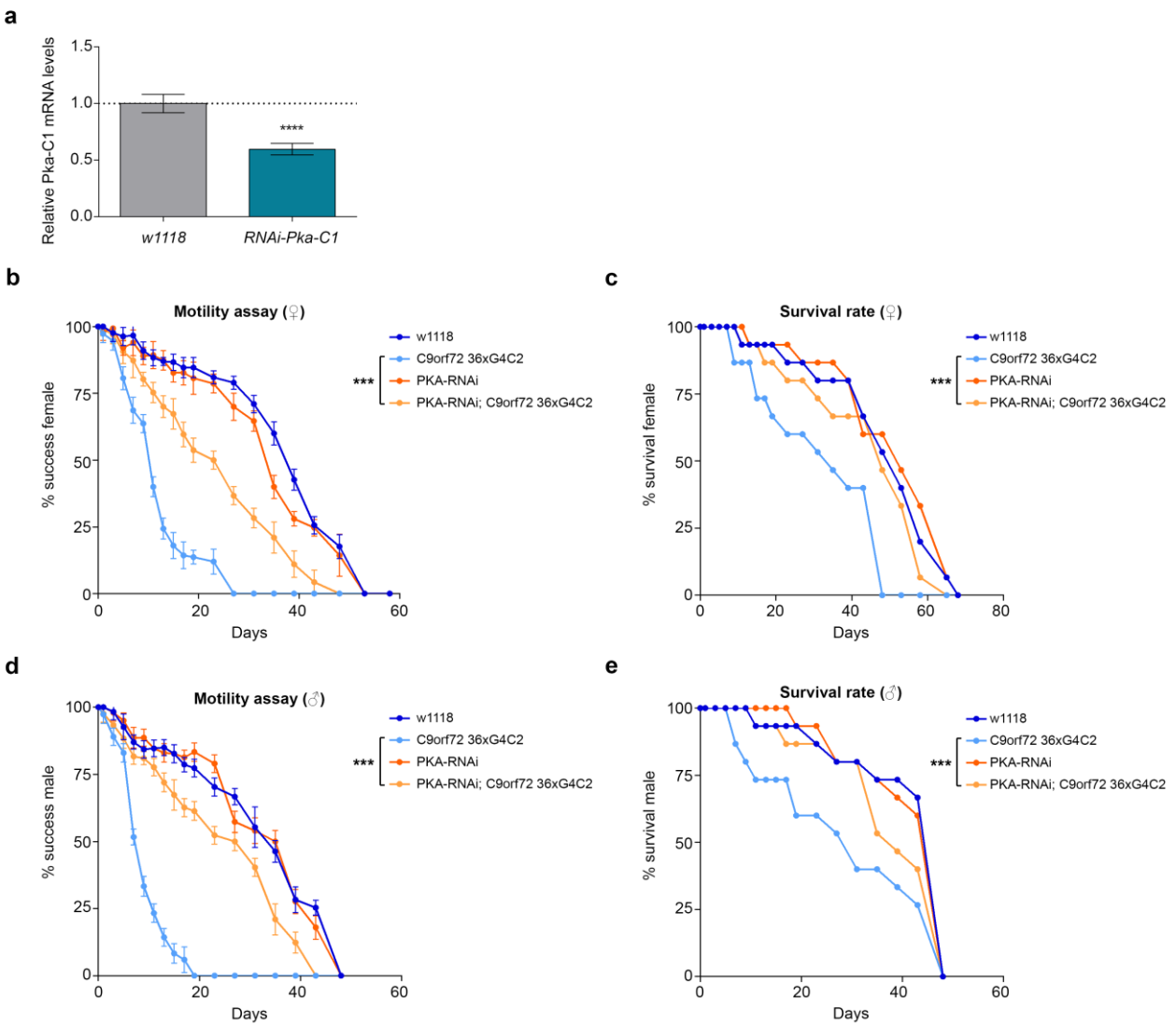


**Figure 12 | PKA inhibition through RNAi interference improves motility defects and extends lifespan in a *Drosophila C9orf72* model.**

**a** Relative expression of *Pka-C1* mRNA in *Drosophila* whole third instar larvae expressing *Pka-RNAi* under the control of the *actin* promoter. Data are expressed as the mean ± SEM from 5 animals for each genotype (n=5). Two-tailed, unpaired t test with Welch's correction ****$P < 0.0001$. **b** Graph showing climbing activity of female flies (♀) co-expressing the *UAS-PKA-RNAi* construct in combination with *UAS C9ORF72 36xG4C2* in neurons using the *elav-gal4* promoter. Data are mean ± SD. 1-way ANOVA followed by Dunnet's multiple comparisons, ***$P$ 0.0002 C9ORF72 36xG4C2 *versus* PKA-RNAi/ C9ORF72 36xG4C2. **c** Survival curves of female flies (♀) reported in (b). Data are mean. 1-way ANOVA followed by Dunnet's multiple comparisons, ***$P$ 0.0001 C9ORF72 36xG4C2 *versus* PKA-RNAi/ C9ORF72 36xG4C2. **d** Graph showing climbing activity of male flies (♂) co-expressing the *UAS-PKA-RNAi* construct in combination with *UAS C9ORF72 36xG4C2* in neurons. Genotypes as in (b). Data are mean ± SD. 1-way ANOVA followed by Dunnet's multiple comparisons, ***$P$ 0.0002 C9ORF72 36xG4C2 *versus* PKA-RNAi/ C9ORF72 36xG4C2. **e** Survival curves of male flies (♂) reported in (d). Data are mean. 1-way ANOVA followed by Dunnet's multiple comparisons, ***$P$ 0.0001 C9ORF72 36xG4C2 *versus* PKA-RNAi/ C9ORF72 36xG4C2.

I performed experiment in (a). Prof Paola Bellosta performed experiments in (b, c, d and e)

# 13. The PKA-substrate eEF2 kinase as candidate involved in modulating DPRs expression

*Flies' experiments were performed in collaboration with Prof Paola Bellosta. I personally contributed to all the other experiments. The polysomal profiling was conducted in collaboration with IBF-CNR (Trento).*

As previously said, PKA phosphorylates several substrates positively or negatively modulating a multiple of cellular pathways[139]. Therefore, I investigated downstream pathways of PKA leading to translation, and I focused on one of the immediate PKA target kinase regulating translation, the eukaryotic Elongation Factor 2 Kinase (eEF2K)[145,146]. eEF2K is principally regulated by $Ca^{2+}$ and CaM (calmodulin)[144] but it can be activated in a $Ca^{2+}$-independent way by PKA-dependent phosphorylation in serine 500 ($Ser^{500}$)[145,146] with the consequence phosphorylation at threonine 56 ($Thr^{56}$) of eEF2[102] (**Figure 13a**). The eEF2 is the only eEF2K substrate and modulates the elongation stage by translocating ribosomes from one codon to the other along mRNAs. The phosphorylation site on eEF2 is close to the site of interaction for ribosomes[103], therefore, when eEF2K phosphorylates eEF2, it inhibits its activity slowing down the total protein synthesis rate[104].

Since others[155] and I observed that the elongation inhibitor CHX did not decrease the level of DPRs, I then reasoned that blocking the activity of eEF2 kinase could decrease the DPRs synthesis. Indeed, the silencing of eEF2K led to the reduction of DPRs (**Figures 13b**, **13c** and **13d**). Polysomal profiling carried out on EEF2K-depleted cells showed no significant changes of polysomal loading on *Gapdh* mRNA (**Figure 8e**, upper inset) and a decrease of the translation of *G4C2* transcripts due to a shift of *G4C2* RNA from heavy to light polysomes (**Figure 13e** lower inset) compared to the control condition.

Conversely, overexpression of *EEF2* in *Drosophila* flies carrying the repeat expansion led to a slight but non-significant worsening in climbing (**Figures 13f** and **13h**) and in survival rate (**Figures 13g** and **13i**) of both genders.

Collectively these data suggest eEF2K as candidate involved in modulating DPRs expression under activation of the AC/PKA signalling pathway, however further experiments are required to elucidate this molecular mechanism.

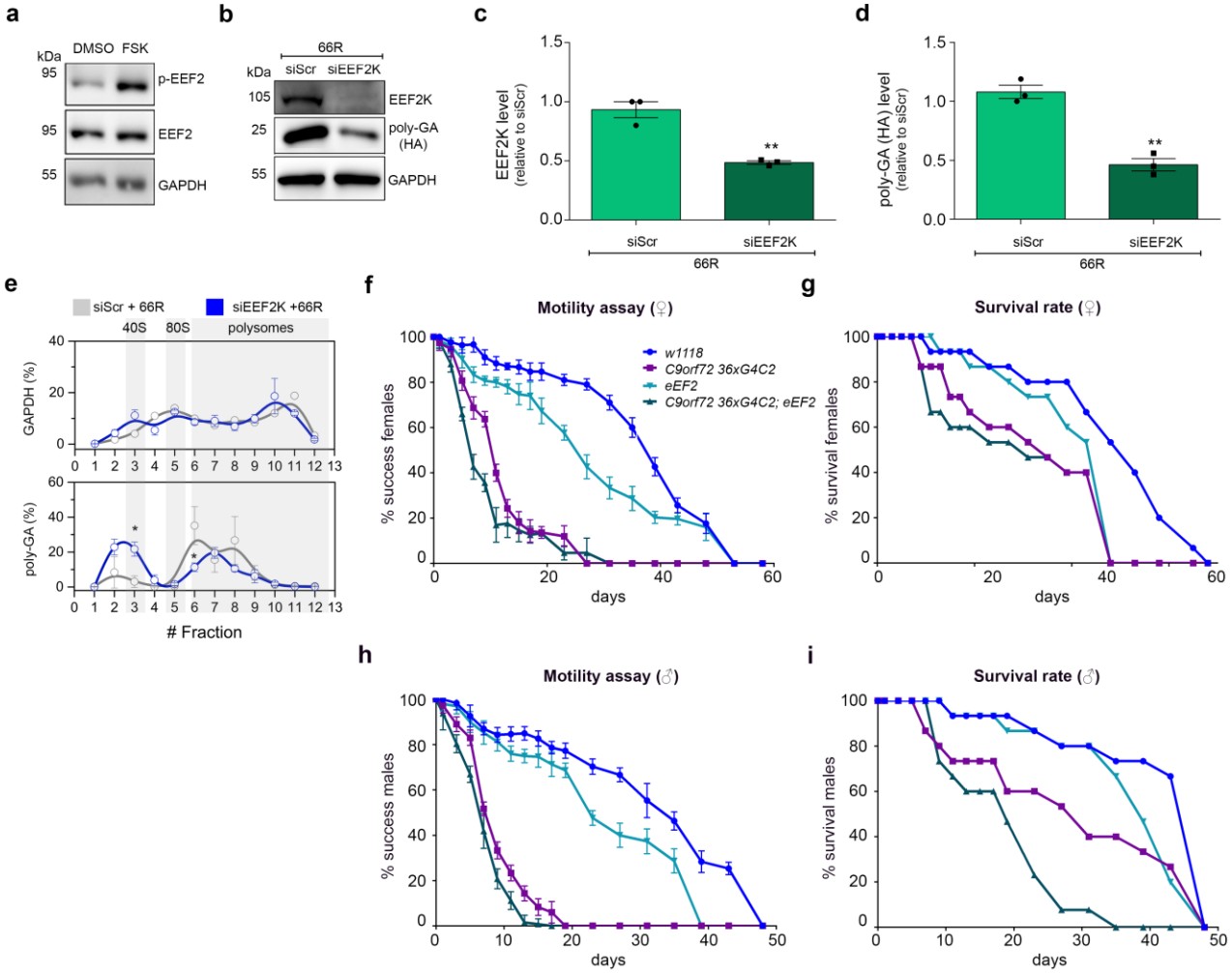


**Figure 13 | Depletion of the PKA-substrate eEF2 kinase slows down DPRs translation**

**a** Lysates from HEK293T cells treated with DMSO or FSK for 24 h and immunoblotted using antibodies for pThr56-EEF2, EEF2 tot and GAPDH expression. **b** Lysates from HEK293T cells, transfected with RNAi scramble or RNAi EEF2K (72 h) and with 66R (24 h), immunoblotted using antibodies for EEF2K, poly-GA (HA tagged) and GAPDH expression. **c** Quantification of EEF2K expression in (b) from three biological replicates. Data are mean ± SEM. Two-tailed, unpaired t-test, $^{**}P < 0.01$. **d** Quantification of poly-GA (HA tagged) expression in (b) from three biological replicates. Data are mean ± SEM. Two-tailed, unpaired t-test, $^{**}P < 0.01$. **e** Co-sedimentation profile of GAPDH (upper panel) and G4C2 (lower panel) mRNAs along the sucrose gradient fractions of polysomal profiles from control (grey lines) and EEF2K-depleted (blue lines) cells. Data are mean ± SEM from three independent biological replicates. One-tailed, t-test, $^{*}P < 0.05$. **f** Graph showing climbing activity of female flies (♀) co-expressing the *UAS-EEF2* construct in combination with *UAS C9ORF72 36xG4C2* in neurons using the *elav-gal4* promoter. Data are mean ± SD. **g** Survival curves of female flies (♀) reported in (f). **h** Graph showing climbing activity of male flies (♂) co-expressing the *UAS-EEF2* construct in combination with *UAS C9ORF72 36xG4C2* in neurons. Genotypes as in (f). Data are mean ± SD. **d** Survival curves of male flies (♂) reported in (c).

I performed experiments in (a, b, c, d and e). I performed polysomal profiling (e) in collaboration with IBF-CNR (Trento). Prof Paola Bellosta (University of Trento) performed the flies' experiments (f, g, h and i).

# *Discussion*

I performed a chemical screening by using libraries of small molecules with known molecular mechanism of action and used the expression level of polyGP-GFP as readout. Contrary to other efforts[176], cell clones stably overexpressing the polyGP-GFP products were not obtained. However, I succeeded in the optimization of a robust assay that allowed the identification of a number of small molecules that modulated the expression level of the RAN products. Among the internal controls, I could observe that blockers of general translation, as mTOR inhibitors (e.g. Torin, Rapamycin) and ribosome targeting antibiotics (as Puromycin), were able to decrease the expression level of both RAN- and AUG-dependent products. Also using genetic deconvolution, I identified 3 small molecules of which 2, GELD and SPL decreased the overall level of DPRs, while in contrast FSK markedly increased DPRs level.

Geldanamycin (GELD) is the “first in class” discovered HSP90 inhibitor[177]. GELD inhibits HSP90 binding to its amino terminus impeding its binding to misfolded proteins, thereby inducing their proteasomal degradation[178]. Since many of these clients are oncogenic proteins, the antitumoral effect of GELD is due to the degradation of these oncodrivers[179]. Unfortunately, no HSP90 inhibitors have been approved for clinical usage, even if a number of HSP90 inhibitors, including some GELD derivatives like 17-AAG and 17-DMAG, are presently in advanced phase II clinical trials for a variety of cancers. Their clinical utilization is based on their capability to induce the heat shock response (HSR), a pro-survival response that upregulates the expression of the protective-stress induced small HSP, like HSPB1 and HSP70[180–182] that is, however, detrimental for the anticancer therapy. HSPB1, like its cognate HSPB8[93,159], show protective effects by inducing proteasome or autophagic degradation of ubiquitinated and misfolded proteins[182]. A plausible explanation of my data is that RAN products might be clients of the HSP90 protein and that GELD inhibits the stabilization effect of the HSP90, by also triggering the HSR and enhancing the DPRs UPS-mediated clearance in cells, as already shown in our previous studies[93,159]. To note, the activation of the UPS by GELD, triggered the degradation of poly-GA and poly-GP that are not normally degraded via this mechanism, but mainly via autophagy[93]. Interestingly, it has been recently demonstrated that poly-GA inhibits the proteasome functionality leading to TDP-43 accumulation and that rolipram has benefit effects as enhances the proteasome activity reducing both poly-GA and TDP-43 aggregation[85]. Therefore, this study[85]

and the results obtained with GELD support that enhancing proteasome activity may represent a promising therapeutic target.

Spironolactone (SPL) is an aldosterone antagonist that targets the Mineralcorticoid Receptor (MR). Its antihypertensive effect was thought to depend primarily on its diuretic and saluretic action. However, it appears that part of its mechanism of action is due to the blockade of the MR in other tissues than the kidneys as the cardiac tissue and the CNS[183]. My results demonstrated that SPL reduces the level of RAN and AUG-DPR (this latter arise from the codon degeneracy, in the absence of G4C2 repeats), suggesting that the effect of SPL might be DPRs protein-dependent. SPL does not induce the autophagy, but enhances the activity of proteasome. However, the co-treatment SPL and the proteasome inhibitor MG132 did not increase the level of AUG-DPRs, suggesting SPL reduces DPRs level by other ways.
Interestingly, SPL is also an inhibitor of DNA repair by inducing the degradation of the helicase XPB through the proteasome[184]. Indeed, SPL is able to induce proteasome-mediated degradation of the helicase XPB independently of its MR blocking effect in HeLA[184] and in human pulmonary artery endothelial cells (PAECs)[185]. Noteworthy, a ChIP-seq analysis of human cells showed that G quadruplexes are targets of the helicases XPB and XPD[186], suggesting that SPL could also act upstream, at the begging of the *C9ORF72*-mediated disease, then acting at different levels (transcription and post-translation).
It is known that SPL with its diuretic effect can act on $Na^+$ and $Ca^{2+}$ metabolism and it has been shown that SPL was able to increase the survival rate of flies carrying CUG-repeat expansions, suppressing their semi-lethal phenotypes[187]. Given the ability of SPL to cross the blood brain barrier[183], its activity should be evaluated in *in vivo* model to reduce the formation of RAN products into neurons. Notably, SPL is a commercially available drug and it is recently available as oral suspension to aid patients with difficult swallowing including ALS patients. Therefore, it might also be interesting to evaluate whether C9ALS/FTD patients may have benefit in disease progression after SPL treatment, compared to non SPL-treated patients.

The screening also identified forskolin (FSK) as a potent inducer of polyGP-GFP expression levels. FSK acts as stimulator of the adenylyl cyclase (AC) enzyme thereby increasing intracellular cAMP levels and regulating several downstream pathways by the activation of PKA[156,158]. I found that FSK increased both poly-GA

and poly-GP in two different cell lines. Conversely, the PKA inhibitor, H89, decreased RAN products expression in different cell models and improved motor dysfunction and survival rates in *Drosophila* model for C9ALS/FTD, showing a generality in the mechanism of action. I also noted a potential gender effect in our C9orf72 *Drosophila* model[188], but this may also be explained by the dosage compensation effect of the X chromosome[189] where the *elav-Gal4* transgene is inserted.

Collectively these data suggest that inducing the AC/PKA signalling pathway entails an increase in DPRs accumulation. However, the rolipram-induced proteasome activity, discussed above, is due to a PKA-dependent phosphorylation of the 26S proteasome non-ATPase regulatory subunit 11 (PSMD11)[85,166]. It is known that PKA modulates the activity of numerous substrates thereby leading to pleiotropic effects into the cells; therefore, it may be reasonable to think that PKA can show positive or negative effects on DPRs depending on downstream substrates phosphorylated.

H89 is thought to inhibit PKA by competitively binding the ATP site on its catalytic subunit[190]. However, several studies demonstrated that H89 shows effects that are PKA independent. To provide evidences of the involvement of PKA in my models, I then silenced its catalytic subunits *in vitro* and *in vivo* with the simultaneous expression of the *G4C2-C9orf72* expansion. Depletion of Cβ showed a marked reduction of poly-GA protein expression more than the silencing of Cα, but no changes in *G4C2* mRNA expression were observed. In addition, the silencing of *PRKACB* also entailed a reduced *Prkaca* mRNA expression, but not conversely.

Polysomal analysis in *PRKACB*-depleted cells showed a strongly repression the translation of *G4C2* transcripts as also observed with minor extent in *PRKACA*-depleted cells, suggesting a specific involvement of Cβ in modulating DPRs translation. Moreover, ablation of its homolog *Pka-C1* in neurons of *Drosophila* significantly ameliorated both motility defects and lethality in flies carrying *C9orf72*-G4C2. Interestingly, Cβ is more specifically expressed in neuronal tissue[191,192] than Cα, and it has been already demonstrated that depletion of *PRKACB* in mice results to be protective by age-related effects[193]. However, it remains to determine whether the benefit effect of H89 in flies' motility depend on a decrease of DPRs protein. As previously said, among all five DPRs, poly-GR expression in the fly eye shows a strong degenerative phenotype and it is widely used to study the C9ALS/FTD disease. Therefore, another idea could be to verify whether H89 and *Pka-C1*

downregulation mitigate the GR-mediated toxicity by utilization of a fly model expressing GFP in GR-frame that also allows assessing the protein level via immunoblot analysis.

Interestingly, there are evidences that PKA is involved in the regulation of translation at different levels. In fungi, PKA is involved in regulating the translation by: i) activation of de-capping enzymes Dcp1/2, via Pat1 (deadenylation factor) phosphorylation, thereby allowing the association of the translational machinery to mRNA and protecting it from degradation and ii) regulation of the abundance of eIF4G[194,195]. Therefore, further experiments will be pursued to better elucidate the role of PKA in translation.

An intriguing hypothesis is that PKA-Cβ regulates translation of specific genes and the mechanism of *G4C2* mRNA regulation is dependent on the translation mechanism driven by the specific activation of PKA. The strong rescue of motility and the enhanced survival of the affected flies using either H89 or the conditional knockout of PKA in the nervous tissue suggest PKA-Cβ as a novel target for ALS due to G4C2 expanded *C9orf72*. A plausible hypothesis explaining the selective involvement of PKA in mediating the neuronal toxicity of the G4C2 expansion could be related to the cross-talk between the neuronal excitatory signalling, leading to cAMP formation that activates the PKA pathway(s). For example, the $Ca^{2+}$-permeable AMPA (CP-AMPA) receptors are normally expressed at low levels at the synapses and its expression on the synapse surface requires the phosphorylation of GluA1 serine 845 by PKA[196]. Interestingly, it has been showed that the increase of intracellular oligomeric amyloid β promotes the synaptic expression of CP-AMPA in a PKA- and CAMKII-dependent way[197], even if how it occurred remains undefined. Therefore, given the involvement of PKA in mediating different signalling pathways at the neuronal tissues, it is important further elucidating its potential role in C9ALS/FTD and in other neurodegenerative diseases characterized by repeat expansion. Indeed, many PKA-substrates can be often regulates in a PKA-independent way by the intracellular level of $Ca^{2+}$ and vice versa.
Noteworthy, FSK is largely sold as a dietary supplement to aid in weight loss and muscle building, but, according to these data, it could lead to serious, long term, adverse events and additional studies should be taken before consumption.

In eukaryotic cells, PKA has been reported to regulate translation elongation by phosphorylating at Ser[500] the eEF2 kinase (eEF2K) that in turn phosphorylates its only substrate eEF2 slowing down the elongation phase[104]. Xie *et al*. reported that when EEF2K is active, slowing the rate of elongation promotes the right recognition of start codons in mRNAs, while conversely its depletion or inactivation leads to faster translation elongation, thereby increasing mistranslation rate[198]. However, my experiments showed that depletion of *EEF2K* led to a reduction of DPRs synthesis as also demonstrated by polysomal loading on *G4C2* mRNA in *EEF2K*-depleted cells. In Kearse *et al*.[155], they showed that slowing the elongation (using the elongation inhibitor CHX) allows ribosomes induce the accumulation of scanning PICs that then positioned over a non-AUG start codon, favouring their translation. This is in agreement with my results relative to eEF2K and to the increase of polyGP-GFP observed in screening under CHX treatment. Moreover, the polysomal loading on *G4C2* transcripts in *EEF2K*-depleted cells was similar to the one in *PRKACA*-depleted cells, suggesting that EEF2K is involved in DPRs translation but with minor extent. In contrast, the overexpression of EEF2 orthologue did not induce significant worsen either in climbing or in survival rate of flies carrying the repeat expansions. However, *Drosophila* lacks the orthologue of EEF2K, therefore EEF2 may be not subjected to regulation[198]. Noteworthy, in agreement with the results I obtained, the unbiased loss-of-function screen for translation factors in *Drosophila* carrying the (G4C2) expansion of Goodman *et al*.[92] identified that depletion of *EEF2* mitigated toxicity in C9-flies.

In summary, in this work, I identified by HTS three small molecules, GELD, SPL and indirectly H89 that reduced the DPRs content. GELD acts by enhancing the function of the UPS, suggesting that targeting degradative machinery may represent a valid therapeutic approach to decrease the C9ALS/FTD disease progression, as already demonstrated[85]. How SPL decreases the level of DPRs remains to determine, but I am going to verify whether it depends on the degradation of the helicase XPB that is able to bind DNA G quadruplexes. By FSK and H89, I identified that the AC/PKA-Cβ pathway regulates the expression of RAN products at the translational level, grounding the work for further exploration of new molecular targets for *G4C2* expanded in *C9ALS/FTD*. Finally, I identified the PKA-substrate EEF2K as potential candidate involved in modulating DPRs expression.

# *Future perspectives and ongoing works*

My experiments demonstrated that SPL reduces the level of RAN and AUG-DPR, suggesting that acts on the DPRs. Moreover, SPL seems no induce the autophagy, but enhances the activity of proteasome. However, the co-treatment SPL and the proteasome inhibitor MG132 do not increase the level of AUG-DPRs, leaving to determine how SPL decreases the level of DPRs. However, collectively, these data suggest that SPL could act on DPRs protein. Since SPL induces the proteasome-mediated degradation of the helicase XPB[184,185,199] that is able to bind DNA G-quadruplexes[186], this evidence does not exclude the possibility that SPL also could act at the transcription level. Therefore as next step, I am going to futher investigate the possible mechanisms of action of SPL. Firstly, I would check if at the concentration I used, SPL induces the degradation of XPB and I would verify if the downregulation of XPB reduces RAN-DPRs in my cell models and in C9 IPSC-derived neurons.

As previously said, it remains to determine whether the benefit effect of H89 and of *Pka-C1* downregulation in flies' motility depend on a decrease of DPRs protein. Since, at the present I did not obtained the expected result in observing the poly-GP band in the C9 fly model I used, most likely due to the antibody I used, an alternative idea should be to use another C9 *Drosophila* model. I would use the same fly model already utilized by Goodman *et al*[92] that also expresses GFP in GR-frame, allowing detecting DPR by immunoblot analysis. Moreover, flies expressing poly-GR from a non-*G4C2* transcript[92] are also commercially available and they could be used to assess whether H89 and *Pka-C1* downregulation act downstream of toxic GR-production (RAN-independent effect).

The identification of protein kinase A (PKA) and Eukaryotic Elongation Factor 2 Kinase (EEF2K) as regulators of the translation of $(G4C2)_n$ repeat expansion highlights the importance of protein kinases in fine-tuning a multiple of cellular processes. As it is well known, translation is tightly regulated by several kinases at different steps. Suffice it to say that eukaryotic initiation factor eIF2α can be phosphorylated at Ser51 by four different kinases in response a specific stress: for example by GCN2 that is activated when essential amino acids lack or by PERK that is active when misfolded proteins induce the endoplasmic reticulum (ER) stress[105]. Phosphorylation of eIF2α allows blocking general translation initiation. Even the eukaryotic elongation factor 2 kinase (eEF2K) instead by phosphorylating

the eEF2 blocks or slows down the translation elongation step[104]. Finally, how previously said, in fungi PKA is involved in regulating the translation by: i) activation of de-capping enzymes Dcp1/2, via Pat1 (a deadenylation factor) phosphorylation, thereby allowing the association of the translational machinery to mRNA and protecting it from degradation and ii) regulation of the abundance of eIF4G[194,195]. Therefore, in addition to better elucidate the role of PKA and EEF2K in C9ALS/FTD, given also the involvement of kinases in mediating different signalling pathways I am going to perform a human kinome RNA interference screen to identify novel kinases involved in regulation of $(G4C2)_n$ translation.

Moreover, new small molecules screening will be performed at the Institute of Molecular and Translational Medicine (IMTM), Palacky University supported by the funding received from the European Union's Horizon 2020 research and innovation programme under the grant agreement No. 823893.

Concerning the role of EEF2K in C9ASL/FTD, I am going to further study it in deep using C9ALS/FTD patient-derived cells.

Finally, the reduction of DPRs by the compounds identified will be tested in four different C9ALS/FTD patient-derived cell lines and isogenic controls in collaboration with the laboratory of Prof Adrian Isaacs from the University College of London (UCL) Institute of Neurology. Specifically, Meso Scale Discovery (MSD) immunoassays will be performed to look at poly-GA and poly-GP levels.

At the present, my ongoing experiments aim at completing the revision of my manuscript.

# *Materials and Methods*

*The materials and methods described below also include the materials and methods used by my collaborators and are marked by an asterisk (*)*

# 1. Cell lines

Human embryo kidney HEK293T cell line was cultured in standard conditions using Dulbecco's modified Eagle's medium (DMEM) (Sigma-Aldrich) with 10% FBS (Sigma-Aldrich), 1% L-glutamine (Sigma-Aldrich) and 1% penicillin–streptomycin (Sigma-Aldrich).

* Mouse motor neuron NSC34 cell line[200,201] was cultured in standard condition using DMEM (Euroclone) with 5% FBS (Sigma-Aldrich), 1 mM L-glutamine (EuroClone) and 1% penicillin–streptomycin (SERVA).

* Human neuroblastoma SH-SY5Y cell line was cultured in DMEM/F12 (EuroClone) supplemented with 10% FBS (Sigma-Aldrich), 1mM L-glutamine (EuroClone) and 1% penicillin–streptomycin (SERVA).

# 2. **Plasmids and siRNAs**

The **pcDNA3.1-CMV-GGGGCCx58-GFP** (G4C2x58-GFP or poly-GP-GFP) vector was kindly provided by J. Paul Taylor[153] (St. Jude Children's Research Hospital, Memphis, TN, USA). The GFP sequence is downstream of the repeat in GP-reading frame and lacking of own AUG start codon. The AUG-RFP vector was kindly provided by Prof Anna Cereseto[202] (University of Trento, Trento, Italy). This couple of vectors was utilized for HTS and dose-response assay.

The **pAG3-CAG-GGGGCCx2** or **GGGGCCx66** (2R or 66R) vectors were kindly provided by Dr. Leonard Petrucelli[70] (Mayo Clinic, Jacksonville, FL, USA). These vectors do not contain either AUG start codon upstream of the repeat or STOP codon downstream, but contain 113 bp of 5′ and 99 bp of 3′ flanking sequence[70]. Downstream of the repeat three epitope tags per frame (HA, +1; His, +2;FLAG, +3) were inserted[70]. The 2R vector was used as negative control of RAN translation. The 66R vector was used for all the experiments that followed the HTS, the confirmatory screening and dose-response assays. Its utilization not only was useful to further validate the results obtained utilizing the previous vector (G4C2x58-GFP), but also allowed to evaluate the expression of poly-GA and poly-GP using antibodies *vs* their tags or dipeptide sequence.

The plasmid expressing the proteasome reporter **GFPu** was kindly provided by Prof. Ron Kopito[164] (Stanford University, Stanford, CA, USA). This vector was used to assess the functionality of proteasome under cell treatments.

The plasmid **pCMV-FLAG-ATG-polyGP-V5-His** was obtained from Prof Daisuke Ito, Keio University School of Medicine, Tokyo, Japan and base pairs to encode polyGP were assembled avoiding GGGGCC repeats (see below). This plasmid was used to verify whether DPRs degradation depends on the UPS.
PolyGP sequence using the degeneracy codons:
ACCATGGACTACAAGGACGACGACGACAAGGGCCCTGGACCTGGCCCAGGACC
AGGACCTGGACCCGGCCCTGGGCCCGGACCGGGGCCTGGTCCAGGACCCGGG
CCAGGACCGGGACCTGGGCCTGGACCTGGTCCCGGCCCTGGTCCAGGACCCG
GACCTGGACCTGGACCAGGACCTGGCCCCGGACCAGGACCAGGACCTGGGCC
AGGACCCGGACCTGGTCCCGGACCCGGACCCGGACCAGGCCCTGGACCCGGA
CCTGGACCTGGTCCTGGCCCTGGACCCGGCCCAGGACCTGGACCCGGTCCCG
GACCTGGACCTGGACCCGGACCAGGGCCAGGGCCTGGACCTGGACCTGGACCT
GGCCCTGGACCTGGGCCTGGGCCCGGACCTGGACCTGGCCCAGGACCCGGAC
CCGGACCTGGGCCTGGACCGGGCCCTGGGCCTGGACCTGGACCTGGACCCGG
ACCAGGACCTGGACCGGGGCCTGGCCCTGGACCAGGACCTGGGCCTGGACCT
GGACCTGGACCAGGACCTGGGCCTGGACCCGGTCCCGGACCCGGCCCTGGGC
CTGGCCCCGGACCTGGGCCTGGACCTGGACCCGGACCTGGTCCCGGACCTGG
ACCT.

The plasmid **pcDNA3.1** (ThermoFisher) was used to normalize the total DNA amount in each transfection.

To silence endogenous human *PKA catalytic* isoforms and human *Eef2k*, were used: siRNAs targeting *PKA catalytic subunit α* (esiRNA human PRKACA, EHU132541), *PKA catalytic subunit β* (esiRNA human PRKACB, EHU075621) and EEF2K (esiRNA human EEF2K, EHU033871) purchased from Sigma-Aldrich.

Plasmid and siRNA transfections were performed using Lipofectamine 3000 (Invitrogen) and Opti-MEM (Thermo Scientific) following the manufacturer's instructions.

# 3. **High-throughput and confirmatory screening**

The screening protocol used in this work lasts 2 days and is the following:

**Day 1st: reverse transfection, cell seeding and treatment with compound-libraries**

### 1.1 Reverse transfection

Human HEK293T cells were seeded into the wells containing pre-aliquoted transfection mixture consisting of 25 ng G4C2x58-GFP and 25 ng AUG-RFP. To allow the complete addiction of the transfection mixture into the well (2.5 µL per well), it was diluted 5 times with Opti-MEM, adding so 12.5 µL per well. The transfection mixture was automatically transferred by Tecan Freedom EVO 200 liquid handler from 96-well plate to 384-well plate (CellCarrier-384 Ultra microplates, Perkin Elmer, #6057300).

### 1.2 Cell seeding

HEK293T cells were cultured in T75 $cm^2$ flaks (Corning®) at 85-90% of confluence. Cells were trypsinized for 30 sec in order to avoid aggregates and re-suspended to a concentration of $3.2x10^5$ cells/mL in DMEM. By Tecan Freedom EVO 200 liquid handler, 37.5 µL of cells were dispensed into each well (containing 12.5 µL of transfection mix) in order to get a final density of $1.2x10^4$ cells per well in 50 µL tot. Plates were spun down briefly and then incubated at 37°C with 5% $CO_2$ for 3 h.

### 1.3 Cell treatment with compound-libraries

Compound-libraries were added after cells adhesion to the well bottom (3 h). The compounds were automatically added by Tecan Freedom EVO 200 liquid handler at the final concentrations of 5 µM in one replicate. CHX was used as positive control at a final concentration of 5 µM, while the vehicle DMSO, at a final concentration of 0.5% was used as negative control. Plates were spun down briefly and then incubated at 37°C with 5% $CO_2$ for 36 h.

**Day 2nd: Cell imaging and analysis**

Cells were imaged after an incubation of 30 min with Hoechst 33342, added by an automated multidispenser (BioTek EL406). Optimized steps gain a GFP S/N higher than 1.5 and a RFP S/N higher than 5 for the negative controls. Image acquisition was performed using an Operetta High-Content Imaging System (Perkin Elmer). Three channels were acquired: Hoechst33342 Ex 380/40nm, Em 445/70nm; GFP

Ex 475/30nm, Em 525/50nm; RFP Ex 535/30nm, Em 595/70nm. Two fields of view were acquired for each well (representing 33% of the entire well) using a 10x Objective 0.4NA. Image analysis was performed using Harmony 4.1 software (Perkin Elmer). Quickly, cell number was estimated counting Hoechst positive nuclei and the transfection rate cells was defined as GFP or RFP positive cells. Hits were defined as compounds capable to selectively reduce or increase the number of cells polyGP-GFP positive and their fluorescence intensity.

**QC of the primary screening and of hits selection**

To determine the QC of the primary screening and of the hits selection, robust Z'-factor and robust Z-score were used. These robust versions differ from the "classic" ones since they utilize the median in place of the mean and the MAD (Median Absolute Deviation) instead of standard deviation and then the outliers do not affect them.

Neither systematic errors nor positional effects were observed in the plates layout heatmap, therefore we preferred not to apply B-score method to normalize the data.

## 4. **Chemicals**

The chemicals utilized in this study are the following: Geldanamycin (GELD; InvivoGen, ant-gl), Erysolin (ERY; Santa Cruz Biotechnology, sc-205679), Spironolactone (SPL; Santa Cruz Biotechnology, sc-204294), Forskolin (FSK; SelleckChem, S2449), Cilostazol (CLZ; Cayman Chemical, 15035), H-89 hydrochloride (H89; Cayman Chemical, 10010556), Cycloheximide (CHX; Sigma-Aldrich, C1988), ActinomycinD (ACTD; Sigma-Aldrich, A9400), Dimethyl sulfoxide (DMSO; Sigma-Aldrich, 41639), Trehalose (TREH, Sigma-Aldrich, T9531), Z-Leu-Leu-Leu-al (MG132, Sigma-Aldrich C2211).

The high-throughput screening was conducted using the following compound libraries:

i) The Spectrum Collection library (MicroSource, USA) containing 60% of FDA/EMA-approved drugs, 25% of natural products and 15% of molecules in preclinical stages for a total of 2000 compounds;

ii) The Anti-cancer compound library (Selleck), a unique collection of 349 bioactive compounds;

iii) The NIH Clinical Collection assembled by the National Institutes of Health (NIH) comprised of 450 molecules that have a history of use in human clinical trials;

iv) The Screen-Well® Autophagy library (Enzo Life Science) containing 94 compounds with defined autophagy-inducing or -inhibitory activity.

## 5. **Cell viability assays**

*In vitro* drug sensitivity was assessed in HEK293T cells by the fluorescent and colorimetric OZBlue CellViability kit (OZbiosciences). HEK293T cells ($1.2x10^4$/well in 96-well plates) were treated for 24 h with different concentrations of compounds (using DMSO as negative control) or plated $2.5x10^3$ in 96-well plates for the silencing experiments (72 h). 8 µL OZBlue Cell Viability Kit was added into the medium and plates incubated for 3 h. The fluorescence measure (560nm Ex/590nm Em) was determined using a plate reading at the following time-points: 1 h, 2 h and 3 h.

* The 3-(4,5-dimethyl-2-thiazolyl)-2,5 diphenyl-2H-tetrazolium bromide-based cell proliferation assay (MTT assay) was carried out on NSC34 cells ($4x10^4$/well in 24-well plates, 6 wells for each condition to be tested; n = 6) after 24 h of treatments with selected compounds. MTT solution was prepared at 1.5 mg/mL in DMEM without phenol red and filtered through a 0.2-mm filter. Then, culture medium was removed and 300 µL of MTT solution was added into each well. Cells were incubated for 30 min at 37°C with 5% $CO_2$. After 30 min, 500 µL of 2-propanol was added into each well and the precipitates were suspended. The optical density (OD) of the wells was determined using a plate reader at a wavelength of 550 nm.

## 6. **Dose-Response assay**

HEK293T cells ($1.2x10^4$/well in 96-well plates) were co-transfected with poly-GP-GFP and AUG-RFP, treated with different concentrations of compounds for 24 h and Heochst 33342 was added in living cells for nuclei staining. Image acquisition was performed using an Operetta High-Content Imaging System (Perkin Elmer). Three channels were acquired: Hoechst33342 Ex 380/40nm, Em 445/70nm; GFP Ex 475/30nm, Em 525/50nm; RFP Ex 535/30nm, Em 595/70nm. Image analysis was performed using Harmony 4.1 software (Perkin Elmer). Cell number was

estimated counting the nuclei Hoechst positive and the transfected cells was defined as polyGP-GFP or AUG-RFP positive cells. Hits were defined as compounds capable to selectively reduce or increase the number of cells polyGP-GFP positive and the GFP fluorescence intensity.

## 7. **RNA and protein click-iT imaging kits**

Click-iT RNA Alexa Fluor 488 Imaging Kit (Thermo Scientific) was used to quantify the level of global RNA synthesis by imaging. Newly synthesized RNA or changes in RNA levels are detected by utilizing an alkyne-modified nucleoside, 5-ethynyl uridine (EU) that is actively incorporated into nascent RNA. Detection utilizes the chemoselective ligation or “click” reaction between azide and the alkyne-modified nucleoside incorporated into nascent RNA.
$1.2x10^4$ HEK293T cells were treated for 24 h with compounds or DMSO and for 3 h with 5 μM ActD (used as positive control of transcriptional inhibition), and then incubated for 1 h with 1 mM 5-ethynyl uridine (EU) working solution without removing the drug-containing media. EU detection was performed following the manufacturer’s protocol after cell fixation and permeabilization by imaging. Heochst33342 was used for DNA staining.

Click-iT Plus OPP Alexa Fluor 488 Protein Synthesis Assay Kit (Thermo Scientific) was used to measure the rate of translation. Newly synthesized proteins, changes in spatial or temporal protein expression patterns, or protein degradation can be detected by utilizing a puromycin analog, O-propargyl-puromycin (OPP), to actively growing cells. OPP inhibits protein synthesis by disrupting peptide transfer on ribosomes causing premature chain termination during translation. The modified proteins are detected by imaged-based analysis following to the chemoselective ligation or “click” reaction between azide and the alkyne moiety-containing OPP.
$1.2x10^4$ HEK293T cells were treated for 24 h with compounds or DMSO and for 3 h with 350 μM CHX (used as positive control of translation inhibition), and then incubated for 30 min with 20 μM O-propargyl-puromycin (OPP) in working solution without removing the drug-containing media. After fixation and permeabilization, OPP incorporation was assessed by imaging. NuclearMask Blue Stain was used for DNA staining and Operetta acquisition and analysis.

## 8. **Total RNA extraction and RT-qPCR**

HEK293T cells were seeded in 12-well plates. Transfection with 66R was performed 24 h after seeding and treatments immediately after transfection. Cells were harvested 24 h after treatments and centrifuged 5 min at 1200 rpm at 4°C; pellets were re-suspended in 300 µL of TRI Reagent (Thermo Scientific) and total RNA isolated according to manufacturer's instructions. RNA quantification was carried out by absorbance at 260 nm.

The retrotranscription reaction was performed starting from 1 µg of RNA using the RevertAid First Strand cDNA synthesis kit (Thermo Scientific) according to the manufacturer's protocol using 0.5 µL random primers and 0.5 µL Oligo(dT) primers (Invitrogen). qPCR was carried out using the CFX Connect Real-Time PCR Detection System (BioRad) and Kapa Syber Fast qPCR Mastermix (Kapa Biosystems).

The primers used for the qPCR are listed in **Table 1**. Relative mRNA quantification was obtained with the ΔCt method using *Gapdh* as housekeeping gene. Relative mRNA quantification of *G4C2* was obtained by normalizing the amount of transfected plasmid.

* $8x10^4$ NSC34 or $1.5x10^5$ SH-SY5Y cells were plated in 12-well plates and treated the day after for 24 h with compounds or DMSO. Cells were harvested and centrifuged 5 min at 100 X g at 4°C. Pellets were resuspended in 300 µL of TRI Reagent (Sigma-Aldrich) and total RNA isolated according to manufacturer's instructions. RNA quantification was carried out by absorbance at 260 nm. Total RNA (1 µg) was treated with DNAse I (Sigma-Aldrich), and reverse transcribed into cDNA using the High-Capacity cDNA Archive Kit (Life Technologies) according to the manufacturer's protocol. qPCR was carried out using the CFX 96 PCR Detection System (BioRad) and iTaq Universal SYBR® Green Supermix (Biorad). All the primers, human and mouse, used for qPCR are listed in **Table 1**. Relative mRNA quantification was obtained with the ΔCt method using *Rplp0*/*RPLP0* as housekeeping genes.

**Table 1. Primer pairs for RT-qPCR**

| **Human genes** | | **Primer** |
|---|---|---|
| *G4C2* | fwd: | TGC GGT TGC GGT GCC T |
| | rev*[1]: | CTT GTC GTC GTC GTC CT |
| | rev*[2]: | AGC GTA ATC TGG AAC GT |
| *Prkaca* | fwd: | CCA CTA TGC CAT GAA GAT CCT CG |
| | rev: | CGA GTT TGA CGA GGA ACG GAA AG |
| *Prkacb* | fwd: | GCA GTG GAT TGG TGG GCA TTA G |
| | rev: | ACT GAA GTG GGA TGG GAA TCG G |
| *Nr4a2f* | fwd: | CGA CCA AGA CCT GCT TTT TGA |
| | rev: | CAA GAC CAC CCC ATT GCA A |
| *Gapdh* | fwd: | AGA AGG CTG GGG CTC ATT T |
| | rev: | CAG GAG GCA TTG CTG ATG AT |
| *Map1LC3-B* | fwd: | CGT CCT GGA CAA GAC CA |
| | rev: | CCA TTC ACC AGG AGG AA |
| *Sqstm1* | fwd: | AGG GAA CAC AGC AAG CT |
| | rev: | GCC AAA GTG TCC ATG TTT CA |
| *Hspb8* | fwd: | ATA CGT GGA AGT TTC AGG CA |
| | rev: | TCT CCA AAG GGT GAG TAC GG |
| *Bag3* | fwd: | ATG GAC CTG AGC GAT CTC A |
| | rev: | CAC GGG GAT GGG GAT GTA |
| *Tfeb* | fwd: | GCG GCA GAA GAA AGA CAA TC |
| | rev: | CTG CAT CCT CCG GAT GTA AT |
| *Rplp0* | fwd: | GGT GCC ACA CTC CAT CAT CA |
| | rev: | AGG CCT TGA CCT TTT CAG TAA GT |
| **Murine Genes** | | **Primer** |
| *MAP1LC3B* | fwd: | CAG CAT CCA ACC AAA ATC CC |
| | rev: | GTT GAC ATG GTC AGG TAC AAG |
| *SQSTM1* | fwd: | CCA GAG AGT TCC AGC ACA GA |
| | rev: | CCG ACT CCA TCT GTT CCT CA |
| *HSPB8* | fwd: | AGA GGA GTT GAT GGT GAA GAC C |
| | rev: | CTG CAG GAA GCT GGA TTT TC |
| *BAG3* | fwd: | GGG TGG AGG CAA AAC ACT AA |
| | rev: | AGA CAG TGC ACA ACC ACA GC |
| *TFEB* | fwd: | CAA GGC CAA TGA CCT GGA C |
| | rev: | AGC TCC CTG GAC TTT TGC AG |
| *RPLP0* | fwd: | GTG GGA GCA GAC AAT GTG GG |
| | rev: | TGC GCA TCA TGG TGT TCT TG |
| **Bacteria Gene** | | **Primer** |
| *Ampicillin*[3] | fwd: | ATG CTT TTC TGT GAC TGG TG |
| | rev: | GCT ATG TGG CGC GGT ATT AT |

*[1] Rev primer designed on HA-tag in frame +1,

*[2] Rev primer designed on His-tag in frame +2

*[3] Antibiotic resistance gene for ampicillin was used to normalize the amount of transfected G4C2 vector

## 9. **Lysates preparation and immunoblotting analysis**

$1x10^5$ HEK293T cells were plated in 12-well plates (3 wells for each condition to be tested; n = 3). 24 h after seeding cells were transfected with 2R (as negative control) or 66R plasmids and treated immediately after transfection with compounds for 24 h. For the silencing of *Prkaca*, *Prkacb* and *Eef2k*, cells were siRNA transfected 24 h after seeding and then transfected with plasmid 48 h after the siRNA transfection. 24 or 72 h after seeding, cells were harvested and centrifuged 5 min at 1,200 rpm at 4°C and then lysed for 15 min in RIPA lysis buffer supplemented with the Protease Inhibitor Cocktail (Sigma-Aldrich). Supernatants were collected after centrifugation at 12,000 rpm for 20 min and protein concentration was determined using the Bradford method (Sigma-Aldrich). Equal amounts of total proteins extract was separated on 12% or 15% SDS–PAGE gels, transferred onto PVDF membranes (Amersham Hybond, GE Healthcare) and blocked with 5% (v/v) nonfat dried milk powder (EuroClone) in Tris–buffered saline with 0.1% Tween 20 (Sigma-Aldrich) (TBS-T; pH 7.5). The membranes were then incubated overnight (O/N) at 4 °C in TBS-T with 5% (v/v) BSA with one of the primary antibodies (listed in **Table 2**) washed twice with TBS-T and then incubated for 1 h with horseradish peroxidase (HRP)-conjugated secondary antibodies (donkey anti-rabbit GE Healthcare Life Sciences #NA934, sheep anti-mouse GE Healthcare Life Sciences #NA931). Then membranes were washed with TBS-T and signal revealed using chemiluminescence detection kit reagents (Amersham ECL Select, GE Healthcare).

* $8x10^4$ NSC34 or $1.5x10^5$ SH-SY5Y cells were plated in 12-well plates (3 wells for each condition to be tested; n = 3). 24 h after seeding, cells were transfected as previously described and treated with compounds for 24 h. In experiments involving autophagy induction, 100 mM trehalose for the last 48 h were added to the cells. 48 or 72 h after seeding, cells were harvested and centrifuged 5 min at 100 X g at 4°C; the cell pellets were resuspended in PBS (Sigma- Aldrich) supplemented with the Protease Inhibitor Cocktail (Sigma-Aldrich) and homogenized using slight sonication to lyse cells and nuclei as previously described[203]. Total proteins were determined with the bicinchoninic acid method (QPRO BCA assay; Cyanagen). Equal amounts

of total proteins extract was separated on 10% or 15% SDS–PAGE gels, transferred onto PVDF membranes (polyscreen transfer membrane; Amersham) and blocked with 5% (v/v) non-fat dry milk powder (EuroClone) in Tris-buffered saline with 0.1% Tween 20 (TBS-T; pH 7.5). The membranes were then incubated O/N at 4°C with the primary antibodies (listed in **Table 2**), washed twice with TBS-T and then incubated for 1 h with horseradish peroxidase (HRP)-conjugated secondary antibodies (goat anti-rabbit Jackson Immunoresearch Laboratories 111–035-003, goat anti-mouse Jackson Immunoresearch Laboratories 115–035-003). Signal was revealed using chemiluminescence detection kit reagents (WESTAR ANTARES Western ECL Blotting Substrate; Cyanagen, XLS142). Membranes were subsequently processed with different antibodies to detect the levels of different proteins in the same sample, after stripping for 20 min at room temperature (RT) (Renew Stripping Buffer, Cyanagen).

**Table 2 | List of antibodies**

| Antibodies | Dilution | Source | Identifier |
|---|---|---|---|
| rabbit anti-HA affinity purified | 1:2,000 | Bethyl | A190-108A |
| rabbit monoclonal anti-P-PKA Substrates (RRXS*/T*) (100G7E) | 1:1,000 | Cell Signaling Technology | 9624 |
| mouse monoclonal anti- PKAα cat (A-2) | 1:500 | Santa Cruz Biotechnology | sc-28315 |
| rabbit polyclonal anti-PKA beta catalytic subunit | 1:500 | Abcam | ab94612 |
| rabbit anti-eEF2K | 1:1,000 | Cell Signaling Technology | 3692 |
| rabbit -Phospho-eEF2 (Thr56) | 1:1,000 | Cell Signaling Technology | 2331 |
| rabbit anti-eEF2 | 1:1,000 | Cell Signaling Technology | 2332 |
| rabbit monoclonal anti-GAPDH (D16H11) | 1:3,000 | Cell Signaling Technology | 5174 |
| mouse monoclonal anti-αTubulin (TU-02) | 1:3,000 | Santa Cruz Biotechnology | sc-8035 |
| rabbit polyclonal anti-LC3A/B | 1:4,000 (WB)<br>1:500 (IF) | Sigma-Aldrich | L8918 |
| rabbit polyclonal anti-SQSTM1 | 1:4,000 (WB) | Sigma-Aldrich | P0067 |
| rabbit polyclonal anti-p62/SQSTM1 | 1:500 (IF) | Abcam | ab91526 |

| | | | |
|---|---|---|---|
| rabbit polyclonal anti-poly-GP | 1:2,000 | Merck | ABN455 |
| mouse monoclonal anti-GFP | 1:5,000 | Immunological Sciences | MAB-943459 |
| mouse monoclonal anti-αTubulin | 1:4,000 | Sigma-Aldrich | T6199 |
| Mouse monoclonal anti-FLAG M2 | 1:2,000 | Sigma-Aldrich | F1804 |

## 10. **Filter retardation assay (FRA) ***

Also known as Filter Trap, it is a technique based on the proteins or protein aggregates retention on 0.22 µm acetate cellulose membrane by vacuum application. FRA was preformed using a Bio-Dot SF Microfiltration Apparatus (Bio-Rad) having 48 wells with dimensions of 7 mm x 0.75 mm. The wells are arranged in 8 rows and 6 columns. 8 µg of the total proteins were filtered through a 0.2-µm cellulose acetate membrane (Whatman). The 0.22 µm acetate cellulose membrane was pre-wetted in PBS and then treated with 20% methanol in water. The membrane was washed twice with 100 µL of PBS, before and after loading the samples. Then membrane was rinsed with 20% MeOH and washed in water. Slot-blots were then probed as described for immunoblotting. ChemiDoc XRS System (Bio-Rad, Hercules, California, USA) was used for the image acquisition of FRA. Optical density of samples assayed with FRA was detected and analysed using the Image Lab software (Bio-Rad). Statistical analyses have been performed using the relative optical densities defined as the ratio between optical densities of each independent biological sample (n = 3) and the mean optical density.

## 11. Immunostaining and confocal microscope analysis *

NSC34 cells were seeded on coverslips at a density of $3x10^4$ cells per well (in 24-well plates), and the day after were transfected and/or treated with compounds. After treatments, cells were fixed at 37°C for 25 min using a solution 1:1 of 4% paraformaldehyde (Sigma-Aldrich) in PB 0.2 M [solution made of $KH_2PO_4$ (0.06 M) and $Na_2HPO_4$ (0.26 M)] and 4% (v/v) sucrose (Sigma-Aldrich) in PB 0.2 M. Then, fixing solution was removed and cold methanol was added for 10min to complete the fixation. Cell permeabilization was performed using a solution of 0.2% TRITON X100 (Sigma-Aldrich) followed by incubation for 1 h in blocking solution. Incubation with the primary antibody was kept O/N at 4°C. Incubation with the fluorescent-tagged secondary antibody was preceded by three washes with PBS, to remove the excess of primary antibody. Nuclei were stained with DAPI (Sigma-Aldrich). The primary antibodies used are listed in **Table 2**. The following secondary antibodies were used: goat anti-rabbit Alexa 594 (Thermo Scientific, A-11012; dilution 1:1,000). All the primary and secondary antibodies were diluted in blocking solution (5% nonfat dried milk in 1X PBS-T). Coverslips were mounted on a glass support using MOWIOL and images were acquired using Eclipse Ti2 (Nikon, Netherlands) confocal microscope equipped with A1 plus camera (Nikon) and processed with the NIS-Elements software (Nikon) processed with Fiji ImageJ distribution[204] based on ImageJ version: 2.0.0-rc-69/1.52p.

## 12. β-galactosidase assay *

NSC34 cells were plated in 24-well plate at density of $4x10^4$ cells/well (6 wells for each condition to be tested) and transfected for 48 h with 0.4 µg of pCMV-βgal or pSV-βgal plasmids. Cells were lysed in 250 µL of lysis buffer (Promega) and 100 µL of samples were added to 750 µL of assay buffer (60 mM $Na_2HPO_4$ 40 mM $NaH_2PO_4$ 10 mM KCl, 1 mM $MgSO_4$, pH 7.0), in presence of 4 mg/mL of β-galactosidase substrate o-nitrophenyl-b-D-galactopyraniside (ONPG; Sigma-Aldrich) and incubated at 37°C until yellow colour appearance. Then, 500 µL of 1 M $Na_2CO_3$ were added and 200 µL of the final solution were transferred into a 96-well plate and 420-nm absorbance was evaluated using Enspire plate-reader (PerkinElmer).

## 13. **Polysomal profiling**

Polysomal profiling was performed according to previously described protocols[205]. Briefly, cells were seeded in 10 $cm^2$ dishes, treated with CHX (10µg/mL) for 4 min and then lysed in 300 µL of cold hypotonic lysis buffer [10 mM NaCl, 10 mM $MgCl_2$•$6H_2O$, 10 mM Tris–HCl, pH 7.5, 1% Triton X-100, 0.2 U/µl Ribolock RNase inhibitor, 0.0005 U/µl DNaseI, CHX 10 µg/mL and 1 mM dithio-threitol, 1% sodium deoxycholate]. Lysates were centrifuged at 4°C for 5 min at 13,000 rpm to pellet cell debris. The cytoplasmic lysates loaded on a linear 10%–40% [w/v] sucrose gradient and centrifuged in a SW41Ti rotor (Beckman) for 1 h 30 min at 39,000 rpm at 4°C in a Beckman Optima XPN-100 Ultracentrifuge. Fractions of 1 mL of volume were then collected monitoring the absorbance at 254 nm with the UA-6 UV/VIS detector (Teledyne Isco).

## 14. **Extraction of polysomal RNA and RT-qPCR analysis**

Polysomal RNAs were isolated from single fractions along sucrose gradient as described in Tebaldi *et al*.[206]. Collected fractions (polysomal and subpolysomal) were incubated with proteinase K (Thermo Scientific) and 1% SDS for 1 h 45 min at 37°C. After acid phenol–chloroform extraction (Ambion) and isopropanol precipitation, polysomal RNA was re-suspended in 20 µL of water and RNA quantification was determined by 260/280 absorbance ratios using NanoDrop 2000 spectrophotometer (Thermo Scientific). The retrotranscription reaction was performed starting from 1 µL of RNA using the RevertAid First Strand cDNA synthesis kit (Thermo Scientific). qPCR was carried out using the CFX Connect Real-Time PCR Detection System (BioRad) and Kapa Syber Fast qPCR Mastermix (Kapa Biosystems). qPCR were run in three biological and three technical replicates. The percentage of each transcript distribution along the profile was obtained using the following formula:

$$\% [mRNA]_n = [2^{\wedge 40-Ct\ mRNA}]_n / \Sigma_{n=0->12} [2^{\wedge 40-Ct\ mRNA}]_n$$

where “n” is the number of the fraction, “% $[mRNA]_n$” is the percentage of mRNA of choice in each fraction.

## 15. Fly husbandry and lines *

Animals were raised at low density, at 25°C, on a standard food medium containing 9 g/L agar (ZN5 B&V), 75 g/L corn flour, 60 g/L white sugar, 30 g/L brewer yeast (Acros Organic), 50 g/L fresh yeast, and 50 ml/L molasses (Biosigma), along with nipagin and propionic acid (Acros Organic). The fly lines were obtained from the Bloomington *Drosophila* Stock Center: p{UAS-GGGGCC.36} attP40 (B58688)[65], and from Vienna Drosophila Research Center $w^{1118}$ (v60000), UAS\Pka-C1-RNAi p{VSH330111} (v330111) (*Pka-C1* UniProtKB code P12370) and M{UAS-eEF2.ORF.3xHA}ZH-86Fb (F001014) from the Zurich ORFeome Project (FlyORF).

## 16. H89 treatment in *Drosophila* *

One day old animals were transferred in a plastic vial (15 animals for each genotype) containing a Whatmann 3 MM paper disc imbibed with 200 µL of H89 diluted to 10 µM final concentration in a 5% sucrose solution with 0.1% DMSO or sucrose and DMSO alone.

## 17. Motility assays *

One day-old animals of each genotype were transferred in a plastic vial without food (15 animals for each genotype), and their ability to climb up the empty vial after a knock-down to the bottom was analyzed, as previously described[175,207] . The number of flies that were able to climb half of the tube in 15 sec was recorded. The total number of flies alive was counted every day. Values were expressed as percentage of success with respect to the total number of flies in the vial. For each genotype the test was repeated 20 times for each time-point. After the test, adults were transferred in vials with food and vials were changed every two days with exception of the animals used for the treatment with the drug that were transferred in vials containing 200 µL of a 5% sucrose solution with 0.1% DMSO or sucrose and DMSO alone. In the motility assay the number of survived flies was scored over time. The number of survived flies was also scored. Data are represented as a curve of progressive motility impairment. The statistical analysis of variance (one-way ANOVA) was performed using PRISM GraphPad Software (CA). Bars represent the standard deviation (SD). Experiments were repeated at least three times.

## 18. RNA extraction from *Drosophila larvae* and RT-qPCR

Total RNAs were isolated, using 1mL TRI Reagent (Thermo Scientific), from larvae (n=5 for each genotype) of the following genotypes: $w^{1118}$ wild-type control and *Actin-Gal4;UAS-Pka-C1-RNAi*. The retrotranscription reaction was performed starting from 1 µg of RNA using the RevertAid First Strand cDNA synthesis kit (Thermo Scientific) according to the manufacturer's protocol. PCR primers were designed as follows:

*Pka* Fw: 5'- TTCAGTTCCCCTTCCTCGTC -3'

*Pka* Rv: 5'- GAGGTCCAAGTAGTGCAGGT -3'

*Actin* Fw: 5'- CAGATCATGTTCGAGACCTTCAAC -3'

*Actin* Rv: 5'- ACGACCGGAGGCGTACAG -3'

## 19. Statistical analysis

Values are expressed as mean ± SD or ± SEM of three independent biological experiments conducted in technical triplicates. Student's t-test, 1-way and 2-way ANOVA were employed to determine statistical significance between control and test groups. Values of $*P<0.05$, $**P<0.01$, $***P<0.001$ and $****P<0.0001$ were considered significant. Data were plotted by GraphPad Prism 6 software.

## Funding

My PhD project was funded by the Fondazione Cassa di Risparmio di Trento e Rovereto (CARITRO) (Drug repositioning project #40102838) coordinated by Prof Alessandro Quattrone and Prof Alessandro Provenzani. Starting from April 2019, my PhD project has been funded by the Fondazione AriSLA (project TARGET RAN #40103385) coordinated by Prof Alessandro Provenzani and in collaboration with Prof Angelo Poletti (University of Milano).

# *References*

1. Rowland, L. P. & Shneider, N. A. Amyotrophic Lateral Sclerosis. *N. Engl. J. Med.* **344**, 1688–1700 (2001).

2. Corcia, P. & Meininger, V. Management of amyotrophic lateral sclerosis. *Drugs* **68**, 1037–48 (2008).

3. Kanouchi, T., Ohkubo, T. & Yokota, T. Can regional spreading of amyotrophic lateral sclerosis motor symptoms be explained by prion-like propagation? *J Neurol Neurosurg Psychiatry* **83**, 739–745 (2012).

4. Wijesekera, L. C. & Leigh, P. N. Amyotrophic lateral sclerosis. *Orphanet J. Rare Dis.* **4**, 1–22 (2009).

5. Kiernan, M. C. *et al.* Amyotrophic lateral sclerosis. *Lancet* **377**, 942–955 (2011).

6. Polkey, M. I., Lyall, R. A., Moxham, J. & Leigh, P. N. Respiratory aspects of neurological disease. *J Neurol Neurosurg Psychiatry* **66**, 5–15 (1999).

7. Brooks, B. R., Miller, R. G., Swash, M. & Munsat, T. L. El Escorial revisited: revised criteria for the diagnosis of amyotrophic lateral sclerosis. *Amyotroph. Lateral Scler. Other Motor Neuron Disord.* **1**, 293–9 (2000).

8. Taylor, J. P., Brown, R. H. & Cleveland, D. W. Decoding ALS: from genes to mechanism. *Nature* **539**, 197–206 (2016).

9. Rosen, D. R. *et al.* Mutations in Cu/Zn superoxide dismutase gene are associated with familial amyotrophic lateral sclerosis. *Nature* **362**, 59–62 (1993).

10. Sreedharan, J. *et al.* TDP-43 mutations in familial and sporadic amyotrophic lateral sclerosis. *Science* **319**, 1668–72 (2008).

11. Mejzini, R. *et al.* ALS Genetics, Mechanisms, and Therapeutics: Where Are We Now? *Front. Neurosci.* **13**, 1310 (2019).

12. Kirby, J., Al Sultan, A., Waller, R. & Heath, P. The genetics of amyotrophic lateral sclerosis: current insights. *Degener. Neurol. Neuromuscul. Dis.* **6**, 49 (2016).

13. Bird, T. D. *et al.* A clinical pathological comparison of three families with frontotemporal dementia and identical mutations in the tau gene (P301L). *Brain* **122 ( Pt 4)**, 741–56 (1999).

14. Goodman, L. D. & Bonini, N. M. Repeat-associated non-AUG (RAN) translation mechanisms are running into focus for GGGGCC-repeat associated ALS/FTD. *Prog. Neurobiol.* 101697 (2019).

15. Snowden, J. S. *et al.* Distinct clinical and pathological phenotypes in frontotemporal dementia associated with MAPT, PGRN and C9orf72 mutations. *Amyotroph. Lateral Scler. Front. Degener.* **16**, 497–505 (2015).

16. Abramzon, Y. A., Fratta, P., Traynor, B. J. & Chia, R. The Overlapping Genetics of Amyotrophic Lateral Sclerosis and Frontotemporal Dementia. *Front. Neurosci.* **14**, 42 (2020).

17. Bensimon, G., Lacomblez, L. & Meininger, V. A controlled trial of riluzole in amyotrophic lateral sclerosis. ALS/Riluzole Study Group. *N. Engl. J. Med.* **330**, 585–91 (1994).

18. Lacomblez, L. *et al.* A confirmatory dose-ranging study of riluzole in ALS. ALS/Riluzole Study Group-II. *Neurology* **47**, S242-50 (1996).

19. Sawada, H. Clinical efficacy of edaravone for the treatment of amyotrophic lateral sclerosis. *Expert Opin. Pharmacother.* **18**, 735–738 (2017).

20. Tsai, R. M. & Boxer, A. L. Treatment of Frontotemporal Dementia. *Curr. Treat. Options Neurol.* **16**, 319 (2014).

21. Fecto, F. <emph type="ital">SQSTM1</emph> Mutations in Familial and Sporadic Amyotrophic Lateral Sclerosis. *Arch. Neurol.* **68**, 1440 (2011).

22. Johnson, J. O. *et al.* Exome Sequencing Reveals VCP Mutations as a Cause of Familial ALS. *Neuron* **68**, 857–864 (2010).

23. Neumann, M. *et al.* A new subtype of frontotemporal lobar degeneration with FUS pathology. *Brain* **132**, 2922–31 (2009).

24. Lamb, R. *et al.* A novel TBK1 mutation in a family with diverse frontotemporal dementia spectrum disorders. *Cold Spring Harb. Mol. case Stud.* **5**, a003913

(2019).

25. Chaussenot, A. *et al.* Screening of CHCHD10 in a French cohort confirms the involvement of this gene in frontotemporal dementia with amyotrophic lateral sclerosis patients. *Neurobiol. Aging* **35**, 2884.e1-2884.e4 (2014).

26. Ji, A.-L., Zhang, X., Chen, W.-W. & Huang, W.-J. Genetics insight into the amyotrophic lateral sclerosis/frontotemporal dementia spectrum. *J. Med. Genet.* **54**, 145–154 (2017).

27. Morita, M. *et al.* A locus on chromosome 9p confers susceptibility to ALS and frontotemporal dementia. *Neurology* **66**, 839–44 (2006).

28. Vance, C. *et al.* Familial amyotrophic lateral sclerosis with frontotemporal dementia is linked to a locus on chromosome 9p13.2-21.3. *Brain* **129**, 868–76 (2006).

29. DeJesus-Hernandez, M. *et al.* Expanded GGGGCC hexanucleotide repeat in noncoding region of C9ORF72 causes chromosome 9p-linked FTD and ALS. *Neuron* **72**, 245–56 (2011).

30. Renton, A. E. *et al.* A hexanucleotide repeat expansion in C9ORF72 is the cause of chromosome 9p21-linked ALS-FTD. *Neuron* **72**, 257–68 (2011).

31. Majounie, E. *et al.* Frequency of the C9orf72 hexanucleotide repeat expansion in patients with amyotrophic lateral sclerosis and frontotemporal dementia: a cross-sectional study. *Lancet Neurol.* **11**, 323–330 (2012).

32. Cooper-Knock, J. *et al.* Clinico-pathological features in amyotrophic lateral sclerosis with expansions in C9ORF72. *Brain* **135**, 751–64 (2012).

33. Ishiura, H. *et al.* C9ORF72 repeat expansion in amyotrophic lateral sclerosis in the Kii peninsula of Japan. *Arch. Neurol.* **69**, 1154–8 (2012).

34. Jang, J.-H. *et al.* Analysis of the C9orf72 hexanucleotide repeat expansion in Korean patients with familial and sporadic amyotrophic lateral sclerosis. *Neurobiol. Aging* **34**, 1311.e7–9 (2013).

35. Balendra, R. & Isaacs, A. M. C9orf72-mediated ALS and FTD: multiple pathways to disease. doi:10.1038/s41582-018-0047-2

36. Gijselinck, I. *et al.* A C9orf72 promoter repeat expansion in a Flanders-Belgian cohort with disorders of the frontotemporal lobar degeneration-amyotrophic lateral sclerosis spectrum: a gene identification study. *Lancet Neurol.* **11**, 54–65 (2012).

37. Waite, A. J. *et al.* Reduced C9orf72 protein levels in frontal cortex of amyotrophic lateral sclerosis and frontotemporal degeneration brain with the C9ORF72 hexanucleotide repeat expansion. *Neurobiol. Aging* **35**, 1779.e5-1779.e13 (2014).

38. Gijselinck, I. *et al.* The C9orf72 repeat size correlates with onset age of disease, DNA methylation and transcriptional downregulation of the promoter. *Mol. Psychiatry* **21**, 1112–1124 (2016).

39. Neumann, M. *et al.* Ubiquitinated TDP-43 in frontotemporal lobar degeneration and amyotrophic lateral sclerosis. *Science* **314**, 130–3 (2006).

40. Stewart, H. *et al.* Clinical and pathological features of amyotrophic lateral sclerosis caused by mutation in the C9ORF72 gene on chromosome 9p. *Acta Neuropathol.* **123**, 409–17 (2012).

41. Al-Sarraj, S. *et al.* p62 positive, TDP-43 negative, neuronal cytoplasmic and intranuclear inclusions in the cerebellum and hippocampus define the pathology of C9orf72-linked FTLD and MND/ALS. *Acta Neuropathol.* **122**, 691–702 (2011).

42. Mann, D. M. A. *et al.* Dipeptide repeat proteins are present in the p62 positive inclusions in patients with frontotemporal lobar degeneration and motor neurone disease associated with expansions in C9ORF72. *Acta Neuropathol. Commun.* **1**, 68 (2013).

43. Cooper-Knock, J., Shaw, P. J. & Kirby, J. The widening spectrum of C9ORF72-related disease; genotype/phenotype correlations and potential modifiers of clinical phenotype. *Acta Neuropathol.* **127**, 333–45 (2014).

44. Lagier-Tourenne, C. Target degradation of sense and antisense C9orf72 RNA foci as theraphy for ALS and FTD. (2013).

45. Mizielinska, S. *et al.* C9orf72 frontotemporal lobar degeneration is

characterised by frequent neuronal sense and antisense RNA foci. *Acta Neuropathol.* **126**, 845–857 (2013).

46. Todd, T. W. & Petrucelli, L. Insights into the pathogenic mechanisms of Chromosome 9 open reading frame 72 (C9orf72) repeat expansions. *J. Neurochem.* **138**, 145–162 (2016).

47. Wen, X., Westergard, T., Pasinelli, P. & Trotti, D. Pathogenic determinants and mechanisms of ALS/FTD linked to hexanucleotide repeat expansions in the C9orf72 gene. *Neurosci. Lett.* **636**, 16–26 (2017).

48. Levine, T. P., Daniels, R. D., Gatta, A. T., Wong, L. H. & Hayes, M. J. The product of C9orf72, a gene strongly implicated in neurodegeneration, is structurally related to DENN Rab-GEFs. *Bioinformatics* **29**, 499–503 (2013).

49. Farg, M. A. *et al.* C9ORF72, implicated in amytrophic lateral sclerosis and frontotemporal dementia, regulates endosomal trafficking. *Hum. Mol. Genet.* **23**, 3579–95 (2014).

50. Jiang, J. & Ravits, J. Pathogenic Mechanisms and Therapy Development for C9orf72 Amyotrophic Lateral Sclerosis/Frontotemporal Dementia. *Neurotherapeutics* **16**, 1115–1132 (2019).

51. Sutcliffe, J. S. *et al.* DNA methylation represses FMR-1 transcription in fragile X syndrome. *Hum. Mol. Genet.* **1**, 397–400 (1992).

52. Greene, E., Mahishi, L., Entezam, A., Kumari, D. & Usdin, K. Repeat-induced epigenetic changes in intron 1 of the frataxin gene and its consequences in Friedreich ataxia. *Nucleic Acids Res.* **35**, 3383–90 (2007).

53. Xi, Z. *et al.* Hypermethylation of the CpG island near the G4C2 repeat in ALS with a C9orf72 expansion. *Am. J. Hum. Genet.* **92**, 981–9 (2013).

54. Haeusler, A. R. *et al.* C9orf72 nucleotide repeat structures initiate molecular cascades of disease. *Nature* **507**, 195–200 (2014).

55. Koppers, M. *et al.* C9orf72 ablation in mice does not cause motor neuron degeneration or motor deficits. *Ann. Neurol.* **78**, 426–38 (2015).

56. Fratta, P. *et al.* Homozygosity for the C9orf72 GGGGCC repeat expansion in

frontotemporal dementia. *Acta Neuropathol.* **126**, 401–409 (2013).

57. Cooper-Knock, J. *et al.* C9ORF72 transcription in a frontotemporal dementia case with two expanded alleles. *Neurology* **81**, 1719–21 (2013).

58. Niblock, M. *et al.* Retention of hexanucleotide repeat-containing intron in C9orf72 mRNA: implications for the pathogenesis of ALS/FTD. *Acta Neuropathol. Commun.* **4**, 18 (2016).

59. Donnelly, C. J. *et al.* RNA toxicity from the ALS/FTD C9ORF72 expansion is mitigated by antisense intervention. *Neuron* **80**, 415–28 (2013).

60. Lee, Y. B. *et al.* Hexanucleotide repeats in ALS/FTD form length-dependent RNA Foci, sequester RNA binding proteins, and are neurotoxic. *Cell Rep.* **5**, 1178–1186 (2013).

61. Sareen, D. *et al.* Targeting RNA foci in iPSC-derived motor neurons from ALS patients with a C9ORF72 repeat expansion. *Sci. Transl. Med.* **5**, 208ra149 (2013).

62. Xu, Z. *et al.* Expanded GGGGCC repeat RNA associated with amyotrophic lateral sclerosis and frontotemporal dementia causes neurodegeneration. *Proc. Natl. Acad. Sci. U. S. A.* **110**, 7778–83 (2013).

63. Cooper-Knock, J. *et al.* Sequestration of multiple RNA recognition motif-containing proteins by C9orf72 repeat expansions. *Brain* **137**, 2040–2051 (2014).

64. Cooper, T. A., Wan, L. & Dreyfuss, G. RNA and disease. *Cell* **136**, 777–93 (2009).

65. Mizielinska, S. *et al.* C9orf72 repeat expansions cause neurodegeneration in Drosophila through arginine-rich proteins. *Science* **345**, 1192–1194 (2014).

66. Moens, T. G. *et al.* Sense and antisense RNA are not toxic in Drosophila models of C9orf72-associated ALS/FTD. *Acta Neuropathol.* **135**, 445–457 (2018).

67. Mori, K. *et al.* Bidirectional transcripts of the expanded C9orf72 hexanucleotide repeat are translated into aggregating dipeptide repeat

proteins. *Acta Neuropathol.* **126**, 881–893 (2013).

68. Mori, K. *et al.* The C9orf72 repeat is translated into aggregating dipeptide-repeat proteins in FTD/ALS. *Sci. Mag* **339**, 1335–1338 (2013).

69. Ash, P. E. A. *et al.* Unconventional translation of C9ORF72 GGGGCC expansion generates insoluble polypeptides specific to c9FTD/ALS. *Neuron* **77**, 639–46 (2013).

70. Gendron, T. F. *et al.* Antisense transcripts of the expanded C9ORF72 hexanucleotide repeat form nuclear RNA foci and undergo repeat-associated non-ATG translation in c9FTD/ALS. *Acta Neuropathol.* **126**, 829–44 (2013).

71. Zu, T. *et al.* RAN proteins and RNA foci from antisense transcripts in C9ORF72 ALS and frontotemporal dementia. *Proc. Natl. Acad. Sci. U. S. A.* **110**, E4968-77 (2013).

72. Mackenzie, I. R. *et al.* Dipeptide repeat protein pathology in C9ORF72 mutation cases: clinico-pathological correlations. *Acta Neuropathol.* **126**, 859–79 (2013).

73. Su, Z. *et al.* Discovery of a Biomarker and Lead Small Molecules to Target r(GGGGCC)-Associated Defects in c9FTD/ALS. *Neuron* **83**, 1043–1050 (2014).

74. Gendron, T. F. *et al.* Poly(GP) proteins are a useful pharmacodynamic marker for C9ORF72-associated amyotrophic lateral sclerosis. *Sci. Transl. Med.* **9**, (2017).

75. Lehmer, C. *et al.* Poly- GP in cerebrospinal fluid links *C9orf72* -associated dipeptide repeat expression to the asymptomatic phase of ALS / FTD. *EMBO Mol. Med.* **9**, 859–868 (2017).

76. Gendron, T. F., Belzil, V. V, Zhang, Y.-J. & Petrucelli, L. Mechanisms of toxicity in C9FTLD/ALS. *Acta Neuropathol.* **127**, 359–76 (2014).

77. Mizielinska, S. & Isaacs, A. M. C9orf72 amyotrophic lateral sclerosis and frontotemporal dementia. *Curr. Opin. Neurol.* **27**, 515–523 (2014).

78. Westergard, T. *et al.* Cell-to-Cell Transmission of Dipeptide Repeat Proteins

Linked to C9orf72-ALS/FTD. *Cell Rep.* **17**, 645–652 (2016).

79. Zhou, Q. *et al.* Antibodies inhibit transmission and aggregation of C9orf72 poly-GA dipeptide repeat proteins. *EMBO Mol. Med.* **9**, 687–702 (2017).

80. Saberi, S. *et al.* Sense-encoded poly-GR dipeptide repeat proteins correlate to neurodegeneration and uniquely co-localize with TDP-43 in dendrites of repeat-expanded C9orf72 amyotrophic lateral sclerosis. *Acta Neuropathol.* **135**, (2018).

81. Wen, X. *et al.* Antisense proline-arginine RAN dipeptides linked to C9ORF72-ALS/FTD form toxic nuclear aggregates that initiate invitro and invivo neuronal death. *Neuron* **84**, 1213–1225 (2014).

82. Freibaum, B. D. *et al.* GGGGCC repeat expansion in C9orf72 compromises nucleocytoplasmic transport. *Nature* **525**, 129–33 (2015).

83. Jovičić, A. *et al.* Modifiers of C9orf72 dipeptide repeat toxicity connect nucleocytoplasmic transport defects to FTD/ALS. *Nat. Neurosci.* **18**, 1226–1229 (2015).

84. Yamakawa, M. *et al.* Characterization of the dipeptide repeat protein in the molecular pathogenesis of c9FTD/ALS. *Hum. Mol. Genet.* **24**, 1630–1645 (2015).

85. Khosravi, B. *et al.* Cell-to-cell transmission of C9orf72 poly-(Gly-Ala) triggers key features of ALS / FTD. *EMBO J.* (2020).

86. Jiang, J. *et al.* Gain of Toxicity from ALS/FTD-Linked Repeat Expansions in C9ORF72 Is Alleviated by Antisense Oligonucleotides Targeting GGGGCC-Containing RNAs. *Neuron* **90**, 535–550 (2016).

87. Zamiri, B., Reddy, K., Macgregor, R. B. & Pearson, C. E. TMPyP4 porphyrin distorts RNA G-quadruplex structures of the disease-associated r(GGGGCC)n repeat of the C9orf72 gene and blocks interaction of RNA-binding proteins. *J. Biol. Chem.* **289**, 4653–9 (2014).

88. Zhang, K. *et al.* The C9orf72 repeat expansion disrupts nucleocytoplasmic transport. *Nature* **525**, 56–61 (2015).

89. Wang, Z.-F. *et al.* The Hairpin Form of r(G4C2)exp in c9ALS/FTD Is Repeat-Associated Non-ATG Translated and a Target for Bioactive Small Molecules. *Cell Chem. Biol.* **26**, 179-190.e12 (2019).

90. Shi, Y. *et al.* Haploinsufficiency leads to neurodegeneration in C9ORF72 ALS/FTD human induced motor neurons. *Nat. Med.* **24**, 313–325 (2018).

91. Goodman, L. D. *et al.* Toxic expanded GGGGCC repeat transcription is mediated by the PAF1 complex in C9orf72-associated FTD. *Nat. Neurosci.* **22**, 863–874 (2019).

92. Goodman, L. D. *et al.* eIF4B and eIF4H mediate GR production from expanded G4C2 in a Drosophila model for C9orf72-associated ALS. *Acta Neuropathol. Commun.* **7**, 62 (2019).

93. Cristofani, R. *et al.* The small heat shock protein B8 (HSPB8) efficiently removes aggregating species of dipeptides produced in C9ORF72-related neurodegenerative diseases. *Cell Stress Chaperones* **23**, 1–12 (2018).

94. Zhang, K. *et al.* Stress Granule Assembly Disrupts Nucleocytoplasmic Transport. *Cell* **173**, 958-971.e17 (2018).

95. Becker, L. A. *et al.* Therapeutic reduction of ataxin-2 extends lifespan and reduces pathology in TDP-43 mice. *Nature* **544**, 367–371 (2017).

96. Sonenberg, N., Morgan, M. A., Merrick, W. C. & Shatkin, A. J. A polypeptide in eukaryotic initiation factors that crosslinks specifically to the 5’-terminal cap in mRNA. *Proc. Natl. Acad. Sci. U. S. A.* **75**, 4843–7 (1978).

97. Jackson, R. J., Hellen, C. U. T. & Pestova, T. V. The mechanism of eukaryotic translation initiation and principles of its regulation. *Nat. Rev. Mol. Cell Biol.* **11**, 113–127 (2010).

98. Kumar, P., Hellen, C. U. T. & Pestova, T. V. Toward the mechanism of eIF4F-mediated ribosomal attachment to mammalian capped mRNAs. *Genes Dev.* **30**, 1573–1588 (2016).

99. Kozak, M. Influences of mRNA secondary structure on initiation by eukaryotic ribosomes. *Proc. Natl. Acad. Sci. U. S. A.* **83**, 2850–4 (1986).

100. Dever, T. E. & Green, R. The elongation, termination, and recycling phases of translation in eukaryotes. *Cold Spring Harb. Perspect. Biol.* **4**, a013706 (2012).

101. Kapur, M., Monaghan, C. E. & Ackerman, S. L. Regulation of mRNA Translation in Neurons — A Matter of Life and Death. *Neuron* **96**, 616–637 (2017).

102. Price, N. T. *et al.* Identification of the phosphorylation sites in elongation factor-2 from rabbit reticulocytes. *FEBS Lett.* **282**, 253–8 (1991).

103. U, C., A, N. & O, N. Functional Properties of Phosphorylated Elongation Factor 2. *Eur. J. Biochem.* **191**, (1990).

104. Liu, R. & Proud, C. G. Eukaryotic elongation factor 2 kinase as a drug target in cancer, and in cardiovascular and neurodegenerative diseases. *Acta Pharmacol. Sin.* **37**, 285–294 (2016).

105. Bellato, H. & Hajj, G. Translational Control by eIF2alpha in Neurons: Beyond the Stress Response. *Cytoskeleton* **565**, 551–565 (2016).

106. Kozak, M. Features in the 5′ non-coding sequences of rabbit α and β-globin mRNAs that affect translational efficiency. *J. Mol. Biol.* **235**, 95–110 (1994).

107. Thakor, N. & Holcik, M. IRES-mediated translation of cellular messenger RNA operates in eIF2α- independent manner during stress. *Nucleic Acids Res.* **40**, 541–52 (2012).

108. Zu, T. *et al.* Non-ATG-initiated translation directed by microsatellite expansions. *Proc. Natl. Acad. Sci. U. S. A.* **108**, 260–5 (2011).

109. Banez-Coronel, M. & Ranum, L. P. W. Repeat-associated non-AUG (RAN) translation: insights from pathology. *Lab. Investig. 2019 997* **99**, 929–942 (2019).

110. Bañez-Coronel, M. *et al.* RAN Translation in Huntington Disease. *Neuron* **88**, 667–677 (2015).

111. Zerylnick, C., Torroni, A., Sherman, S. L. & Warren, S. T. Normal variation at the myotonic dystrophy locus in global human populations. *Am. J. Hum.*

*Genet.* **56**, 123–30 (1995).

112. Kearse, M. G. *et al. CGG Repeat-Associated Non-AUG Translation Utilizes a Cap-Dependent Scanning Mechanism of Initiation to Produce Toxic Proteins*. *Molecular Cell* **62**, (2016).

113. Green, K. M. *et al.* RAN translation at C9orf72-associated repeat expansions is selectively enhanced by the integrated stress response. *Nat. Commun.* (2017).

114. Tabet, R. *et al.* CUG initiation and frameshifting enable production of dipeptide repeat proteins from ALS/FTD C9ORF72 transcripts. *Nat. Commun.* **9**, 152 (2018).

115. Sonobe, Y. *et al.* Translation of dipeptide repeat proteins from the C9ORF72 expanded repeat is associated with cellular stress. *Neurobiol. Dis.* **116**, 155–165 (2018).

116. Starck, S. R. *et al.* Translation from the 5' untranslated region shapes the integrated stress response. *Science (80-. ).* **351**, aad3867–aad3867 (2016).

117. Starck, S. R. *et al.* Leucine-tRNA initiates at CUG start codons for protein synthesis and presentation by MHC class I. *Science* **336**, 1719–23 (2012).

118. Yamada, S. B. *et al.* RPS25 is required for efficient RAN translation of C9orf72 and other neurodegenerative disease-associated nucleotide repeats. *Nat. Neurosci.* **22**, 1383–1388 (2019).

119. Hertz, M. I., Landry, D. M., Willis, A. E., Luo, G. & Thompson, S. R. Ribosomal protein S25 dependency reveals a common mechanism for diverse internal ribosome entry sites and ribosome shunting. *Mol. Cell. Biol.* **33**, 1016–26 (2013).

120. Shi, Y. *et al.* Therapeutic potential of targeting IRES-dependent c-myc translation in multiple myeloma cells during ER stress. *Oncogene* **35**, 1015–24 (2016).

121. Cheng, W. *et al.* C9ORF72 GGGGCC repeat-associated non-AUG translation is upregulated by stress through eIF2α phosphorylation. *Nat. Commun.* **9**,

(2018).

122. Westergard, T. *et al.* Repeat-associated non-AUG translation in C9orf72-ALS/FTD is driven by neuronal excitation and stress. *EMBO Mol. Med.* e9423 (2019).

123. Rogers, G. W., Richter, N. J., Lima, W. F. & Merrick, W. C. Modulation of the helicase activity of eIF4A by eIF4B, eIF4H, and eIF4F. *J. Biol. Chem.* **276**, 30914–22 (2001).

124. Satoh, J.-I. *et al.* Molecular Network Analysis Suggests a Logical Hypothesis for the Pathological Role of C9orf72 in Amyotrophic Lateral Sclerosis/Frontotemporal Dementia. *J. Cent. Nerv. Syst. Dis.* **6**, JCNSD.S18103 (2014).

125. Tai, H.-C. & Schuman, E. M. Ubiquitin, the proteasome and protein degradation in neuronal function and dysfunction. *Nat. Rev. Neurosci.* **9**, 826–38 (2008).

126. Kraft, C., Peter, M. & Hofmann, K. Selective autophagy: ubiquitin-mediated recognition and beyond. *Nat. Cell Biol.* **12**, 836–41 (2010).

127. Feng, Y., He, D., Yao, Z. & Klionsky, D. J. The machinery of macroautophagy. *Cell Res.* **24**, 24–41 (2014).

128. Rubinsztein, D. C. The roles of intracellular protein-degradation pathways in neurodegeneration. *Nature* **443**, 780–6 (2006).

129. Lippai, M. & Lőw, P. The role of the selective adaptor p62 and ubiquitin-like proteins in autophagy. *Biomed Res. Int.* 1–11 (2014).

130. Thrower, J. S., Hoffman, L., Rechsteiner, M. & Pickart, C. M. Recognition of the polyubiquitin proteolytic signal. *EMBO J.* **19**, 94–102 (2000).

131. Coux, O., Tanaka, K. & Goldberg, A. L. Structure and functions of the 20S and 26S proteasomes. *Annu. Rev. Biochem.* **65**, 801–47 (1996).

132. Baumeister, W., Walz, J., Zühl, F. & Seemüller, E. The proteasome: paradigm of a self-compartmentalizing protease. *Cell* **92**, 367–80 (1998).

133. Klionsky, D. J., Cuervo, A. M. & Seglen, P. O. Methods for monitoring autophagy from yeast to human. *Autophagy* **3**, 181–206 (2007).

134. Mizushima, N., Yoshimori, T. & Ohsumi, Y. The role of Atg proteins in autophagosome formation. *Annu. Rev. Cell Dev. Biol.* **27**, 107–32 (2011).

135. Kenney, D. L. & Benarroch, E. E. The autophagy-lysosomal pathway: General concepts and clinical implications. *Neurology* **85**, 634–645 (2015).

136. Kuma, A., Matsui, M. & Mizushima, N. LC3, an autophagosome marker, can be incorporated into protein aggregates independent of autophagy: caution in the interpretation of LC3 localization. *Autophagy* **3**, 323–8 (2007).

137. Rubinsztein, D. C. *et al.* In search of an 'autophagomometer'. *Autophagy* **5**, 585–9 (2009).

138. Pohl, C. & Dikic, I. Cellular quality control by the ubiquitin-proteasome system and autophagy. *Science* **366**, 818–822 (2019).

139. Sassone-Corsi, P. The Cyclic AMP Pathway. *Cold Spring Harb. Perspect. Biol.* **4**, (2012).

140. Bruce, J. I. ., Straub, S. V & Yule, D. I. Crosstalk between cAMP and Ca2+ signaling in non-excitable cells. *Cell Calcium* **34**, 431–444 (2003).

141. Goraya, T. A. & Cooper, D. M. F. Ca2+-calmodulin-dependent phosphodiesterase (PDE1): current perspectives. *Cell. Signal.* **17**, 789–97 (2005).

142. Taylor, S. S., Knighton, D. R., Zheng, J., Ten Eyck, L. F. & Sowadski, J. M. Structural Framework for the Protein Kinase Family. *Annu. Rev. Cell Biol.* **8**, 429–462 (1992).

143. Mayr, B. & Montminy, M. Transcriptional regulation by the phosphorylation-dependent factor CREB. *Nat. Rev. Mol. Cell Biol.* **2**, 599–609 (2001).

144. Tavares, C. D. J. *et al.* The Molecular Mechanism of Eukaryotic Elongation Factor 2 Kinase Activation. *J. Biol. Chem.* **289**, 23901 (2014).

145. Redpath, N. T. & Proud, C. G. Cyclic AMP-dependent protein kinase

phosphorylates rabbit reticulocyte elongation factor-2 kinase and induces calcium-independent activity. *Biochem. J.* **293 ( Pt 1)**, 31–4 (1993).

146. Diggle, T. A., Redpath, N. T., Heesom, K. J. & Denton, R. M. Regulation of protein-synthesis elongation-factor-2 kinase by cAMP in adipocytes. *Biochem. J.* **336 ( Pt 3)**, 525–9 (1998).

147. Yan, K., Gao, L.-N., Cui, Y.-L., Zhang, Y. & Zhou, X. The cyclic AMP signaling pathway: Exploring targets for successful drug discovery (Review). *Mol. Med. Rep.* **13**, 3715–23 (2016).

148. Lugnier, C. Cyclic nucleotide phosphodiesterase (PDE) superfamily: A new target for the development of specific therapeutic agents. *Pharmacol. Ther.* **109**, 366–398 (2006).

149. Schaal, S. M. *et al.* The Therapeutic Profile of Rolipram, PDE Target and Mechanism of Action as a Neuroprotectant following Spinal Cord Injury. *PLoS One* **7**, e43634 (2012).

150. Bedenis, R. *et al.* Cilostazol for intermittent claudication. *Cochrane Database Syst. Rev.* CD003748 (2014).

151. Lochner, A. & Moolman, J. A. The Many Faces of H89: A Review. *Cardiovasc. Drug Rev.* **24**, 261–274 (2006).

152. Murray, A. J. Pharmacological PKA inhibition: all may not be what it seems. *Sci. Signal.* **1**, re4 (2008).

153. Freibaum, B. D. *et al.* GGGGCC repeat expansion in C9orf72 compromises nucleocytoplasmic transport. *Nature* **525**, 129–33 (2015).

154. Zhang, J.-H., Chung, T. D. Y. & Oldenburg, K. R. A Simple Statistical Parameter for Use in Evaluation and Validation of High Throughput Screening Assays. *J. Biomol. Screen.* **4**, 67–73 (1999).

155. Kearse, M. G. *et al.* Ribosome queuing enables non-AUG translation to be resistant to multiple protein synthesis inhibitors. *Genes Dev.* **33**, 871–885 (2019).

156. Seamon, K. B., Padgett, W. & Daly, J. W. Forskolin: unique diterpene activator

of adenylate cyclase in membranes and in intact cells. *Proc. Natl. Acad. Sci. U. S. A.* **78**, 3363–7 (1981).

157. Sapio, L. *et al.* Targeting protein kinase A in cancer therapy: an update. *EXCLI J.* **13**, 843–55 (2014).

158. Kanne, H., Prasanna, V., Burte, N. & Gujjula, R. Extraction and elemental analysis of Coleus forskohlii extract. *Pharmacognosy Res.* **7**, 237 (2015).

159. Cristofani, R. *et al.* Inhibition of retrograde transport modulates misfolded protein accumulation and clearance in motoneuron diseases. *Autophagy* **13**, 1280–1303 (2017).

160. Zhang, Y.-J. *et al.* Aggregation-prone c9FTD/ALS poly(GA) RAN-translated proteins cause neurotoxicity by inducing ER stress. *Acta Neuropathol.* **128**, 505–524 (2014).

161. May, S. *et al.* C9orf72 FTLD/ALS-associated Gly-Ala dipeptide repeat proteins cause neuronal toxicity and Unc119 sequestration. *Acta Neuropathol.* **128**, 485–503 (2014).

162. Guo, Q. *et al.* In Situ Structure of Neuronal C9orf72 Poly-GA Aggregates Reveals Proteasome Recruitment. *Cell* **172**, 696-705.e12 (2018).

163. Rusmini, P. *et al.* Trehalose induces autophagy via lysosomal-mediated TFEB activation in models of motoneuron degeneration. *Autophagy* **15**, 631–651 (2019).

164. Bence, N. F., Sampat, R. M. & Kopito, R. R. Impairment of the ubiquitin-proteasome system by protein aggregation. *Science* **292**, 1552–5 (2001).

165. Tydlacka, S., Wang, C.-E., Wang, X., Li, S. & Li, X.-J. Differential activities of the ubiquitin-proteasome system in neurons versus glia may account for the preferential accumulation of misfolded proteins in neurons. *J. Neurosci.* **28**, 13285–95 (2008).

166. Lokireddy, S., Kukushkin, N. V. & Goldberg, A. L. cAMP-induced phosphorylation of 26S proteasomes on Rpn6/PSMD11 enhances their activity and the degradation of misfolded proteins. *Proc. Natl. Acad. Sci. U. S.*

*A.* **112**, E7176-85 (2015).

167. Huang, H., Wang, H. & Figueiredo-Pereira, M. E. Regulating the Ubiquitin/Proteasome Pathway Via cAMP-signaling: Neuroprotective Potential. *Cell Biochem. Biophys.* **67**, 55–66 (2013).

168. Fuse, M. *et al.* Regulation of geranylgeranyl pyrophosphate synthase in the proliferation of rat FRTL-5 cells: involvement of both cAMP-PKA and PI3-AKT pathways. *Biochem. Biophys. Res. Commun.* **315**, 1147–1153 (2004).

169. Hoshino, T. *et al.* Suppression of Alzheimer's Disease-Related Phenotypes by Geranylgeranylacetone in Mice. *PLoS One* **8**, e76306 (2013).

170. Marunouchi, T., Inomata, S., Sanbe, A., Takagi, N. & Tanonaka, K. Protective effect of geranylgeranylacetone via enhanced induction of HSPB1 and HSPB8 in mitochondria of the failing heart following myocardial infarction in rats. *Eur. J. Pharmacol.* **730**, 140–147 (2014).

171. Davies, S. P., Reddy, H., Caivano, M. & Cohen, P. Specificity and mechanism of action of some commonly used protein kinase inhibitors. *Biochem. J.* **351**, 95–105 (2000).

172. Limbutara, K., Kelleher, A., Yang, C.-R., Raghuram, V. & Knepper, M. A. Phosphorylation Changes in Response to Kinase Inhibitor H89 in PKA-Null Cells. *Sci. Rep.* **9**, 2814 (2019).

173. Tang, X. *et al.* Divergence, Convergence, and Therapeutic Implications: A Cell Biology Perspective of C9ORF72-ALS/FTD. *Mol. Neurodegener.* **15**, 34 (2020).

174. Yuva-Aydemir, Y., Almeida, S. & Gao, F.-B. Insights into C9ORF72-Related ALS/FTD from Drosophila and iPSC Models. *Trends Neurosci.* **41**, 457–469 (2018).

175. Zhang, S., Feany, M. B., Saraswati, S., Littleton, J. T. & Perrimon, N. Inactivation of Drosophila Huntingtin affects long-term adult functioning and the pathogenesis of a Huntington's disease model. *Dis. Model. Mech.* **2**, 247–266 (2009).

176. Cheng, W. *et al.* CRISPR-Cas9 Screens Identify the RNA Helicase DDX3X as a Repressor of C9ORF72 (GGGGCC)n Repeat-Associated Non-AUG Translation. *Neuron* **104**, 885-898.e8 (2019).

177. Whitesell, L., Mimnaugh, E. G., De Costa, B., Myers, C. E. & Neckers, L. M. Inhibition of heat shock protein HSP90-pp60v-src heteroprotein complex formation by benzoquinone ansamycins: essential role for stress proteins in oncogenic transformation. *Proc. Natl. Acad. Sci. U. S. A.* **91**, 8324–8 (1994).

178. Ochel, H. J., Eichhorn, K. & Gademann, G. Geldanamycin: the prototype of a class of antitumor drugs targeting the heat shock protein 90 family of molecular chaperones. *Cell Stress Chaperones* **6**, 105–12 (2001).

179. Sidera, K. & Patsavoudi, E. HSP90 inhibitors: current development and potential in cancer therapy. *Recent Pat. Anticancer. Drug Discov.* **9**, 1–20 (2014).

180. Manaenko, A. *et al.* Heat shock protein 70 upregulation by geldanamycin reduces brain injury in a mouse model of intracerebral hemorrhage. *Neurochem. Int.* **57**, 844–850 (2010).

181. Putcha, P. *et al.* Brain-permeable small-molecule inhibitors of Hsp90 prevent alpha-synuclein oligomer formation and rescue alpha-synuclein-induced toxicity. *J. Pharmacol. Exp. Ther.* **332**, 849–57 (2010).

182. Parcellier, A. *et al.* HSP27 is a ubiquitin-binding protein involved in I-kappaBalpha proteasomal degradation. *Mol. Cell. Biol.* **23**, 5790–802 (2003).

183. Gomez-Sanchez, E. P. Third-generation Mineralocorticoid Receptor Antagonists: Why Do We Need a Fourth? *J. Cardiovasc. Pharmacol.* **67**, 26–38 (2016).

184. Alekseev, S. *et al.* A Small Molecule Screen Identifies an Inhibitor of DNA Repair Inducing the Degradation of TFIIH and the Chemosensitization of Tumor Cells to Platinum. *Chem. Biol.* **21**, 398–407 (2014).

185. Elinoff, J. M. *et al.* Spironolactone-induced degradation of the TFIIH core complex XPB subunit suppresses NF-κB and AP-1 signalling. *Cardiovasc. Res.* **114**, 65–76 (2018).

186. Gray, L. T., Vallur, A. C., Eddy, J. & Maizels, N. G quadruplexes are genomewide targets of transcriptional helicases XPB and XPD. *Nat. Chem. Biol.* **10**, 313–318 (2014).

187. Garcia-Lopez, A. *et al.* Genetic and Chemical Modifiers of a CUG Toxicity Model in Drosophila. *PLoS One* **3**, e1595 (2008).

188. Vegeto, E. *et al.* The Role of Sex and Sex Hormones in Neurodegenerative Diseases. *Endocr. Rev.* **41**, (2020).

189. Lucchesi, J. C. & Kuroda, M. I. Dosage compensation in Drosophila. *Cold Spring Harb. Perspect. Biol.* **7**, 1–21 (2015).

190. Engh, R. A., Girod, A., Kinzel, V., Huber, R. & Bossemeyer, D. Crystal structures of catalytic subunit of cAMP-dependent protein kinase in complex with isoquinolinesulfonyl protein kinase inhibitors H7, H8, and H89. Structural implications for selectivity. *J. Biol. Chem.* **271**, 26157–64 (1996).

191. Ørstavik, S. *et al.* Identification of novel splice variants of the human catalytic subunit cβ of cAMP-dependent protein kinase. *Eur. J. Biochem.* **268**, 5066–5073 (2001).

192. Kvissel, A.-K. *et al.* Induction of Cβ splice variants and formation of novel forms of protein kinase A type II holoenzymes during retinoic acid-induced differentiation of human NT2 cells. *Cell. Signal.* **16**, 577–587 (2004).

193. Enns, L. C., Pettan-Brewer, C. & Ladiges, W. Protein kinase A is a target for aging and the aging heart. *Aging (Albany. NY).* **2**, 238–243 (2010).

194. Tudisca, V. *et al.* PKA isoforms coordinate mRNA fate during nutrient starvation. *J. Cell Sci.* **125**, 5221–32 (2012).

195. Leipheimer, J., Bloom, A. L. M. & Panepinto, J. C. Protein Kinases at the Intersection of Translation and Virulence. *Front. Cell. Infect. Microbiol.* **9**, 318 (2019).

196. He, K. *et al.* Stabilization of Ca2+-permeable AMPA receptors at perisynaptic sites by GluR1-S845 phosphorylation. *Proc. Natl. Acad. Sci. U. S. A.* **106**, 20033–8 (2009).

197. Whitcomb, D. J. *et al.* Intracellular oligomeric amyloid-beta rapidly regulates GluA1 subunit of AMPA receptor in the hippocampus. *Sci. Rep.* **5**, 10934 (2015).

198. Xie, J. *et al.* Regulation of the Elongation Phase of Protein Synthesis Enhances Translation Accuracy and Modulates Lifespan. *Curr. Biol.* **29**, 737-749.e5 (2019).

199. Ueda, M., Matsuura, K., Kawai, H., Wakasugi, M. & Matsunaga, T. Spironolactone-induced XPB degradation depends on CDK7 kinase and SCF $^{FBXL18}$ E3 ligase. *Genes to Cells* **24**, 284–296 (2019).

200. Cashman, N. R. *et al.* Neuroblastoma x spinal cord (NSC) hybrid cell lines resemble developing motor neurons. *Dev. Dyn.* **194**, 209–221 (1992).

201. Durham, H. D., Dahrouge, S. & Cashman, N. R. Evaluation of the spinal cord neuron X neuroblastoma hybrid cell line NSC-34 as a model for neurotoxicity testing. *Neurotoxicology* **14**, 387–95 (1993).

202. Francis, A. C. *et al.* Second Generation Imaging of Nuclear/Cytoplasmic HIV-1 Complexes. *AIDS Res. Hum. Retroviruses* **30**, 717–726 (2014).

203. Rusmini, P. *et al.* Aggregation and proteasome: the case of elongated polyglutamine aggregation in spinal and bulbar muscular atrophy. *Neurobiol. Aging* **28**, 1099–111 (2007).

204. Schindelin, J. *et al.* Fiji: An open-source platform for biological-image analysis. *Nature Methods* **9**, 676–682 (2012).

205. Bernabò, P. *et al.* In Vivo Translatome Profiling in Spinal Muscular Atrophy Reveals a Role for SMN Protein in Ribosome Biology. *Cell Rep.* **21**, 953–965 (2017).

206. Tebaldi, T. *et al.* Widespread uncoupling between transcriptome and translatome variations after a stimulus in mammalian cells. *BMC Genomics* **13**, 220 (2012).

207. Vernizzi, L. *et al.* Glutamine Synthetase 1 Increases Autophagy Lysosomal Degradation of Mutant Huntingtin Aggregates in Neurons, Ameliorating

Motility in a Drosophila Model for Huntington's Disease. *Cells* **9**, 196 (2020).

# *Acknowledgements*

At the end of this 4-year experience, I wish to thank various people for their fundamental contribution to my Ph.D.

Firstly, I would like to express my gratitude to my tutor Prof Alessandro Provenzani, who gave me the opportunity to join his Laboratory of Genomic Screening and encouraged me to pursue this challenging and ambitious project. I truly enjoyed working in a research environment that stimulates original thinking and initiative, which he created. His skilful guidance, constructive critiques and stoic patience are greatly appreciated. I also want to say many thanks to Prof Provenzani for believing in me, giving me often *carte blanche* to plan and propose project, and for always interesting in hearing my opinion. It means a lot to me because he contributed to my personal and professional growth.

I would like to thank Prof Angelo Poletti from the University of Milano. Prof Poletti welcomed me to his lab for my master's thesis and continued in contributing many discussions during my Ph.D. research that helped me to shape this project.

I would like to acknowledge helpful suggestions from my committee members Dr Gabriella Viero, Prof Alberto Inga, Prof Adriano Chiò and Dr Eugenio Fava.

The Department of Cellular, Computational and Integrative Biology (CIBIO) of the University of Trento offered me the possibility to work in a young, highly dynamic, and stimulating research environment. I would also like to express my very great appreciation for the training provided by the International Ph.D. program I was enrolled in, headed by Prof Anna Cereseto and subsequently by Prof Alberto Inga.

I wish to acknowledge the help provided by internal and external collaborators.
I would like to acknowledge the valuable input of Dr Riccardo Cristofani, from the University of Milano, who contributed to this project with his knowledge and experience about the mechanism of proteins clearance.
Valuable technical support on this project came from Dr Valentina Adami, and Michael Pancher of HTS & Validation Core Facility.

A special thanks to Prof Paola Bellosta from the Laboratory of Metabolism of Cell Growth and Neuronal Survival of the University of Trento for her valuable collaboration concerning the part on flies. My deepest thanks also go to Dr Alessia Soldano that granted my wish teaching me how to work with flies and allowing me to discover the fascinating world of *Drosophila*.

My deep thanks go to Dr Gabriella Viero, researcher and group leader at the Institute of Biophysics of CNR not only for teaching me how to do and interpreter a polysomal profiling, but also and especially to have enriched me with precious advices for my professional and personal growth.

This work would not have materialized without the financial support of grants from Fondazione Cassa di Risparmio di Trento e Rovereto and from Fondazione AriSLA.

These acknowledgements would not be complete without mentioning my past and present research lab colleagues: Rosa Loffredo, Vito D'Agostino, Preet Lal, Natthakan Thongon, Chiara Zucal, Isabelle Bonomo, Mariachiara Micaelli, Daniele Pollini, Caterina Ciani and Àgata Carreira, who shared with me good and bad times and have always helped me. It was a great pleasure working with them and I appreciate their ideas, help and good humour.
Special thanks goes to Vito for sharing valuable data and to Rosa that she has been much more than a mentor. I am thankful to Rosa for all that taught me and for our true friendship that continues from miles away.

Finally, my deepest appreciation belongs to my family and all the people who love me. They have always believed in me and gave me their complete support, patience and understanding.

Grazie infinite a tutti voi!